NC STATE UNIVERSITY

CENTER

FOR

TRANSPORTATION

ENGINEERING

STUDIES

INTERPRETATION OF FWD DATA WHEN PAVEMENT LAYERS ARE NOT INTACT

by

Y. Richard Kim, Ph.D., P.E.
Yung-Chien Lee
Sunwoo Park, Ph.D.
S. Ranji Ranjithan, Ph.D.

DEPARTMENT OF CIVIL ENGINEERING

INTERPRETATION OF FWD DATA WHEN PAVEMENT LAYERS ARE NOT INTACT

by

Y. Richard Kim, Ph.D., P.E.
Yung-Chien Lee
Sunwoo Park, Ph.D.
S. Ranji Ranjithan, Ph.D.

INTERPRETATION OF FWD DATA WHEN PAVEMENT LAYERS ARE NOT INTACT

by

Y. Richard Kim, Ph.D., P.E.
Associate Professor

Yung-Chien Lee
Graduate Research Assistant

Sunwoo Park, Ph.D.
Research Associate

S. Ranji Ranjithan, Ph.D.
Assistant Professor

Final Report Submitted to the
North Carolina Department of Transportation

Department of Civil Engineering
North Carolina State University
Raleigh, NC

March 1999

Technical Report Documentation Page

1. Report No.	2. Government Accession No.	3. Recipient's Catalog No.
FHWA/NC/99-002		

4. Title and Subtitle	5. Report Date
Interpretation of FWD Data When Pavement Layers Are Not Intact	March, 1999
	6. Performing Organization Code
	8. Performing Organization Report No.
7. Author(s)	
Y. Richard Kim, Ph.D., P.E.	
9. Performing Organization Name and Address	10. Work Unit No. (TRAIS)
Center for Transportation Engineering Studies North Carolina State University Campus Box 7908 Raleigh, NC 27695-7908	11. Contract or Grant No. 23241-96-5
12. Sponsoring Agency Name and Address	13. Type of Report and Period Covered
North Carolina Department of Transportation Raleigh, NC 27611 Federal Highway Administration Raleigh, NC 27611	Final Report July 1995 - June 1997
	14. Sponsoring Agency Code

15. Supplementary Notes

16. Abstract

The falling weight deflectometer (FWD) has become a popular tool worldwide for the evaluation of the structural capacity and integrity of existing pavements. Most of the deflection analysis programs used today are based on multi-layered elastic analysis which assumes static loading and continuous, homogeneous, and isotrophic layers. When FWD tests are performed on broken or cracked pavements (of which information is crucial in making rehabilitation and overlay decisions), the multi-layered elastic theory-based backcalculation programs assume that the effect of these discontinuities in a cracked layer on deflection basins would be accounted for by the reduction of the elastic modulus for that layer. However, it has been concluded and confirmed by researchers and practioners that the backcalculation algorithms based on the multi-layered elastic theory produce large variation in the "effective" moduli of the cracked layers. Studies have also shown that significant errors in the backcalculated pavement moduli can accrue from performing a static analysis of what is inherently a dynamic test. Unfortunately, dynamic analysis usually involves complex calculations and requires significant computation time, thus making it impractical for routine applications.

This study presents a methodology based on deflection basin parameters and artificial neural networks (ANNs) for processing dynamic FWD measurements to estimate layer strengths. Two-dimensional, dynamic, finite element analysis using the ABAQUS program was employed to develop the deflection information for this
(continued)

17. Key Words	18. Distribution Statement
falling weight deflectometer, flexible pavement, back calculation, deflection basin parameter, finite element analysis, artificial neural network, asphalt concrete	No restrictions 125 copies of this document were printed at a cost of $4.02 per copy

19. Security Classif. (of this report)	20. Security Classif. (of this page)	21. No. of Pages	22. Price
		134	

Form DOT F 1700.7 (8-72) Reproduction of completed page authorized

study. Unlike the majority of the existing backcalculation programs that iteratively adjust the layer moduli to match the measured deflections, the proposed method first determines the subgrade modulus by means of two deflection basin parameters, Base Damage Index and Shape Factor F2, and then applies the estimated subgrade modulus and other parameters as input variables to a trained ANN to estimate the upper layers' moduli. Procedures in predicting layer moduli for both two- and three-layer pavement systems are presented. In contrast to other programs that require the input of seed values for layer moduli, this method does not require initial estimates as input.

Field FWD measurements were analyzed both by this method and by the MODULUS program. Results reveal that the proposed method is better able to predict the asphalt concrete (AC) layer modulus while taking into account the dynamic effects of the FWD test. This method is also computationally efficient which makes it applicable for routine tasks and field use.

Effects of discontinuities in the AC layer of a pavement on the resulting deflections under an FWD test load were also studied using the finite element method. It was discovered that the condition of an AC layer, whether it is intact or damaged, may be detected using two deflection basin parameters, Shape Factor F2 and AREA.

ACKNOWLEDGMENTS

This research was sponsored by the North Carolina Department of Transportation and the Federal Highway Administration. Our Technical Advisory Committee consisted of W. K. Creech, P.E., Chair; Moy Biswas, Ph.D., P.E.; S. S. Wu, Ph.D., P.E.; Judith Corley-Lay, Ph.D., P.E.; and Mr. Jim Travis. These advisors have given invaluable direction and support to us throughout the project. Mr. Thomas Hearne of the Pavement Management Unit has also provided helpful suggestions, constructive criticism, and support throughout the project. The principal investigator wishes to thank these people for their significant contributions to the research.

ABSTRACT

The falling weight deflectometer (FWD) has become a popular tool worldwide for the evaluation of the structural capacity and integrity of existing pavements. Most of the deflection analysis programs used today are based on multi-layered elastic analysis which assumes static loading and continuous, homogeneous, and isotropic layers. When FWD tests are performed on broken or cracked pavements (of which information is crucial in making rehabilitation and overlay decisions), the multi-layered elastic theory-based backcalculation programs assume that the effect of these discontinuities in a cracked layer on deflection basins would be accounted for by the reduction of the elastic modulus for that layer. However, it has been concluded and confirmed by researchers and practitioners that the backcalculation algorithms based on the multi-layered elastic theory produce large variations in the "effective" moduli of the cracked layers. Studies have also shown that significant errors in the backcalculated pavement moduli can accrue from performing a static analysis of what is inherently a dynamic test. Unfortunately, dynamic analysis usually involves complex calculations and requires significant computation time, thus making it impractical for routine applications.

This study presents a methodology based on deflection basin parameters and artificial neural networks (ANNs) for processing dynamic FWD measurements to estimate layer strengths. Two-dimensional, dynamic, finite element analysis using the ABAQUS program was employed to develop the deflection information for this study. Unlike the majority of the existing backcalculation programs that iteratively adjust the layer moduli to match the measured deflections, the proposed method first determines the subgrade modulus by means of two deflection basin parameters, Base Damage Index and Shape Factor *F*2, and then applies the estimated subgrade modulus and other parameters as input variables to a trained ANN to estimate the upper layers' moduli. Procedures in predicting layer moduli for both two- and three-layer pavement systems are presented. In contrast to other programs that require the input of seed values for layer moduli, this method does not require initial estimates as input.

Field FWD measurements were analyzed both by this method and by the MODULUS program. Results reveal that the proposed method is better able to predict the asphalt concrete (AC) layer modulus while taking into account the dynamic effects of the FWD test. This method is also computationally efficient which makes it applicable for routine tasks and field use.

Effects of discontinuities in the AC layer of a pavement on the resulting deflections under an FWD test load were also studied using the finite element method. It was discovered that the condition of an AC layer, whether it is intact or damaged, may be detected using two deflection basin parameters, Shape Factor *F*2 and *AREA*.

TABLE OF CONTENTS

TABLE OF CONTENTS (CONTINUED)

TABLE OF CONTENTS (CONTINUED)

LIST OF TABLES

LIST OF FIGURES

LIST OF FIGURES (CONTINUED)

LIST OF FIGURES (CONTINUED)

LIST OF FIGURES (CONTINUED)

PART I: PROJECT SUMMARY

1. INTRODUCTION

The falling weight deflectometer (FWD) has become a principal means of evaluating structural condition of pavements. A great deal of effort has been made to interpret FWD deflection basins for the determination of rehabilitation strategies and overlay thickness. Such efforts have mainly centered around the backcalculation of layer material properties within the framework of continuum mechanics, in particular, the multi-layered elastic theory [1].

This theory assumes that each layer is intact and is characterized by its Young's modulus and Poisson's ratio. When FWD tests are performed on broken or cracked pavements (of which information is crucial in making rehabilitation and overlay decisions), the multi-layered elastic theory-based backcalculation programs assume that the effect of these discontinuities in a cracked layer on deflection basins would be accounted for by the reduction of the elastic modulus for that layer. However, it has been concluded and confirmed by researchers and practitioners that the backcalculation algorithms based on the multi-layered elastic theory produce large variations in the "effective" moduli of the cracked layers [2, 3]. This difficulty forces some researchers to place more emphasis on interpretation of deflections than on backcalculation of elastic moduli using the multi-layered elastic theory-based programs, when FWD tests are performed on severely cracked pavements. However, Uddin et al. [4] recently reported their success in backcalculating the "effective" moduli of cracked layers in portland cement concrete pavements using three-dimensional finite element analysis instead of the traditional multi-layered elastic analysis.

Another deficiency of the multi-layered elastic theory-based backcalculation programs is that they are based on a static analysis procedure. Studies have shown that significant errors in the backcalculated pavement moduli can accrue from performing a static analysis of what is inherently a dynamic test. Chang et al. [5] reported that static analysis-based programs often underestimate the subgrade strength when deflections obtained from dynamic tests are used. Although many dynamic analysis-based programs are readily available today, they usually involve complex calculations and require extensive computation time. As a result, they are impractical for use in routine tasks.

The urgent need to develop a deflection analysis procedure that provides accurate information on the condition of distressed flexible pavements has been recognized by the North Carolina Department of Transportation, resulting in a two-year research project entitled "Interpretation of FWD Data When Pavement Layers Are Not Intact." This report presents research results from this project. The remaining sections in Part I will briefly describe the objectives and research approach taken in this study and summarize

the proposed deflection analysis procedure that has resulted. Detailed research findings and information regarding the basis for the proposed procedure will then be presented in Part II.

2. OBJECTIVES AND RESEARCH APPROACH

The objectives of this research are:

1. to determine the effects of distresses in flexible pavement systems on FWD deflection basins,
2. to develop a method or guideline of determining, based on the interpretation of FWD deflection basins, layer conditions of existing flexible pavements which require rehabilitation, and
3. to verify the recommended procedure using the deflections measured from pavements with known distress conditions.

These objectives are challenging tasks owing to the large number of factors to be considered, their interactions, and the randomness of the distresses with regard to location, severity, and extent. One approach to developing a reliable deflection analysis procedure is to conduct deflection tests on a number of pavements with varying distress characteristics under different environmental conditions and to relate the observed deflection behavior to the input variables, a so-called empirical approach. Considering the large number of combinations of these factors, this approach will be time consuming and costly, if not impossible, due to the large data requirements.

The other approach, a mechanistic approach, is to employ mechanics of materials equations that relate an input such as a FWD loading to an output or to pavement responses such as deflections. Depending upon the type of layer materials used, appropriate material models can be employed with varying complexities. The effects of environmental conditions are usually reflected through these material models. Then the main question becomes, "How accurate and realistic is the analytical model in predicting pavement responses under varying conditions?"

The research approach taken in this study is the so-called mechanistic-empirical approach that optimizes the application of the two approaches described above to develop a more reliable procedure. ABAQUS, a powerful general purpose finite element computer program, was employed for developing the structural analysis model. This forward model was used as the vehicle for effectively estimating deflections of damaged synthetic pavements with varying designs, distress characteristics, and environmental conditions. Both the field deflection data and the calculated synthetic deflections were then used in estimating a set of damage indicators, including deflection basin parameters and effective moduli. The employment of the FEM model allowed the relationship(s) between damage

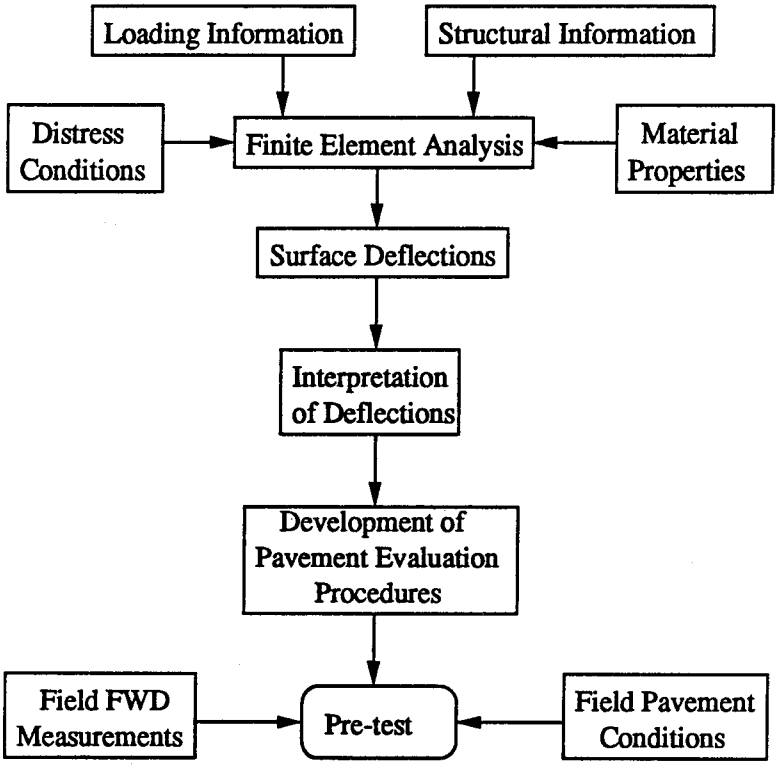

Figure 2.1: An overview of the research plan.

indicators and known distress characteristics to be studied systematically without costing much money and time in collecting field FWD data. An overview of this research plan is displayed in Figure 2.1.

There are two types of cracked flexible pavements that pavement engineers frequently encounter: one covered with an intact overlay, and the other with cracks present on the pavement surface. The condition of cracks present on the pavement surface is not a major concern of highway agencies because the condition of that pavement can be measured visually. It is, however, the hidden cracks or weak layers covered by an intact layer (e.g., an overlay) that makes a pavement condition difficult to identify or measure. Two types of flexible pavements are often employed in a highway system - asphalt concrete surface layer with aggregate base course and full-depth asphalt concrete layer on top of subgrade. In this study, a full factorial of intact pavement analyses with various combinations of layer thicknesses and moduli was carried out. Table 2.1 shows the variables considered in selecting pavement configurations and the number of levels for each of the variables.

Table 2.1. Variables and number of levels to be considered in the forward calculation for intact pavements.

	Number of Levels	
Variables	Full-depth AC Pavements	AC with Granular Base Pavements
AC Modulus	7	6
ABC Modulus	---	5
SG Modulus	8	5
AC Thickness	4	4
ABC Thickness	---	4
SG Thickness	Fixed (∞)	Fixed (∞)

Distress types considered in this study are hidden vertical cracks and stripping in the asphalt concrete layer. The results from the distressed pavement analyses were compared against those of intact pavements to identify the key characteristics of deflections for distress conditions. It is noted here that the weak conditions of aggregate base and subgrade layers are represented by reductions in the base and subgrade moduli instead of considering discontinuities in these layers.

3. PROPOSED DEFLECTION ANALYSIS PROCEDURE

The following conditions must be met before using the current model:

1. The depth to a stiff layer is assumed to be infinity or larger than 20 feet.
2. The distances of the seven deflections are 0, 203, 305, 457, 610, 914, and 1219 mm (0, 8, 12, 18, 24, 36, 48 inches) from the loading center.

3. Pavement structure must be a pavement consisting of an AC layer and subgrade (2-layer system) or a pavement consisting of an AC layer, an aggregate base layer, and subgrade (3-layer system).
4. For the 3-layer pavement system, the thickness of the aggregate base layer must be less than 450 mm (17.7 in.).
5. The current model is not valid for pavements with a cement-treated base.

The proposed deflection analysis procedures are described in the following steps:

1. Obtain the FWD measurements with the load magnitude in pound-force and the seven deflections in mils (typical current DOT FWD measurements).
2. Estimate the depth to a stiff layer. At present, the MODULUS program is used for the estimation of the depth to a stiff layer. It should be noted that the current model can handle pavements with infinite (or deeper than 4 m) depth to a stiff layer only.
3. Normalize the seven deflections with the applied load and the loading area to mils/psi or in./kip.
4. Convert the normalized deflections from English units to metric units (1 mils/psi = 1 in./kip = 404.238 mm/MPa).
5. Compute *Do*, *AREA*, Base Damage Index (*BDI*), Base Curvature Index (*BCI*), and Shape Factor *F2*. These parameters are defined as follows.

$$D_0 = \delta_0 \tag{3.1}$$

$$BDI = \delta_1 - \delta_2 \tag{3.2}$$

$$BCI = \delta_2 - \delta_3 \tag{3.3}$$

$$F2 = \frac{\delta_1 - \delta_3}{\delta_2} \tag{3.4}$$

$$AREA = \frac{12 \times 2.54}{2} \times \frac{\delta_0 + 2\delta_1 + 2\delta_2 + \delta_3}{\delta_0} \tag{3.5}$$

where BCI = Base Curvature Index (mm/MPa),
BDI = Base Damage Index (mm/MPa),
$F2$ = shape factor (dimensionless),
$AREA$ = deflection basin area (cm),
δ_0 = deflection at the loading center (mm/MPa),
δ_1 = deflection at distance 305 mm (12 in.) from the loading center,
δ_2 = deflection at distance 610 mm (24 in.) from the loading center, and
δ_3 = deflection at distance 914 mm (36 in.) from the loading center.

6. Use *BDI* and *F2* to determine the subgrade modulus (E_{sg}) using the *BDI-F2* and E_{sg} relationships. The relationships are presented in figures which have been implemented using a trained Artificial Neural Network (ANN) and the MATLAB program. This step is valid for both full-depth AC pavements and AC pavements with an aggregate base layer.
7. If the pavement is a 2-layer system, use the estimated E_{sg}, H_{ac}, D_o, and *AREA* to estimate E_{ac} using figures or the computer program.

8. If the pavement is a 3-layer system, use the estimated E_{sg}, H_{ac}, H_{abc}, *BCI*, *Do*, and *AREA* to estimate E_{ac}. After obtaining E_{ac}, use E_{sg}, E_{ac}, H_{ac}, H_{abc}, *BCI*, *Do*, and *AREA* to estimate E_{abc}. This step should be conducted using the computer program to ensure an accurate estimation because of the number of variables involved.
9. Use the AC thickness and the values of *F2* and *AREA* for the prediction of the AC layer condition (whether it is damaged or not). If the *F2-AREA* is located above the envelope (developed from an intact pavement model) then the AC layer may have been damaged.

Steps 3 through 8 have been automated using the MATLAB program. It should be noted that the prediction accuracy of the layer moduli can be improved by adding more cases to the data base which was used to train the artificial neural networks.

PART II: RESEARCH FINDINGS

4. PAVEMENT ANALYSIS USING FINITE ELEMENT METHOD

To study the behavior of cracked pavements, the multi-layered linear elastic theory is not appropriate because it assumes that pavement layers are continuous. In contrast, the finite element method (FEM) allows for the consideration of discontinuities in the cracked layers. Finite element models can replicate the results of proven theories such as the multi-layered elastic theory, as well as hold the possibility of adding levels of complexity (e.g., discontinuity effects) to pavement analysis that would be impossible otherwise.

Many finite element computer programs have been developed specifically for pavement structural analysis; for example, ILLI-PAVE [6] for flexible pavements and ILLI-SLAB for rigid pavements. These programs consider the non-linearity of the pavement materials in analysis, in particular, the stress-state dependency of the soil materials. However, these programs do not incorporate the discontinuity effects of the distressed layer into analysis.

Modern finite element codes (e.g., ABAQUS) are available for comprehensive pavement structural response analysis that considers static and dynamic loads (e.g., impulse, moving wheel load, etc.), linear and nonlinear elastic material models, viscoelastic material models, and crack conditions in pavement layers. Using appropriate element and material models, it is possible to approximate the actual behavior of a pavement system in the field.

4.1. ABAQUS FEM Program

ABAQUS [7], a commercially available FEM program, has been proven suitable for pavement analysis. Chen et al. [8] made a comprehensive study of various FEM pavement analysis programs and showed that the ABAQUS program yielded results comparable to those of other programs. Zaghloul and White [9] have successfully employed ABAQUS for 3-D dynamic analysis of intact flexible pavements. Three-dimensional rigid pavement analyses using ABAQUS were also performed by Kuo et al. [10], Mallela and George [11], and Zaghloul et al. [12]. Recently, Uddin et al. [4] investigated the behavior of a joint concrete pavement under a standard FWD load with discontinuities using ABAQUS with 3-D dynamic analysis.

ABAQUS provides many element and material models that are useful for pavement analysis. For example, the infinite element model can be used to model the infinite horizontal and vertical boundaries of a pavement profile, the interface element may be used to simulate cracked conditions in the asphalt concrete (AC) layer, and the viscoelastic material model can be incorporated to model the behavior of the asphalt

concrete material, etc. The use of these models in pavement analysis has been demonstrated by other researchers [4,9,12]. A case study using the linear viscoelastic model to simulate a cyclic loading test on laboratory compacted specimens is also presented by Lee [13]. This study showed good agreement between the measured and the computed responses on asphalt concrete specimens with a cyclic loading test. Findings from the results of these research activities indicate that ABAQUS is a suitable tool for analyzing pavement problems.

4.2. Infinite Element Model

A pavement system is usually modeled with infinite boundary in the lateral direction and with semi-infinite depth for the subgrade layer. This assumption works well except when a load is applied close to the pavement edge or with a shallow rigid base. Another consideration of assuming infinite boundary in the analysis model is where the region of interest is small in size as compared to the surrounding medium. Usually, the effect of infinite boundary is modeled using a larger size of the model in analysis. This increases the size of the FEM model and results in unnecessary computation time. ABAQUS provides 1-D, 2-D, and 3-D element models, called infinite elements, for modeling the infinite boundary conditions that can produce similar infinite boundary effect while conserving CPU time.

The solution in the infinite elements (far-field) is assumed to be linear, so that only linear behavior is provided in the infinite elements. In the dynamic analysis, the material response in the infinite elements is assumed to be isotropic. In the direct integration dynamic response analysis, these elements provide "quiet" boundaries to the finite element model. They also maintain the static force that was present at the start of the dynamic response analysis on this boundary and, as a consequence, the far-field nodes in the infinite elements will not displace during the dynamic response.

A set of analyses was performed to study the appropriateness of using infinite elements for typical FWD testing configurations of flexible pavements. The pavement models were comprised of an AC layer, a granular base layer, and the subgrade. The corresponding layer properties are presented in Table 4.1. The lengths of the pavement models to the loading center were set to 2.032, 4.064, 8.128 m (80, 160, 320 in.), and infinite. Finite elements were used throughout the pavement models except for the case of infinite length at which the outer-most elements were modeled using 2-D infinite elements (Figure 4.1). Two-dimensional, axisymmetric, 4-node elements were employed in the pavement models. Roller constraints were assigned to the model boundaries except where the infinite elements were used. The applied load given was 40 kN (9,000 lbf), uniformly distributed over a circular area with a 150 mm (5.91 in.) radius (typical FWD loading configuration). Both static and dynamic analyses were carried out for all the cases.

Table 4.1. Layer properties used for the investigation of the infinite elements.

	AC Layer	Aggregate Base	Subgrade
Thickness (cm)	13.97	27.94	609.6
Modulus (MPa)	5516	345	103
Poisson's Ratio	0.35	0.4	0.45
Density (kg/m^3)	2565	2244	1763
Damping (%)	5	5	5

Figure 4.2 presents the results obtained from the analyses. As can be seen, the surface deflections computed by the static analysis with a model length of 8.128 m and those of infinite length are essentially the same. When the dynamic analysis is employed, the computed deflections all fall onto the same curve when the length of the pavement model is greater than 4.064 m. This result demonstrates that the infinite element model can be used to generate the infinite boundary effect of a pavement profile without needing to use a large FEM model. In this study, the infinite elements will be used for modeling the infinite boundaries in both the lateral direction and the infinite depth of the subgrade.

4.3. Dynamic Analysis

The dynamic effect is one of the most significant factors affecting the results of pavement analysis. Deflection basins measured from dynamic FWD tests differ in several respects from the deflection basins estimated from static analysis. Davies and Mamlouk [14] and Roesset and Shao [15] have incorporated the inertial effects into a rigorous elasto-dynamic analysis of pavement response which indicates that the dynamic effects are significant. Sebaaly et al. [16] indicated that static analysis of the FWD overestimates the stiffness of the pavement layers. Chang et al. [5] also reported that the modulus of the subgrade is generally underestimated and the moduli of the base and the surface layers are overestimated when dynamic effects occurring in the measurements are not taken into account in the analysis. A recent study conducted by Nazarian and Boddapati [17] also concluded that the dynamic nature of an FWD load may more significantly affect the deflections measured away from the load. These findings emphasize the importance of considering the dynamic nature of FWD loads.

Two approaches, IMPLICIT and EXPLICIT, are provided in ABAQUS. The IMPLICIT method computes the deflections at any time step n by solving a set of nonlinear equations to determine the deflections at time step n-1. The direct integration method is usually used when nonlinear problems are being studied. The standard method in ABAQUS/Standard is one of the approaches of direct integration. This method implies that the nonlinear dynamic equilibrium equations must be solved at each time increment. Uddin et al. [18] concluded that the IMPLICIT method is more appropriate and generally converges better for pavement analysis. The direct integration method of the dynamic analysis procedure is employed throughout this study.

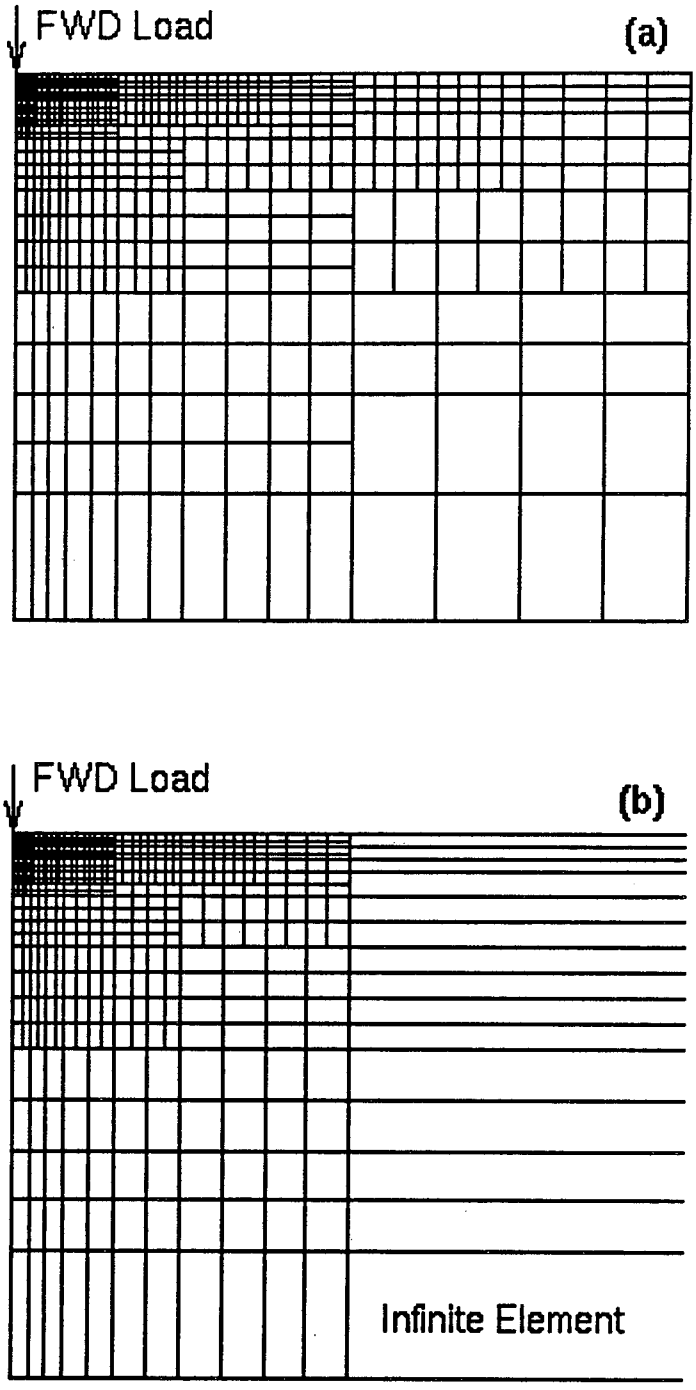

Figure 4.1: Finite and infinite element models of a pavement system; (a) finite elements, (b) infinite elements.

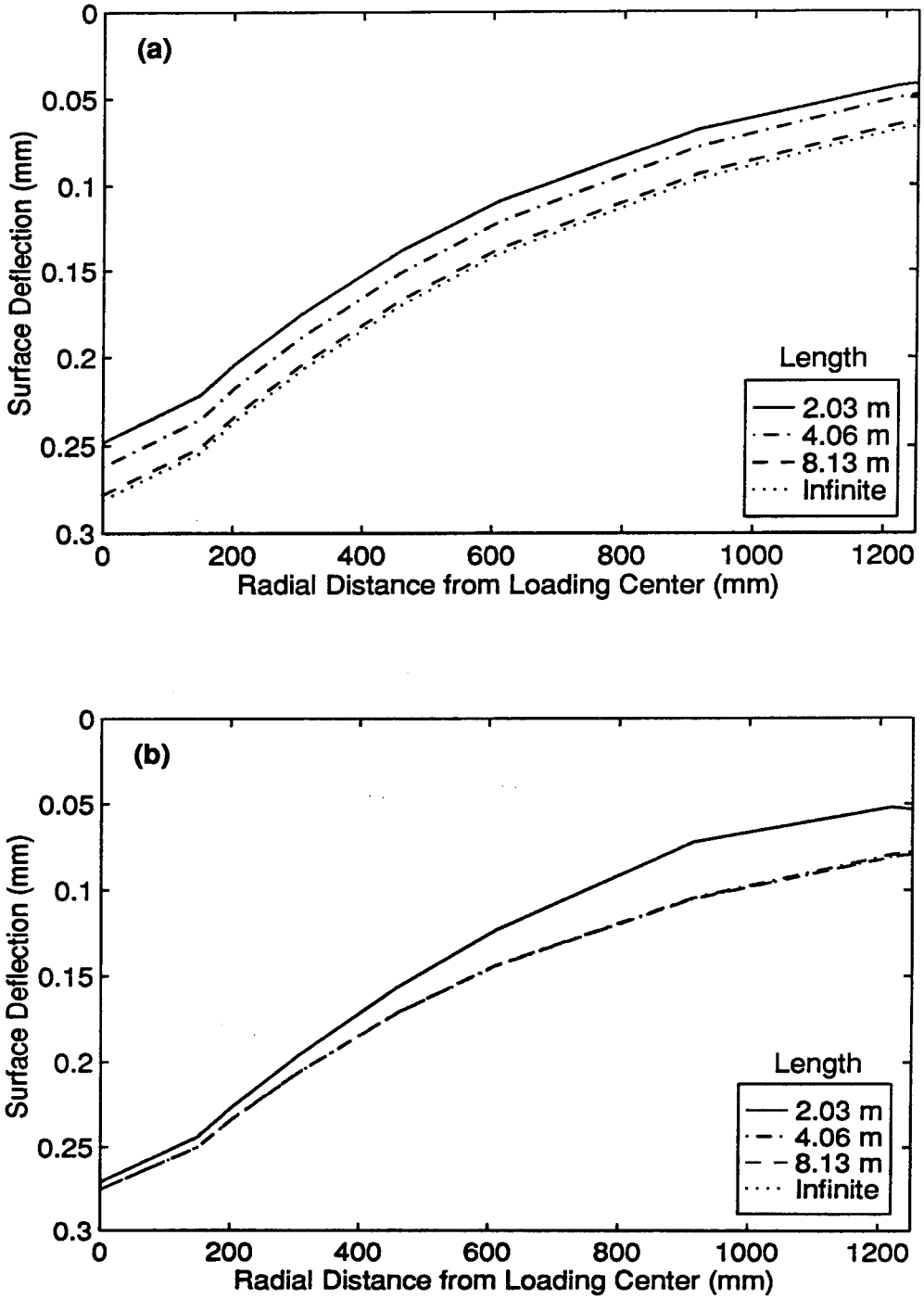

Figure 4.2: Computed peak surface deflections for various pavement length configurations; (a) static analysis, (b) dynamic analysis.

To demonstrate the need to employ dynamic analysis for pavement evaluation, five pavement models were analyzed. These models had the same pavement structure but the subgrade thickness was set at 1.524, 3.048, 6.096, 12.192 m (60, 120, 240, 480 inches) and at infinite depth. The length of the pavement model was infinite and was modeled with infinite elements as described in the previous section. The pavement layer properties are given in Table 4.2. A two-dimensional, axisymmetric element model was employed for the pavement model. A haversine load with 40 kN peak load and duration of 0.03 ms that simulates a typical FWD load (Figure 4.3) was used for dynamic analysis. Both static and dynamic analyses were carried out on these five pavement models.

The computed results are presented in Figure 4.4. It can be seen that surface deflection increases as the subgrade thickness increases when static analysis is employed. On the other hand, when dynamic analysis is employed, the effect of the subgrade thickness to the surface deflections vanishes when the subgrade thickness is greater than (or equal to) 6.096 m (240 in.). It is unlikely, according to the theory of wave propagation, that the zone of influence of a dynamic load will extend to an infinite depth. This result shows the importance of using dynamic analysis to analyze the pavement responses under an FWD load. Therefore, dynamic analysis will be employed throughout this study.

Table 4.2. Layer properties used for the investigation of dynamic analysis.

	AC Layer	Aggregate Base	Subgrade
Thickness (cm)	11.3	30	varies
Modulus (MPa)	5516	345	103
Poisson's Ratio	0.35	0.4	0.45
Density (kg/m^3)	2565	2244	1763
Damping (%)	5	5	5

4.4. 2-D and 3-D Analyses

For intact pavements when the applied load is away from the edges, a 2-D axisymmetric model is proved to yield good approximations [19]. However, when considering distress conditions (e.g., transverse cracking, longitudinal cracking, etc.), 2-D pavement models may not be adequate. FWD load may be reasonably modeled by 2-D axisymmetric elements with uniformly distributed pressure if the test load is away from the pavement edges. However, transverse or longitudinal cracks can not be modeled using 2-D axisymmetric elements since cracks do not occur in a circular shape. Longitudinal cracks may be modeled by plane strain problems. However, FWD load can not be simulated by plane strain elements. A combination of the loading conditions and the geometries of cracks make the use of 3-D analysis for distressed pavements necessary.

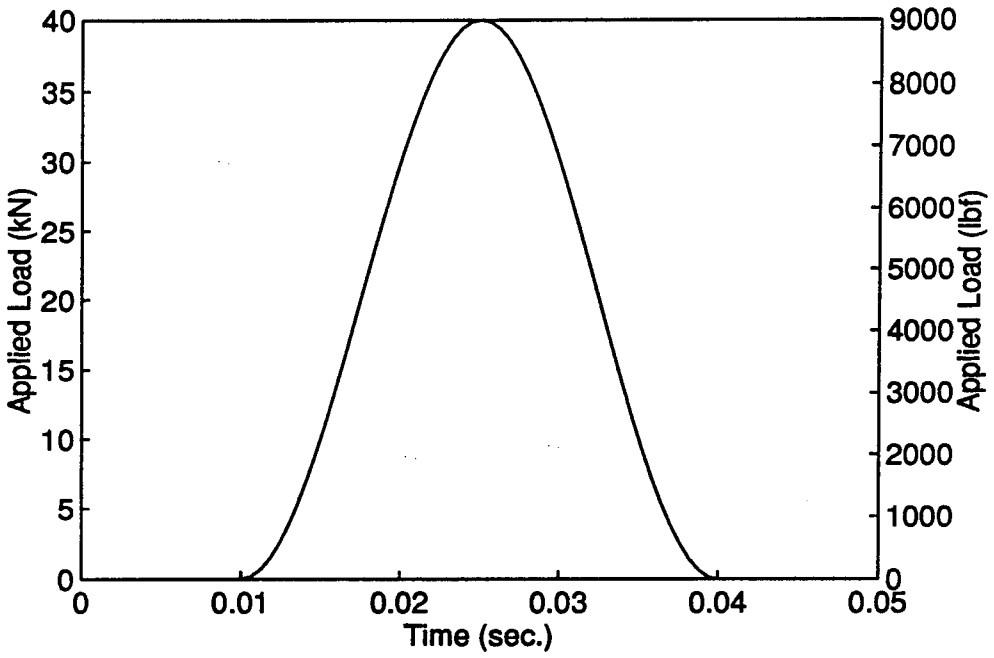

Figure 4.3: Load used for dynamic analysis.

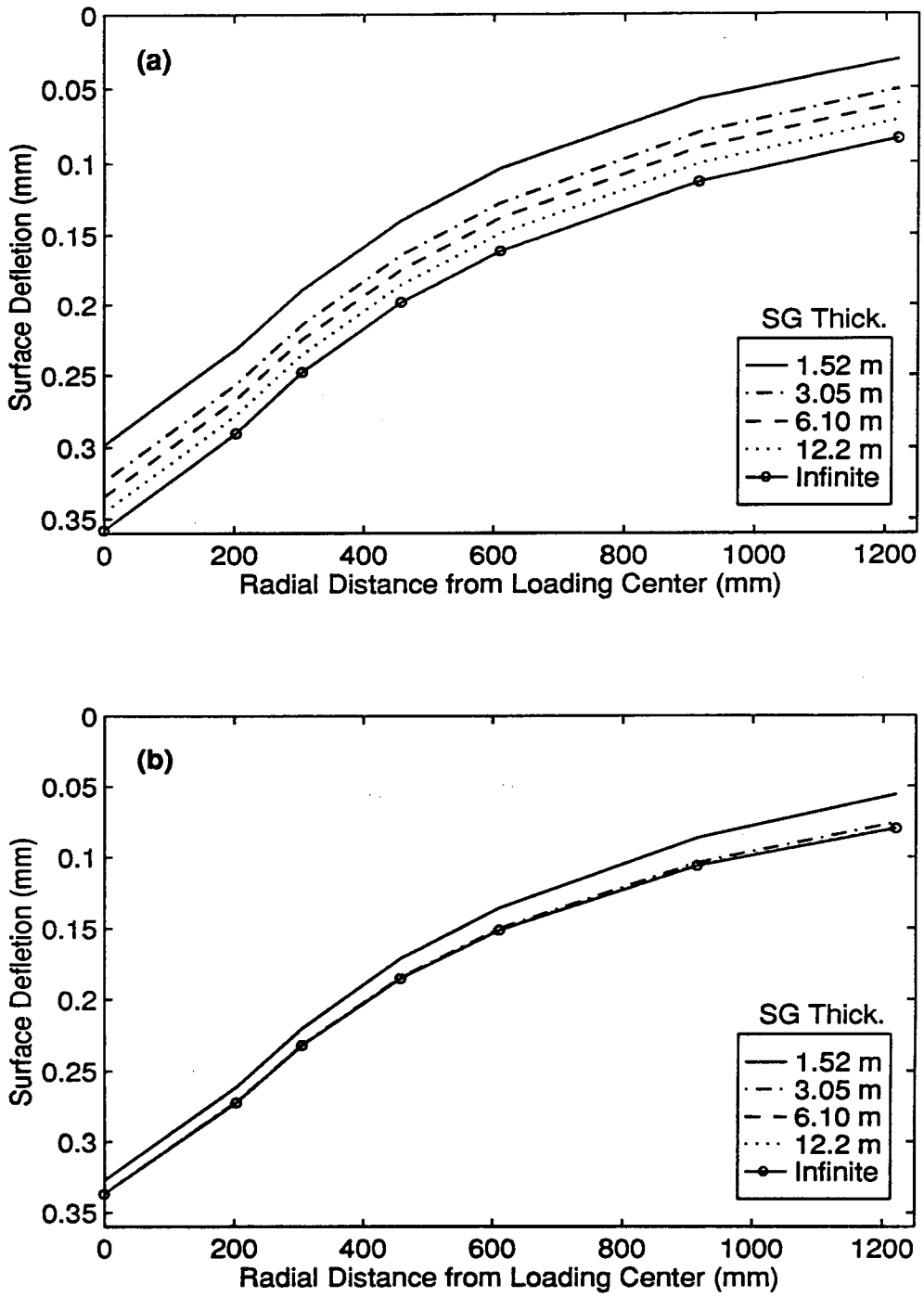

Figure 4.4: Computed peak surface deflections for various subgrade thicknesses; (a) static analysis, (b) dynamic analysis.

To investigate the effects of 2-D and 3-D analysis on surface deflections, a study was performed on a pavement model with intact and cracked conditions. Figure 4.5 presents the pavement model in the form of 2-D and 3-D for this case study. The 3-D finite element mesh is displayed in Figure 4.6. Vertical cracks were placed at 203 mm (8 in.) from the applied load and at every 305 mm (12 in.) thereafter through the AC layer. Surface deflections in three directions of the 3-D model were considered. They are; (a) along the traffic direction, (b) from the load toward the edge, and (c) from the load toward the lane center as depicted in Figure 4.5(b). These are marked with A, B, and C, respectively.

Results are presented in Figure 4.7. As can be seen, surface deflections obtained from intact models are very close for the 2-D model and for those in directions A, B, and C of the 3-D model. This indicates that a pavement system may be analyzed by 2-D axisymmetric models when pavement layers are intact. When cracks are present in the pavement AC layer, not only does the center deflection increase, but the shape of the deflection basin changes (discontinuous deflection basin) as well. This is expected because the stiffness of the AC layer is reduced due to the presence of the discontinuity, thus the surface deflections are increased. However, deflection basins obtained in directions B and C of the 3-D model remain smooth. It must be noted that the discontinuous deflection basins obtained from the cracked models are less likely to occur in actual FWD measurements unless the crack condition in the field is very distinctive and unless deflection sensors are placed across the cracks. In fact, this "idealized" crack model magnifies the discontinuity effect that would occur in the field. Though the magnitudes are different for the 2-D and 3-D cracked models, the characteristics of the deflection basins are similar. Therefore, the 2-D axisymmetric model and the interface elements will be suitable to investigate the effects of discontinuity on deflection basins which is the objective of this study.

4.5. Interface Element

Typical discontinuities in flexible pavements are longitudinal, transverse, and alligator cracks. Cracks are caused by fatigue or load repetitions, by environmental factors, or by interactions of the two. Two element types provided in ABAQUS may be used to simulate crack conditions in a pavement layer. They are gap elements and interface elements. Gap elements may be used to model contact between discrete points. Results are reported for those elements in the form of contact forces between nodes. Interface elements are designed for problems involving contact over parts of an element's surface. The elements are provided with interpolation that is compatible with the various elements in ABAQUS, so that an appropriate choice can be made to match the elements that are used to model the components that may be in contact. The interface element can be either no thickness (surfaces in contact) or can have a thickness equal to the distance between two surfaces of nodes to simulate an initial gap. Normal stress will not be developed until two surfaces are in contact. Whether the two surfaces can slide against each other is governed by the maximum allowable shear stress and friction coefficient.

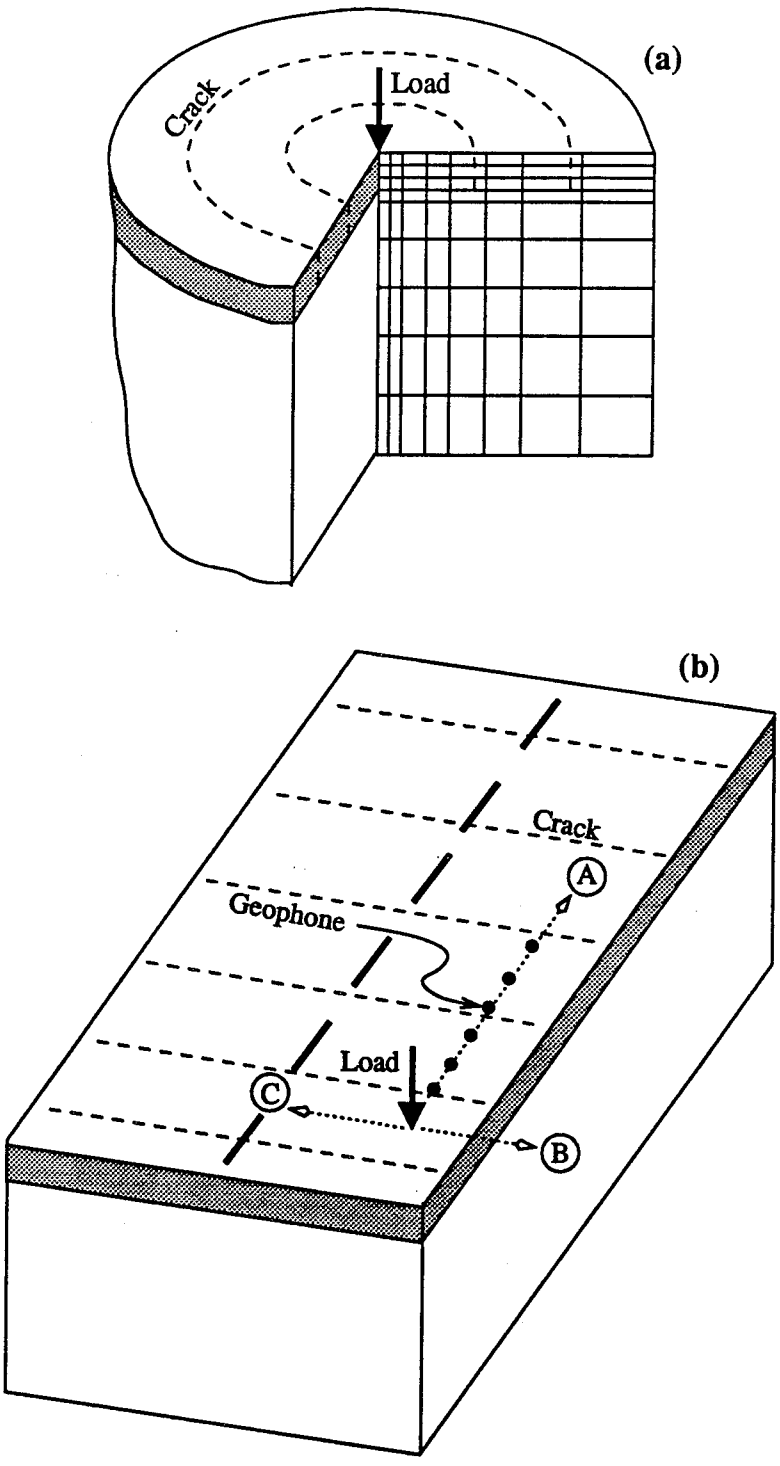

Figure 4.5: Crack modeling of a pavement system; (a) 2-D axisymmetric, (b) 3-D.

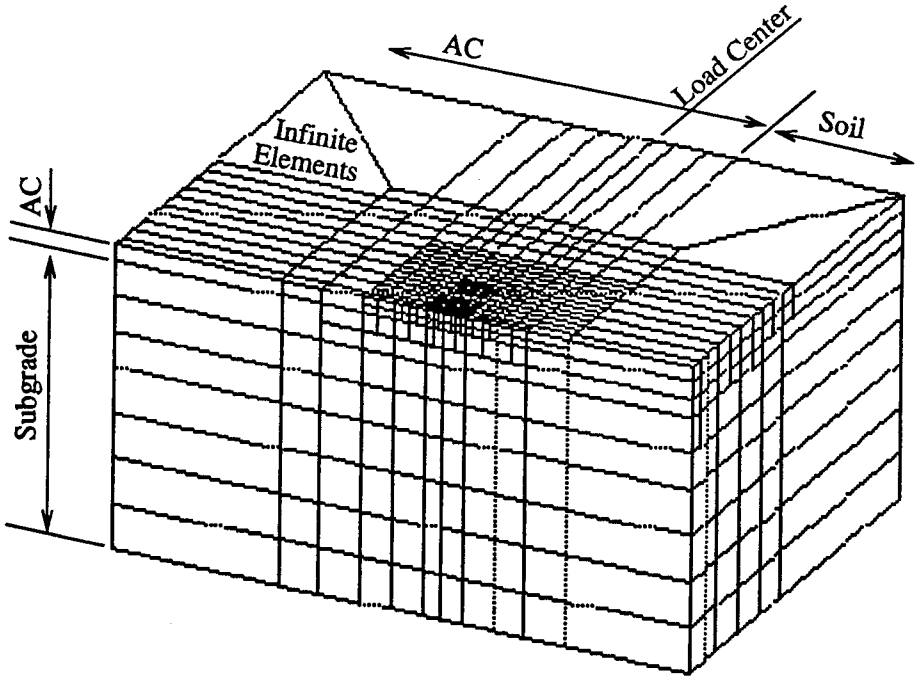

Figure 4.6: A 3-D FEM model of a pavement with transverse cracks.

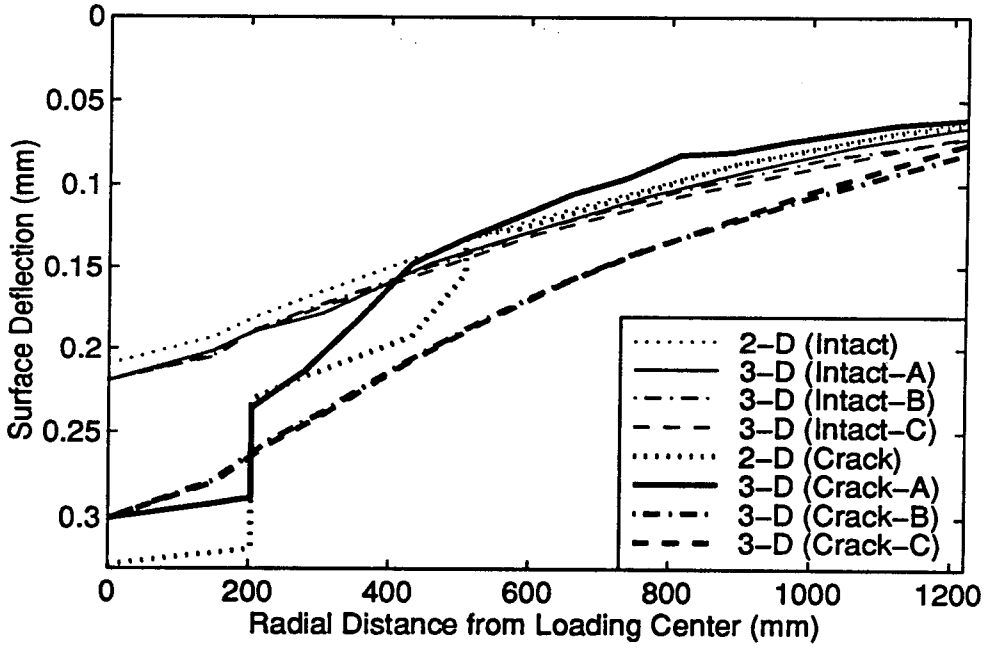

Figure 4.7: Computed surface deflections of 2-D and 3-D pavement models for intact and cracked conditions.

A study was conducted to investigate the effects of initial gap and friction coefficient on surface deflections under FWD load. Interface elements were used to simulate the crack condition in the pavement model. Cracks were placed in the AC layer and were located at the distances of 229, 381, 553, and 686 mm (9, 15, 21, and 27 in.) from the loading center. A two-dimensional, axisymmetric model was employed to analyze the pavement using dynamic analysis. A haversine load with peak magnitude of 40 kN and duration of 30 ms was used to simulate the standard FWD load. The initial crack gap and friction coefficient were varied as described in Figure 4.8. The same pavement model but without cracks was also analyzed for comparison. As can be seen in Figure 4.8, pavements with initial gaps of 0.254 and 1.27 mm (0.01 and 0.05 in.) yield the same deflections. This is because the deformations between the crack surfaces are smaller than 0.254 mm, and thus the gap remains separate throughout the analysis under the standard FWD load. In such cases, the friction coefficient does not play a role in the analysis. On the other hand, when the initial gap is smaller than 0.254 mm, the resulting deflections decrease as the initial gap decreases and the friction coefficient increases. Similar conclusions were also reached by Uddin et al. [4].

It must be noted that the actual crack condition in the field is extremely complicated, especially the fatigue cracking, and can not be described completely. The purpose of using an interface element for "idealized" crack simulation is to introduce discontinuities into the system so that the effects of crack conditions can be studied. Despite the changes in magnitudes of initial gaps, the deflection shapes are similar (Figure 4.8). The deflection basin shapes are very distinctive when compared with the intact ones. An initial gap of 0.254 mm and a friction coefficient of 0.5 for the interface element will be used in this study.

4.6. Material Models

A flexible pavement system usually consists of an asphalt concrete surface layer, an aggregate or asphalt concrete base, stabilized or treated (cement or asphalt) subbase, and subgrade. Thus, materials in a flexible pavement can be categorized into asphalt concrete mixture, granular soils, and cohesive soils.

Asphalt concrete is a viscoelastic particulate composite comprised of aggregate particles (rigid, elastic) and asphalt binder (viscoelastic). Therefore, its current stress is a function of the current strain and strain rate and/or past values of strain rate. Unlike elastic materials, the response of a viscoelastic material under load is a function of time. Asphalt concrete is also known as a thermo-rheological material whose response under load depends upon temperature in addition to the time-dependent behavior. For a non-aging, linear viscoelastic medium, the uniaxial stress and strain relationship can be described by the following convolution integrals:

$$\sigma(t) = \int_0^t E(t-\tau)\frac{d\varepsilon(\tau)}{d\tau}d\tau \qquad (4.1)$$

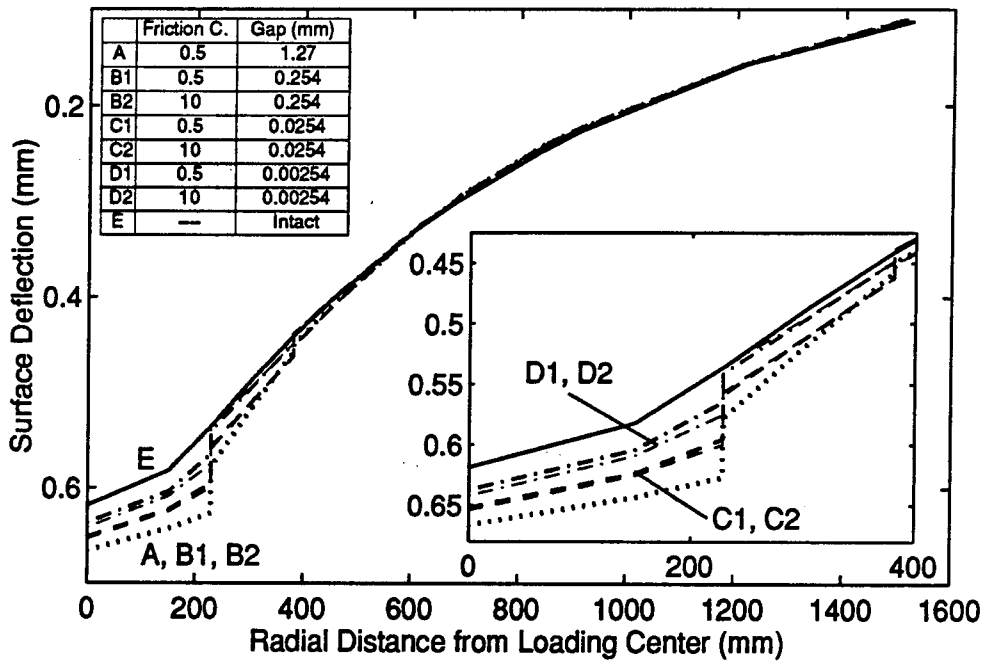

Figure 4.8: Investigation of 2-D interface element for pavement analysis.

$$\varepsilon(t) = \int_0 D(t-\tau)\frac{d\sigma(\tau)}{d\tau}d\tau \qquad (4.2)$$

where $\sigma(t)$ = stress at time t,
$\varepsilon(t)$ = strain at time t,
$D(t)$ = creep compliance as a function of time, t,
$E(t)$ = relaxation modulus as a function of time, t, and
τ= the integration parameter.

Thus, the behavior of a linear viscoelastic material can be characterized by either its creep compliance or relaxation modulus. A case study using the linear viscoelastic material model to investigate the asphalt concrete behaviors under the cyclic load and the FWD load was presented by Lee [13]. This case study showed much agreement between the laboratory measurements and the ABAQUS-calculated responses under cyclic loading tests. Results also revealed that the use of the viscoelastic model can describe the actual flexible pavement responses more closely than those deflections carried out by the linear elastic material model. The temperature effect of a viscoelastic material can also be incorporated using the Williams-Landell-Ferry (WLF) approximations [20]. The study demonstrates that ABAQUS is capable of analyzing the behavior of the asphalt concrete material using the linear viscoelastic constitutive model.

Properties of a soil material are complex and can change dramatically from one location to another. It has been shown that whether a soil material can be assumed to be elastic or not is governed by the shear strains of that soil [21]. Elastic behavior may be reasonably assumed if the shear strain is smaller than 0.005%. A preliminary study from a three-layer pavement system using the elastic material model under a 40 kN FWD load reveals that the maximum shear strain in the base layer is usually within the ranges of elasticity. Therefore, it is reasonable to assume the soils are elastic materials in this study. It is also known that soils are stress-state dependent materials; e.g., sandy or granular soils undergo stress-stiffening while clayey soils undergo stress-softening. Due to the time limitations of this research study, the stress-state dependent behavior will not be studied.

4.7. Summary

Capabilities when using the finite element method to analyze pavement problems were discussed in this chapter. The dynamic analysis procedure is needed to better describe the response of a pavement under a dynamic FWD load. It is also preferable to use an infinite element to model the infinite boundary of a pavement profile. The discontinuity condition in the AC layer can be simulated using the interface element. A 2-D axisymmetric FEM model will be suitable for the objectives in this study. The success of using more realistic material models (e.g., viscoelasticity) in pavement analysis is heavily affected by the accuracy of the parameters characterized from the material being used. It is well known that the material properties of a pavement section can vary significantly from one location to another and are affected by the environmental

conditions, e.g., temperature, moisture, etc. Therefore, the most "accurate" analysis method is not necessarily the most "appropriate" method for the evaluation of in-service pavement conditions. Given the time limitation in this study, it is impossible to utilize these more realistic material models in the analysis. As the majority of pavement design and evaluation methods are based on the elastic model, and the elastic model has been proven to yield reasonable results, it is practical to assume the materials are elastic. Therefore, the linear elastic material model will be employed throughout this study.

5. FWD DEFLECTION DATA BASE AND ANALYSIS OF FIELD FWD DEFLECTION BASINS

5.1. Synthetic Deflections

This study focuses on the interpretation of the deflection data measured by the FWD device. Therefore, finite element models were designed particularly for FWD testing configurations. In North Carolina, a typical FWD test is performed by dropping a 40 kN (9,000 lbf) on top of a circular plate with a radius of 150 mm (5.91 in.) resting on the pavement surface. The loading duration is about 30 ms. The deflection sensors are placed at distances of 0, 203, 305, 457, 610, 914, and 1219 mm (0, 8, 12, 18, 24, 36, and 48 in.) from the loading center (see Figure 5.1).

For this study pavement structures were modeled using two-dimensional, axisymmetric finite elements. This configuration was chosen because it is a reasonable approximation of pavement behavior under FWD load, as well as the fact that it conserves computation time. The subgrade thickness was fixed to be of infinite depth. The horizontal and vertical boundaries were modeled using the infinite element. Both two- and three-layer pavements were considered. In all cases, the dynamic analysis was performed with an elastic material model and a haversine load with a duration of 30 ms and a magnitude of 40 kN.

5.1.1 Intact Pavements

Table 5.1 shows the array of layer thicknesses and material properties used in this study for intact pavements. When analyzing deflections measured by the FWD, difficulty in identifying whether a pavement layer is damaged or not arises because there are no reference values, e.g., deflections obtained from an intact condition. Therefore, surface deflections computed from intact pavements will serve as the basis for the study of the effects of distress conditions on FWD deflections.

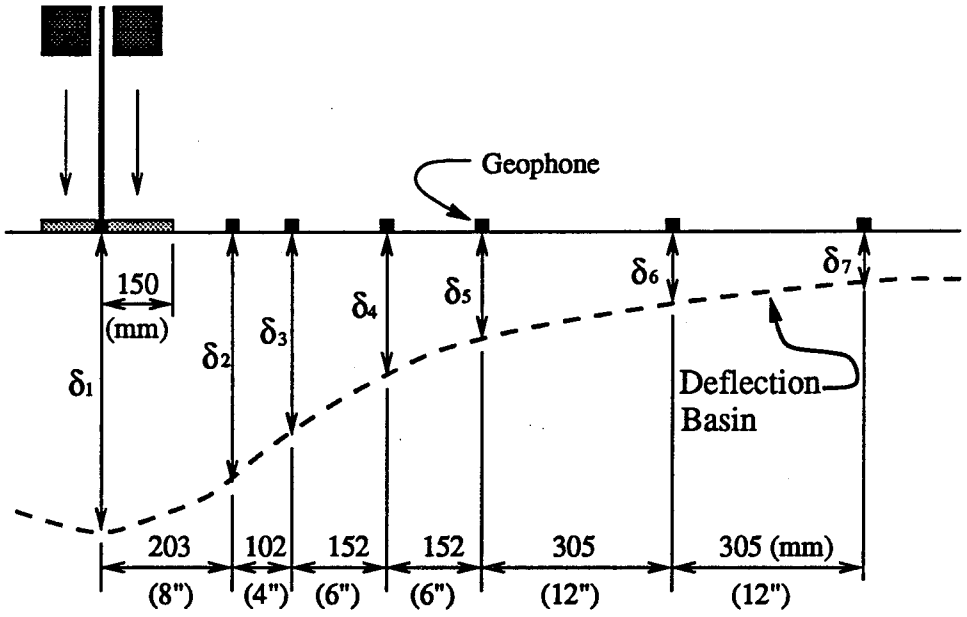

Figure 5.1: FWD testing configuration used in this study.

Table 5.1. Pavement configurations and material properties considered for intact pavements.

		AC Layer	Base Layer	Subgrade
Modulus (MPa)	2-layer	345, 690, 1380, 2760 5520, 11040, 16560	--- ---	34.5, 69,103.5, 138 172.5, 207, 276, 345
	3-layer	690, 1380, 2760, 5520, 11040, 16560	172.5, 345, 517.5 690, 1380	34.5, 69, 103.5 138, 172.5
Thickness (mm)	2-layer	112, 225, 338, 450	---	Infinity
	3-layer	112, 225, 338, 450	150, 300, 450, 600	Infinity
Poisson's Ratio		0.3	0.35	0.45
Density (kg/m^3)		2560	2240	1760
Damping (%)		5	5	5

5.1.2 Distressed Pavements

Discontinuities of distressed pavements were also considered. This was a necessary step since distress conditions usually have great impact on FWD measurements. Figure 5.2 presents the distress conditions modeled in this study. Crack conditions are introduced using interface elements and are placed at every 152 mm starting at a distance of 102 mm from the loading center. Crack-1 represents cracks that are placed at the bottom of the AC layer with one-fourth of the AC layer at the top being intact. Crack-2 represents cracks in the bottom half of the AC layer. As noted previously, actual crack conditions in the field are very complicated and cannot be modeled completely. Nevertheless, introducing these idealized cracks into FEM models will allow us to study how these discontinuities may influence FWD deflections.

Another distress condition to be considered is the stripping which is modeled by reducing the elastic modulus within the designated region in the AC layer. The severities of the stripping conditions are represented as Strip-1, Strip-2, Strip-3, and Strip-4 as depicted in Figure 5.2. Only a few pavement configurations from the intact pavement models were selected for modeling the distressed pavements. The computed deflections will be studied together with the deflections obtained from the intact models for the development of pavement evaluation procedures.

5.2. Field FWD Measurements

Field FWD deflections measured from various pavements were incorporated to verify the findings concluded from the synthetic data. These pavements were selected because their layer information, conditions, and the AC temperatures at the time of the

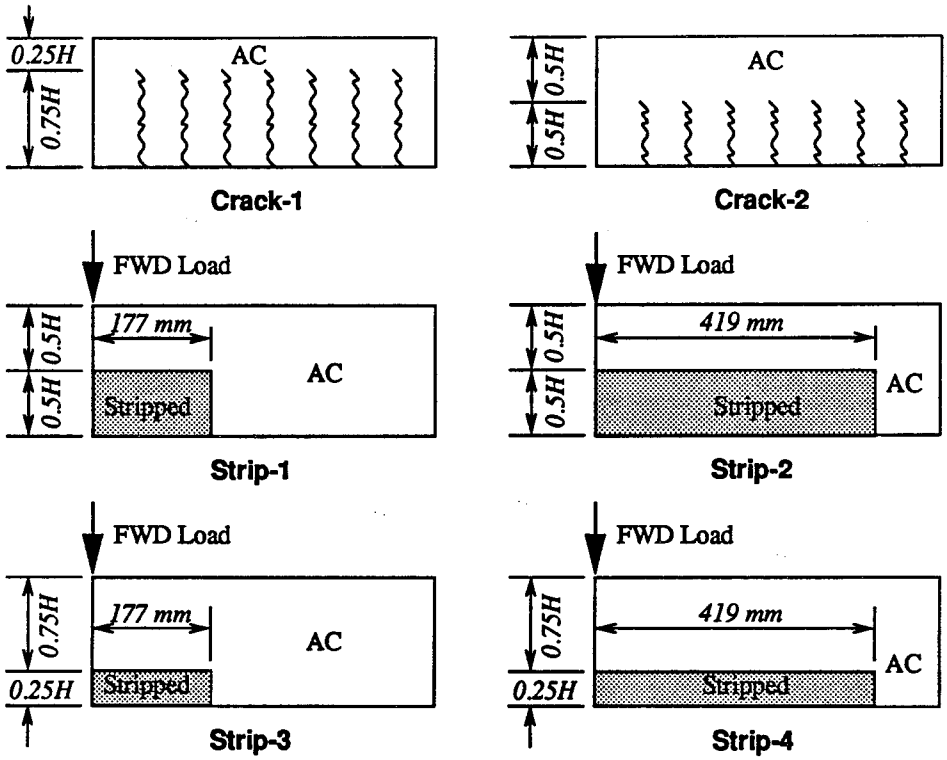

Figure 5.2: Distress conditions considered in this study.

FWD tests were known. Cores were also obtained from some sections to determine the layer thickness and the distress condition in depth. The conditions of these pavements ranged from intact to damaged. Detailed information about these pavements is given in the following sections.

5.2.1 Intact Pavements

FWD data obtained from six pavements that were tested during the previous NCDOT temperature correction projects [22,23], were used in this study. The layer information and their locations are presented in Table 5.2. These sections were evaluated as good or intact pavements at the time of the FWD tests. Thermocouples were installed in the AC layer at different depths to measure the temperature gradient when the FWD test was performed. FWD tests were performed in four different seasons during 1994 and 1995, except for the US 421 section which was tested in 1992 and 1993. On each trip, FWD tests were made at the same four locations every hour during daytime to incorporate temperature variations. The depth to a stiff layer was estimated using the MODULUS program. Deflections from one of the four locations in each section were used in this study.

Table 5.2. Layer information and their locations in the tested pavements.

Highway	US 421	NC 54	US 264	NC 24	US 17	US 74
County	Chatham	Durham	Pitt	Carteret	N.Hanover	Polk
H_{ac}	229 mm	267 mm	114 mm	184 mm	254 mm	178 mm
H_{abc}	---	---	203 mm	---	---	305 mm
Subgrade Type	A-7-6	A-4, A-6	A-2-3, A-3 A-4, A-6	A-3	A-2-4, A-3	Unknown
DRL[a]	2.1 m	3.3 m	1.8 m	2.3 m	5.7 m	6.8 m

[a]Depth to a Stiff Layer (estimated by the MODULUS program)

5.2.2 Damaged Pavements

US Highway 1

A pavement section of US 1 near Vass, North Carolina was selected for the FWD test during this study. This section has experienced various distress conditions, primarily fatigue cracking, and was scheduled for an overlay in October 1996. Six locations were selected for FWD tests at about 91 m (300 ft) intervals, and the distress conditions were identified to be intact, mildly cracked, and severely cracked as presented in Table 5.3. Two trips were made to conduct the FWD test, one in October 1996 before the overlay and the other in November 1996 after the overlay. PK nails, a metal detector, and posts were utilized to relocate the FWD testing locations after the overlay. A total of five passes of FWD test were conducted in each trip with an hour interval between passes to gain the temperature variations. The pavement surface temperatures as well as the

weather conditions were recorded while the FWD test was performed. Cores were retrieved from the tested spots immediately after the FWD test was complete, and the dynamic corn penetrometer (DCP) test was performed to determine the strengths of the base layer and the subgrade. It was found that location 4 had the lowest CBR value while location 6 had the highest, according to the results of the DCP tests conducted during each trip.

Table 5.3. Layer information and distress conditions of the pavement section of US 1 near Vass, North Carolina.

Location	1	2	3	4	5	6
Overlay Thick.	25 mm	38 mm	25 mm	32 mm	38 mm	25 mm
AC Thick.	114 mm	127 mm	121 mm	108 mm	114 mm	114 mm
Surface Condition	Intact	Intact	Mild Fatigue	Severe Fatigue	Mild Figure	Severe Fatigue
CABC[a] Thick.	89 mm	0 mm	76 mm	76 mm	76 mm	51 mm
ABC Thick.	152 mm	292 mm	184 mm	152 mm	152 mm	127 mm
DRL[b]	1.01 m	1.21 m	0.88 m	1.02 m	0.87 m	1.14 m

[a]Cemented Aggregate Base Course
[b]Depth to a Stiff Layer (estimated by the MODULUS program)

US Highway 421

A series of test sections with different designs was constructed on US 421 Bypass near Siler City, North Carolina in 1989 and 1990 [24]. The test road consisted of 12 different types of pavement sections with different materials and thicknesses but all with an asphalt concrete surface course. For each type, two sections were considered for replication in each direction of traffic, and thus a total of 48 sections were constructed. The twelve different types of sections are regrouped into the following 6 categories by base and subgrade type: (1) asphalt concrete over an aggregate base course (ABC), (2) asphalt concrete over an aggregate base course with stabilized subgrade (ABC on Stab. SG), (3) full-depth asphalt concrete (HB), (4) full-depth asphalt concrete with stabilized subgrade (HB on Stab. SG), (5) asphalt concrete over cement-treated base (CTB), and (6) asphalt concrete over cement-treated base with stabilized subgrade (CTB on Stab. SG). Of a total of 48 sections, only data from 12 selected sections (including at least one representative section from each of the six categories) are presented and discussed in this paper. The layer thicknesses and the subgrade condition for each test section considered are presented in Table 5.4. A series of FWD tests was performed on these test sections in August 1993 with a 40 kN test load with seven sensors located at 0, 203, 305, 457, 610, 914, and 1219 mm from the loading center. In order to know the type and degree of distresses at each test station, cores of bound layers were retrieved from the field at the time of FWD tests. Varying degrees of different types of distresses were observed. Some core logs cited later are presented in Tables 5.5 to 5.12.

Table 5.4. Layer information of the pavement sections of US 421 near Siler City, North Carolina.

Sections Considered	HDS (mm)	HDB (mm)	HB (mm)	ABC (mm)	CTB (mm)	Subgrade Stabilization
1,23 (ABC)	50.8 (2")	38.1 (1.5")	-	304.8 (12")	-	No
3,16 (ABC)	50.8 (2")	76.2 (3")	-	203.2 (8")	-	No
17 (ABC on tab. SG)	50.8 (2")	38.1 (1.5")	-	203.2 (8")	-	Lime
7,20 (HB)	50.8 (2")	38.1 (1.5")	139.7 (5.5")	-	-	No
9,22 (HB)	50.8 (2")	76.2 (3")	101.6 (4")	-	-	No
13 (HB on Stab. SG)	50.8 (2")	38.1 (1.5")	101.6 (4")	-	-	Lime
21 (CTB)	50.8 (2")	76.2 (3")	-	-	139.7 (5.5")	No
19 (CTB on Stab. SG*)	50.8 (2")	-	-	-	190 (7.5")	Lime

* CTB on Stab. SG section has additional 76.2 (3") to 88.9 mm (3.5") of AC overlay.

Nomenclature:

HDS = asphalt surface course
HDB = asphalt binder course
HB = asphalt-stabilized base course
ABC = aggregate base course
CTB = cement-treated base course
SG = subgrade

Table 5.5. Core information of pavement section 1 of US Highway 421 (H_{abc}=305mm).

Loc. #	H_{ac} (mm)	DRL[a] (m)	AC Core Condition
0	89	1.26	Fatigue throughout depth, failed
1	76	1.57	Longitudinal cracking (L.C.) through depth
2	89	1.95	Good condition
3	89	1.81	Low Severity, L.C. on surface of core
4	89	1.27	L.C. through depth
5	114	1.57	Core broken up
6	---	1.31	Non-recoverable
7	89	1.47	Stripping in binder layer
8	102	1.19	Good condition
9	102	2.20	Good condition

[a]Depth to a Stiff Layer (estimated by the MODULUS program)

Table 5.6. Core information of pavement section 23 of US Highway 421 (H_{abc}=305mm).

Loc. #	H_{ac} (mm)	DRL[a] (m)	AC Core Condition
0	---	2.26	Coring through patch, could not remove
1	86	1.85	On fatigue
2	89	1.91	On fatigue, core broken
3	114	1.85	Patch (surface), cracked through original AC
4	127	1.59	Patch (surface), same as previous
5	89	1.89	Cracked through core
6	---	1.36	Full depth patch, could not recover core
7	89	1.81	On fatigue
8	89	1.63	Fatigue cracking through core
9	89	1.45	Cracked through, separated

[a]Depth to a Stiff Layer (estimated by the MODULUS program)

Table 5.7. Core information of pavement section 3 of US Highway 421 (H_{abc}=203mm).

Loc. #	H_{ac} (mm)	DRL[a] (m)	AC Core Condition
0	114	1.39	Slight strip. In binder (51 mm overlay)
1	114	1.16	Stripping in binder (38 mm overlay)
2	89	1.40	Good condition (64 mm overlay)
3	114	1.89	Good condition (38 mm overlay)
4	114	1.55	Stripping in binder (25 mm overlay)
5	127	1.39	Good condition (25 mm overlay)
6	108	1.31	Good condition (38 mm overlay)
7	114	1.26	--- (38 mm overlay)
8	114	1.08	Severe stripping in overlay (102 mm overlay)
9	114	1.69	Severe stripping in binder (89 mm overlay)

[a]Depth to a Stiff Layer (estimated by the MODULUS program)

Table 5.8. Core information of pavement section 16 of US Highway 421 (H_{abc}=203mm).

Loc. #	H_{ac} (mm)	DRL[a] (m)	AC Core Condition
0	140	1.09	Slight stripping in surface
1	152	1.00	Good condition
2	127	2.20	Longitudinal cracks through core
3	127	0.86	Slight strip. in binder
4	127	0.94	Good condition
5	127	1.38	Slight stripping in both layers
6	279	0.69	Severe stripping at bottom (full depth patch)
7	127	1.15	Longitudinal cracks through core
8	108	0.71	Good condition
9	114	0.93	Good condition

[a]Depth to a Stiff Layer (estimated by the MODULUS program)

Table 5.9. Core information of pavement section 7 of US Highway 421.

Loc. #	H_{ac} (mm)	DRL[a] (m)	AC Core Condition
0	216	1.17	Slight stripping in base layer
1	197	0.80	Good condition
2	210	1.48	Good condition
3	203	0.61	Severe stripping in base
4	203	1.46	Good condition
5	203	1.27	Stripping in base
6	203	1.71	Slight stripping in top base layer
7	203	1.30	Stripping at bottom of base
8	203	1.17	Slight stripping in all layers
9	229	1.09	Good condition

[a]Depth to a Stiff Layer (estimated by the MODULUS program)

Table 5.10. Core information of pavement section 20 of US Highway 421.

Loc. #	H_{ac} (mm)	DRL[a] (m)	AC Core Condition
0	216	1.60	Intact
1	216	1.41	Intact
2	216	1.39	Stripping at bottom of HB
3	241	2.23	---
4	222	1.72	Stripping at bottom of HB
5	229	2.00	Slight stripping in HB layer
6	229	1.45	Slight stripping at bottom of HB
7	210	1.22	Slight stripping
8	187	1.41	Stripping at each layer surface and in HB

[a]Depth to a Stiff Layer (estimated by the MODULUS program)

Table 5.11. Core information of pavement section 9 of US Highway 421.

Loc. #	H_{ac} (mm)	DRL[a] (m)	AC Core Condition
0	216	2.13	Stripping at bottom of base layer
1	216	1.55	Cracked through core
2	216	1.54	Cracked halfway through core
3	216	0.84	Stripping in base layer
4	203	0.96	Stripping in base layer
5	216	1.80	Slight Stripping in base layer
6	229	1.28	Full depth patch, stripping all layers
7	190	0.94	Stripping in all layers
8	216	0.86	Severe stripping in base and binder
9	216	2.21	Slight stripping at bottom of base layer

[a]Depth to a Stiff Layer (estimated by the MODULUS program)

Table 5.12. Core information of pavement section 22 of US Highway 421.

Loc. #	H_{ac} (mm)	DRL[a] (m)	AC Core Condition
0	235	1.13	HB severely stripped
1	229	1.06	Stripping at bottom of HB and binder
2	222	1.68	Some stripping at bottom of HB
3	222	2.33	Stripping at bottom of HB
4	235	2.84	Stripping at bottom of HB
5	229	2.33	Less stripping
6	229	1.06	Stripping
7	232	0.95	Stripping in HB, mild at binder
8	229	0.96	Stripping in HB
9	235	0.89	HB severely stripped

[a]Depth to a Stiff Layer (estimated by the MODULUS program)

5.3. Analysis of Field FWD Deflection Basins

5.3.1 Variation and Characteristics of Deflection Basins from Different Pavement Types

In order to observe the station-to-station variation of deflection basins along the project and their characteristics for different pavement types, basins are plotted at each test station within each of the six typical pavement sections as shown in Figures 5.3(a) through (f). There are ten equally-spaced (30.5 m) stations within the 305 meter-long stretch of each section. For an easier identification of basin shapes and characteristics, a complete, symmetric deflection basin was generated by adding a mirror image on the negative radial axis. Smoothing of curves between data points was applied to simulate the actual basins more naturally. All the deflections were temperature-corrected using the phenomenological method described in Appendix C.

Overall, a significant station-to-station variation was observed for most cases. The section with an aggregate base course without stabilized subgrade shows the highest variability, and the section with a cement-treated base with stabilized subgrade shows the least variability among them. In general, the subgrade stabilization significantly reduces the variability.

In order to view the station-to-station variation of deflection basins more clearly, the center deflections (D_0) and the AREA are plotted in Figures 5.4(a) and (b), respectively, for each station within each of the six representative sections as identified in Figures 5.3(a) to (f). The center deflection is known to be an indicator of the overall compliance (or reciprocal of the overall stiffness) of the pavement section and was used by many earlier engineers as a primary structural index for the pavement [25,26]. In Figure 5.4(a), it is seen that, in general, D_0's from ABC are greater than those from HB which, in turn, are greater than those from CTB, roughly in reverse order of overall stiffness of the pavement section. Also observable in Figure 5.4(a) is the fact that the sections without stabilized subgrade yield higher D_0's than the corresponding sections with stabilized subgrade, indicating that the sections with stabilized subgrade possess higher overall stiffness. This difference due to subgrade stabilization is most noticeable in the ABC section probably due to the lower stiffness of this section.

The AREA is known as an indicator of the spreadability of the load by the upper layer or, in other words, the relative stiffness of the upper layer to that of the subgrade. In Figure 5.4(b), it is seen that, in general, AREA's for either HB or CTB are greater than those for ABC, because HB and CTB sections provide stiffer upper layers than ABC section. Also noticeable is that the sections without stabilized subgrade yield higher AI's than the corresponding sections with stabilized subgrade, which can be expected because higher AREA's are associated with higher stiffnesses of the upper layers relative to the subgrade.

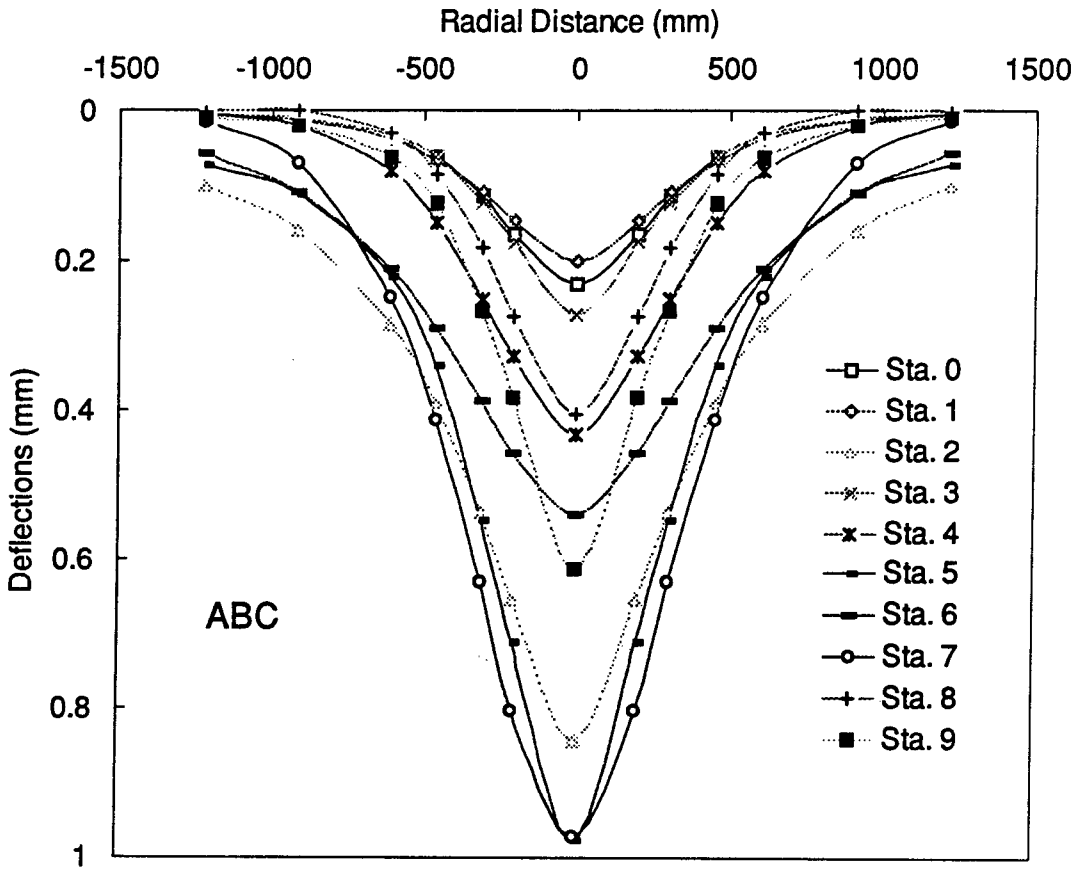

Figure 5.3: Sample station-to-station variation of FWD deflection basin along the project for different flexible pavement constructions. (a) With aggregate base (Section 16).

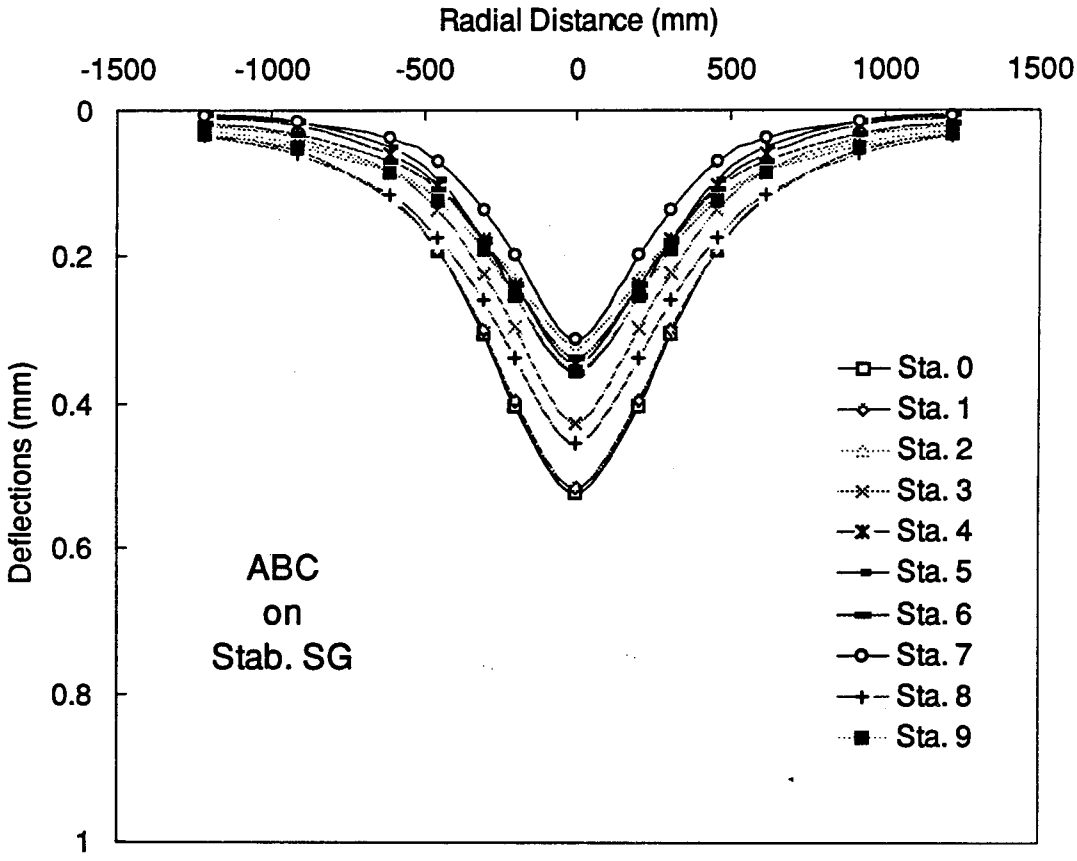

Figure 5.3: (Continued). (b) With aggregate base on lime-stabilized subgrade (Section 17).

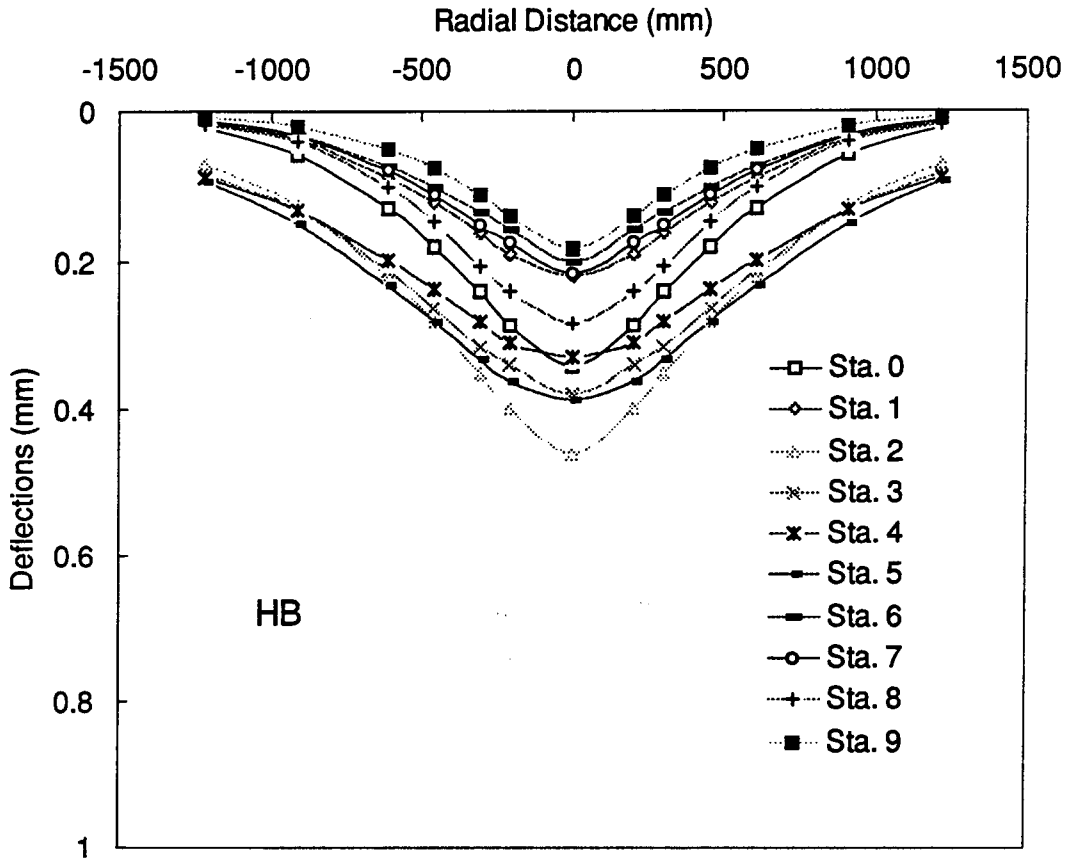

Figure 5.3: (Continued). (c) With asphalt-treated base (Section 22).

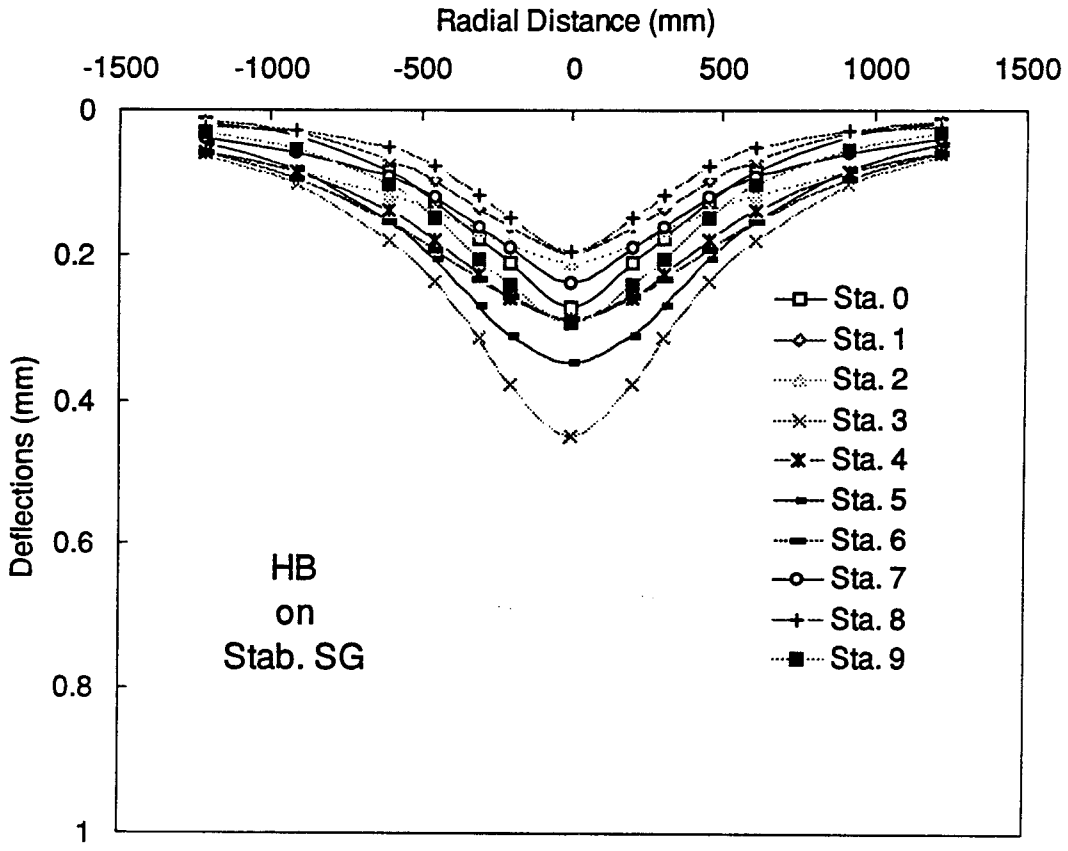

Figure 5.3: (Continued). (d) With asphalt-treated base on lime-stabilized subgrade (Section 13).

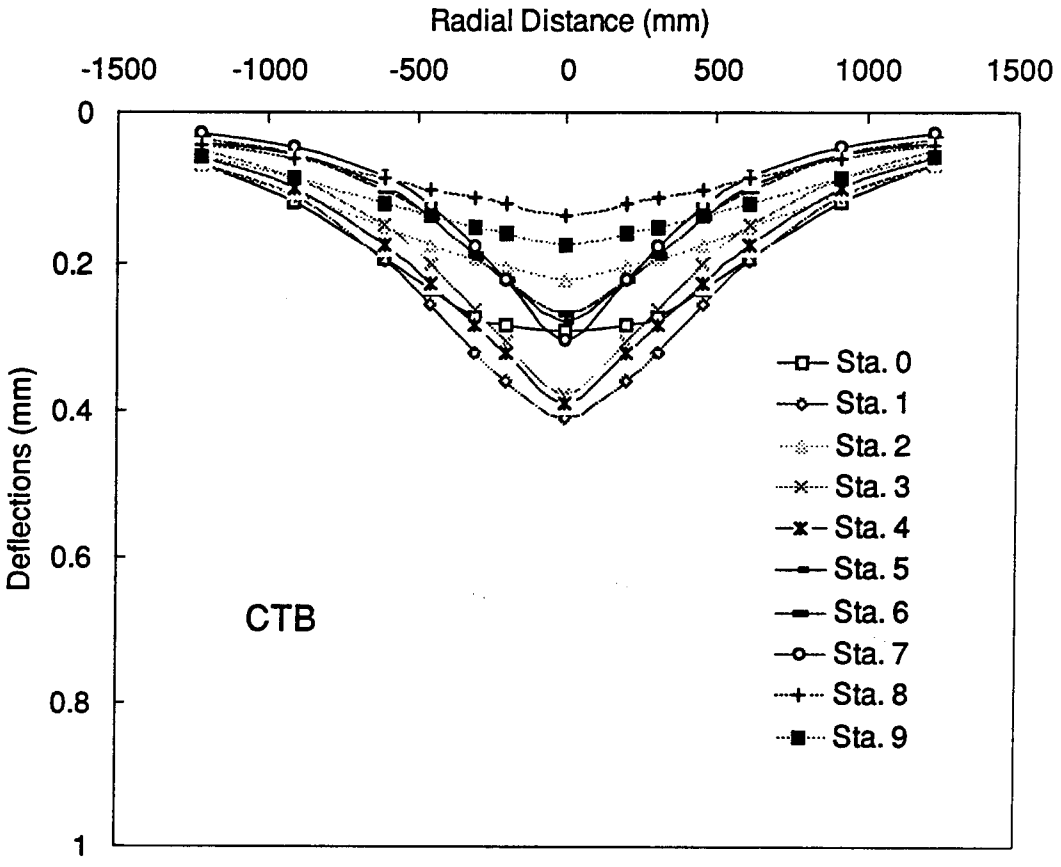

Figure 5.3: (Continued). (e) With cement-treated base (Section 21).

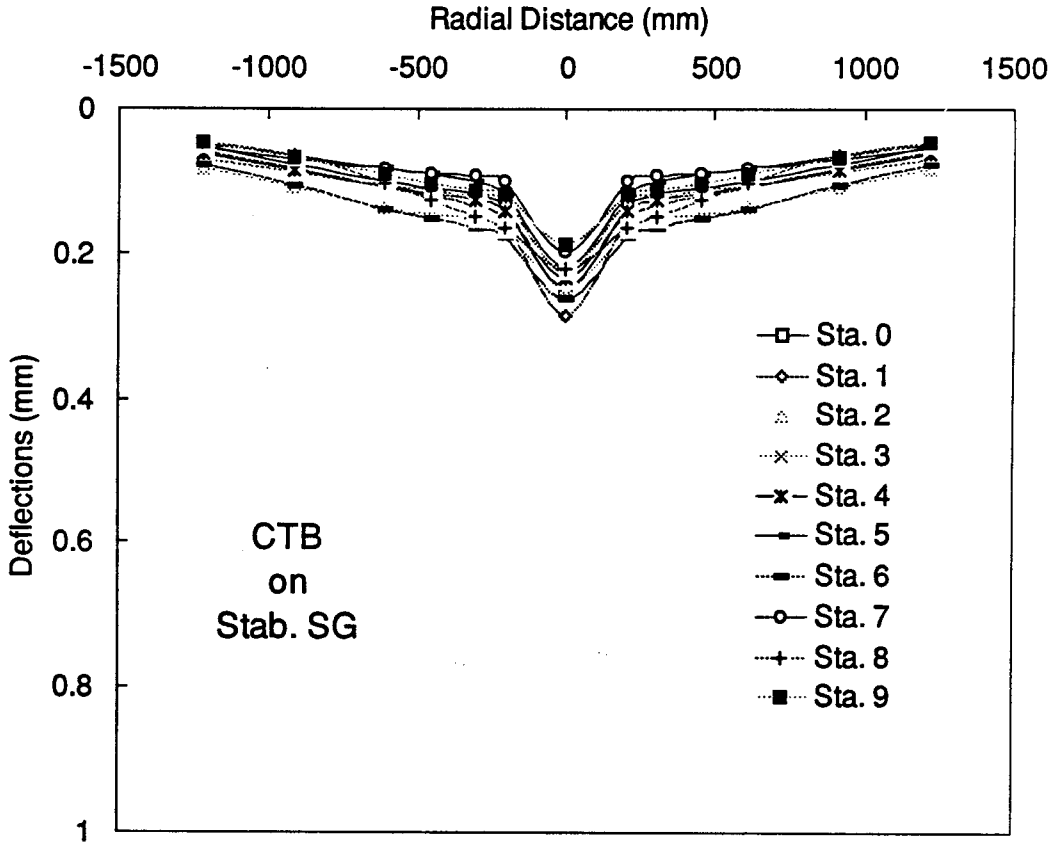

Figure 5.3: (Continued). (f) With cement-treated base on lime-stabilized subgrade (Section 19).

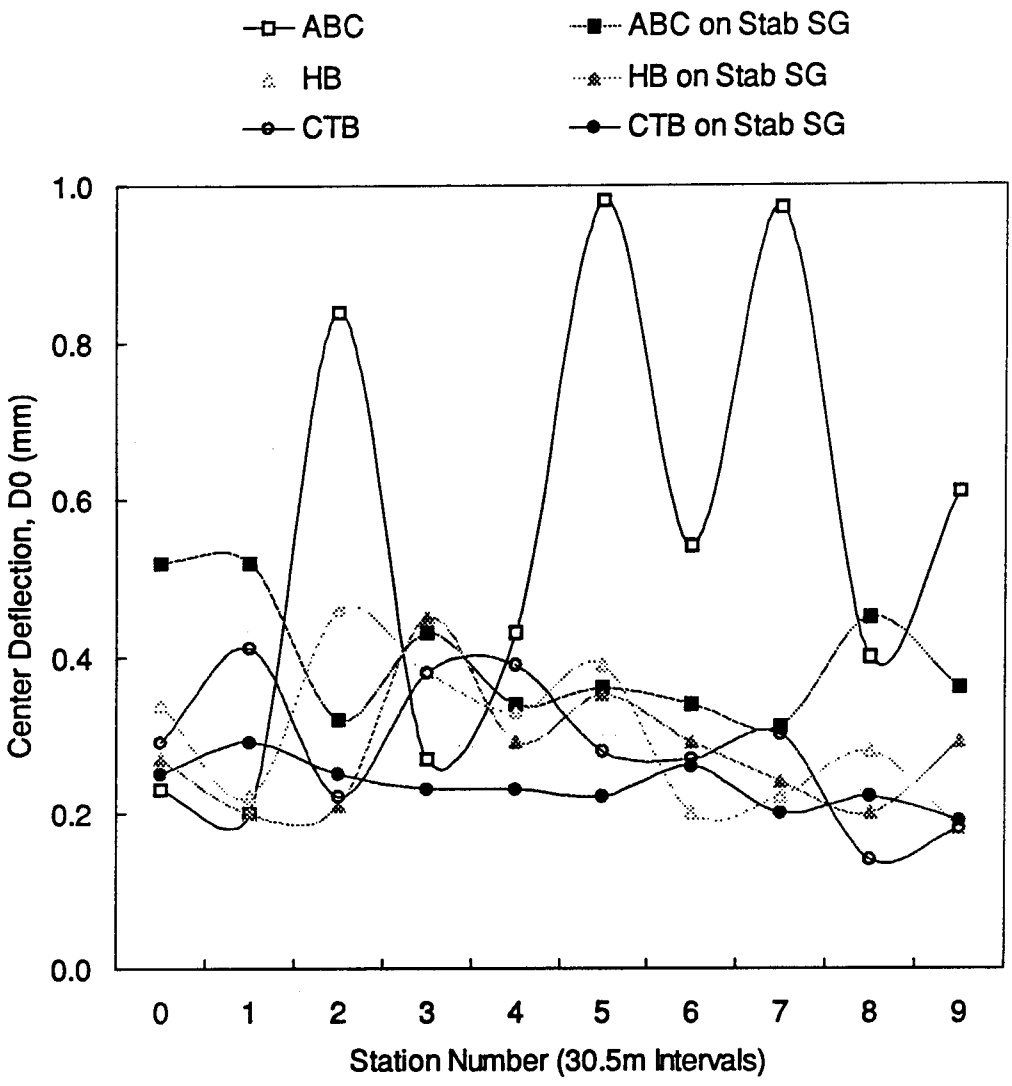

Figure 5.4: Variation of FWD center deflection (D_0) and basin Area Index (AI) in the longitudinal project direction for the six pavement sections considered. (a) Center deflection.

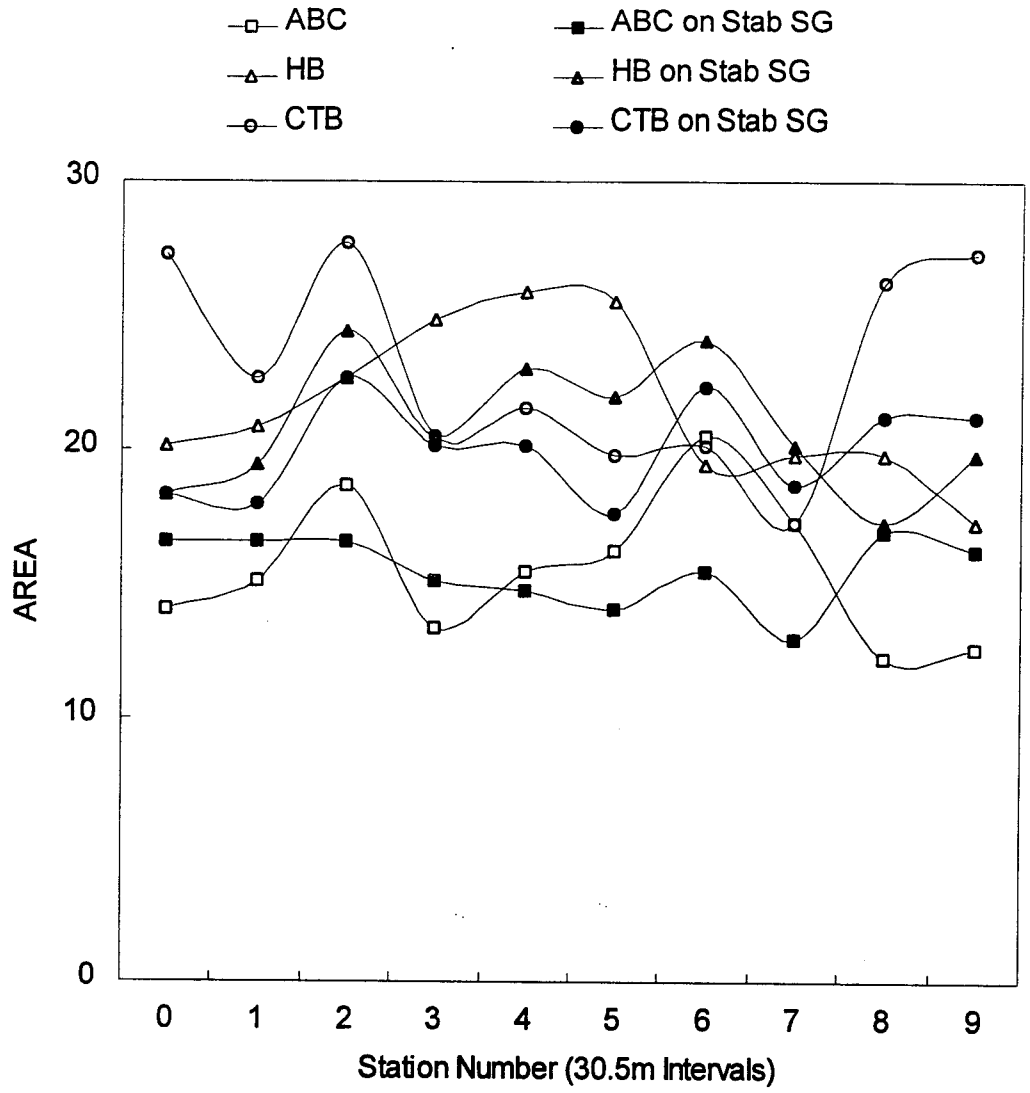

Figure 5.4. (Continued). (b) Area Index, defined as $\frac{6(\delta_0 + 2\delta_1 + 2\delta_2 + \delta_3)}{\delta_0}$

Based on a comparison of the sample core logs and the corresponding deflection basins, one may easily see that assessing the pavement conditions solely based on the core logs is not always successful. We assume here that the FWD deflections represent the actual pavement responses and thus the pavement's structural conditions. For example, the center deflection at station 9 of section 16 (ABC) is fairly large and the AREA is low, suggesting a weak upper layer; however the log description does not indicate any distresses in the core. Also, at station 5 of section 16, the basin indicates a large center deflection and medium-to-low AREA, indicating a very weak section; the log merely indicates *slight* stripping in the surface and binder course. In these cases, the weakness of the upper layers could be originated from other mixture deficiencies (e.g., low density or high asphalt content) which cannot be detected by visual observation of cores.

There exist many variables other than distresses that affect deflection responses but are not recorded in core logs. The core logs usually do not contain any information on the unbound layers and subgrade, and the FWD deflections are sensitively influenced by the properties of the unbound layers and subgrade. Therefore, it is often difficult to judge the accuracy and effectiveness of the core logs simply based on their comparison with the FWD responses.

Figure 5.5 shows the quantified results of a surface visual condition survey performed on each pavement section during the time of FWD tests. Section ABC has the most fatigue cracking, and the most severe longitudinal cracking was observed in section HB; these are more or less consistent with the overall deflection responses shown in Figures 5.3(a) and (c), for ABC and HB, respectively. However, it is difficult to find a definitive correlation between the condition indices (Figure 5.5) and the deflection basin parameters (Figures 5.4(a) or (b)). Comparing the core logs and the condition indices also indicates that it is not easy to estimate the subsurface condition from the surface condition survey; for example, no particular indication of the presence of fatigue cracking was made in the core logs for ABC section, while the surface condition survey indicates substantial fatigue cracking. According to Figure 5.5, the magnitude of rutting is more or less constant in all sections considered, which is difficult to deduce from the inspection of the deflection basins. No condition survey data was available for the section CTB on stabilized SG because the sections have been rehabilitated.

5.3.2 Sample Deflection Responses for Different Distress Types

Now we shall examine the basin characteristics in relation to pavement distresses. We attempted to find a correlation between distress types and basin characteristics by comparing the available core logs and the corresponding FWD deflection basins. Generally, it was difficult to extract any definitive correlation because of the enormous variability of the basins even within a given category of pavement and distress type. For instance, within a particular section with *longitudinal cracks*, the basins normally vary significantly in magnitude and shape, and establishing any meaningful correlation

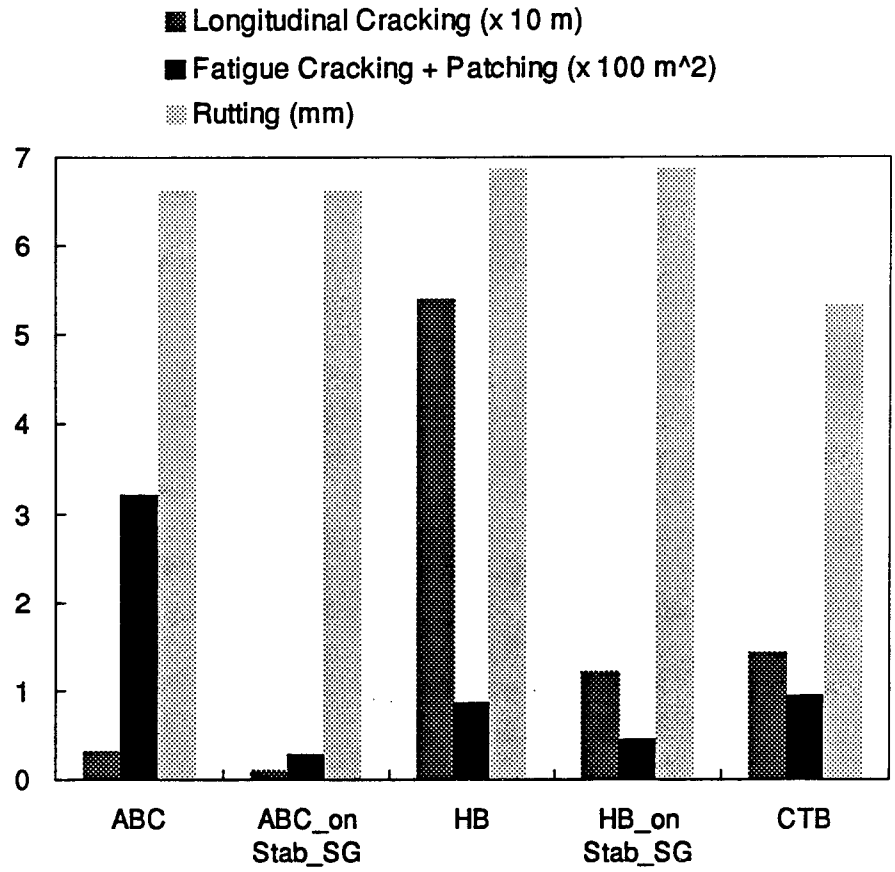

Figure 5.5: Data from surface visual condition survey for each section (when 18k ESAL = 631,064).

between the basin characteristics and the longitudinal cracks for that particular pavement type was not easy.

However, despite the difficulty associated with variability, we were able to find some trends that may give a useful clue to interpreting deflection basins with respect to structural conditions (including distresses). We examined the deflection data from all 24 north-bound sections with known distress conditions (based on the core logs) and known pavement designs. First, we classified the data according to the six pavement types (i.e., four sections per pavement type). Then, primary distresses were identified from the core logs and the corresponding deflection basins were examined. Among the distresses considered were longitudinal cracking, fatigue cracking (or simply, cracking), stripping, and broken CTB.

The *representative* deflection basins for different distress conditions for each of the six pavement types are presented in Figures 5.6(a) through (f). No quantitative statistical analysis was used in selecting the representative basins because it was difficult to quantify the descriptions in the core logs and the basin characteristics. Also, without realistic engineering judgment, such a nominal analysis may lead one to an erroneous conclusion. Representative deflection basins were selected by first categorizing deflection basins with respect to pavement type and distress type and then carefully sorting out the common trends between deflection basins from intact and distressed pavements.

For section ABC, the longitudinal and fatigue cracking in the AC layer resulted in narrow basins with large center deflections, while the stripping in the binder layer yielded a rather broad basin with a uniform increase in all seven deflections. No particular distresses were found in ABC on Stab. SG section. For section HB, when cracks ran through the full-depth the resulting basin was narrow with a large center deflection, and when full-depth stripping was present the basin was roughly in between the intact and cracked cases both in size and shape. Similarly, for section HB on Stab. SG, full-depth cracks yielded a deep and narrow basin. For section CTB, when the CTB layer was broken all seven deflections significantly increased compared to those of the intact section. Stripping again induced an overall increase of deflections. Finally, for section CTB on Stab. SG, when the CTB layer was broken a large increase of the center deflection was observed. This characteristic shape was also observed in most of the basins shown in Figure 5.3(f). Stripping in the binder course also resulted in a basin with large deflections in the central portion of the basin, although the change in deflection basin slope is much more gradual in the stripping case.

Overall, a cracked (either longitudinal or fatigue) pavement yielded a deep and narrow basin compared to the intact one. Apparently, the load spreadability of the upper layers significantly drops due to the presence of cracks in these layers. On the other hand, stripping resulted in an overall downward shift of the basin (i.e., overall increase in all deflections), which suggests a substantial stiffness reduction of the pavement section as a whole. Significant jumps of central deflections were observed within the section with a broken CTB layer on the stabilized subgrade. It appears that the reinforcement of the

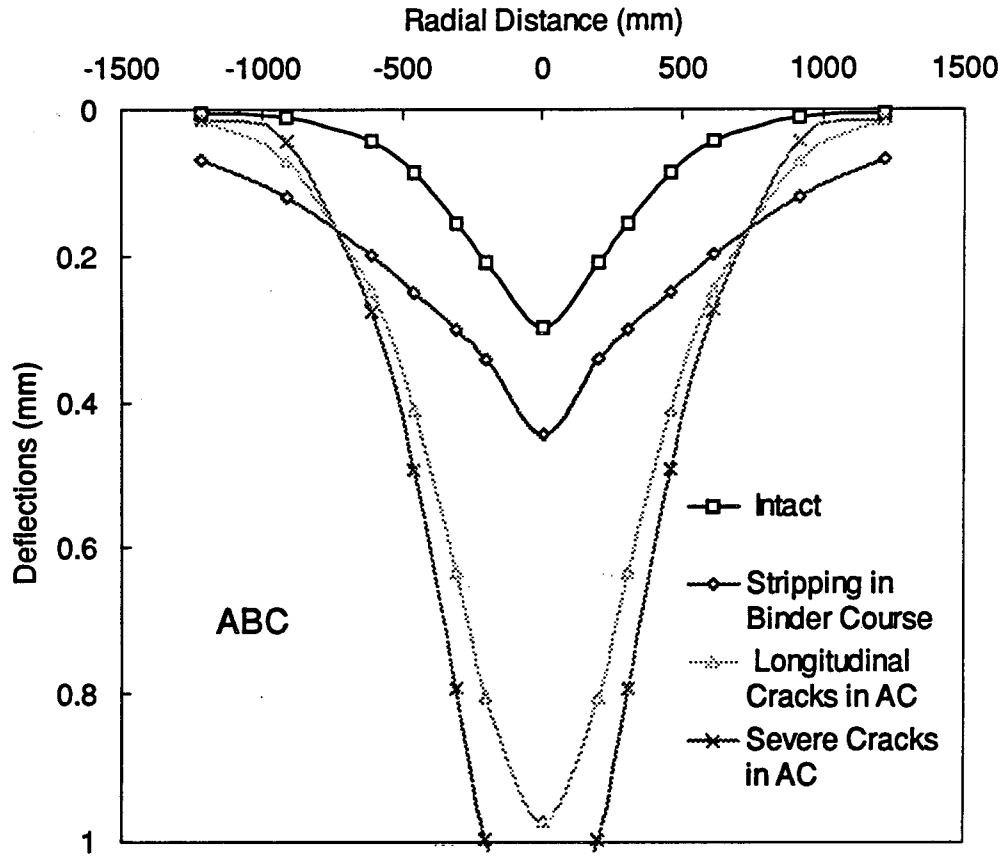

Figure 5.6: Typical FWD deflection basins for different flexible pavement constructions with different distresses. (a) With aggregate base (Section 16).

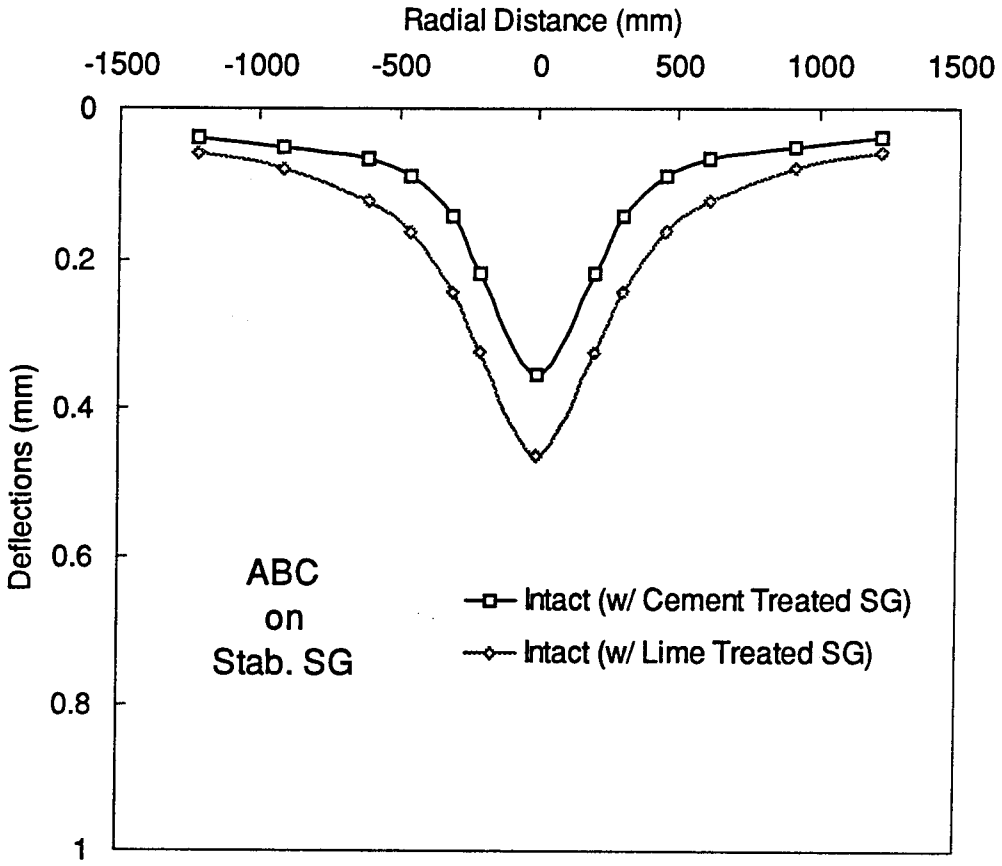

Figure 5.6: (Continued). (b) With aggregate base on lime-stabilized subgrade (Section 17).

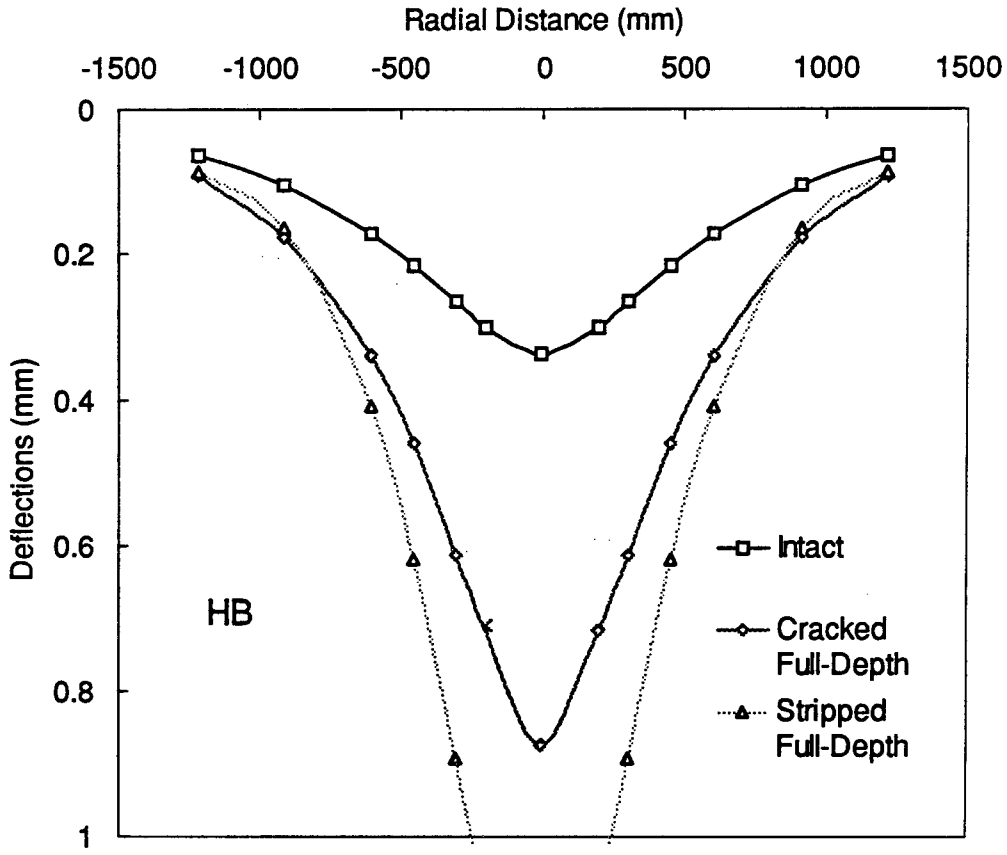

Figure 5.6: (Continued). (c) With asphalt-treated base (Section 22).

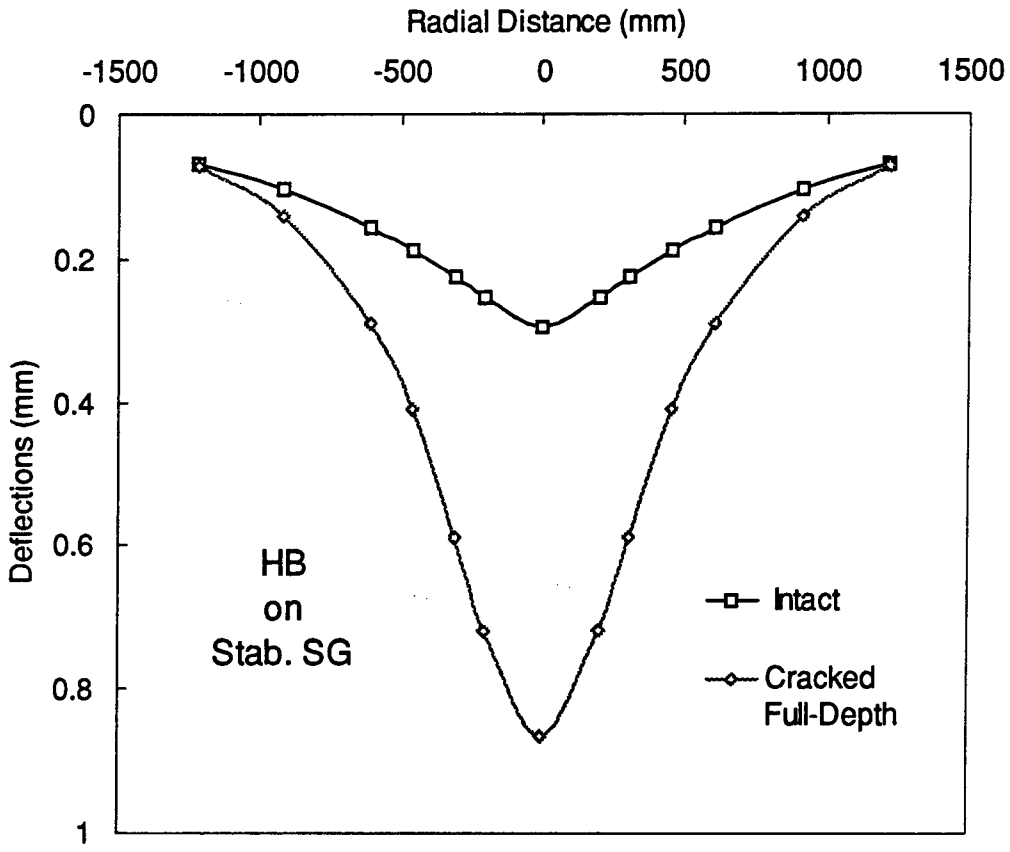

Figure 5.6: (Continued). (d) With asphalt-treated base on lime-stabilized subgrade (Section 13).

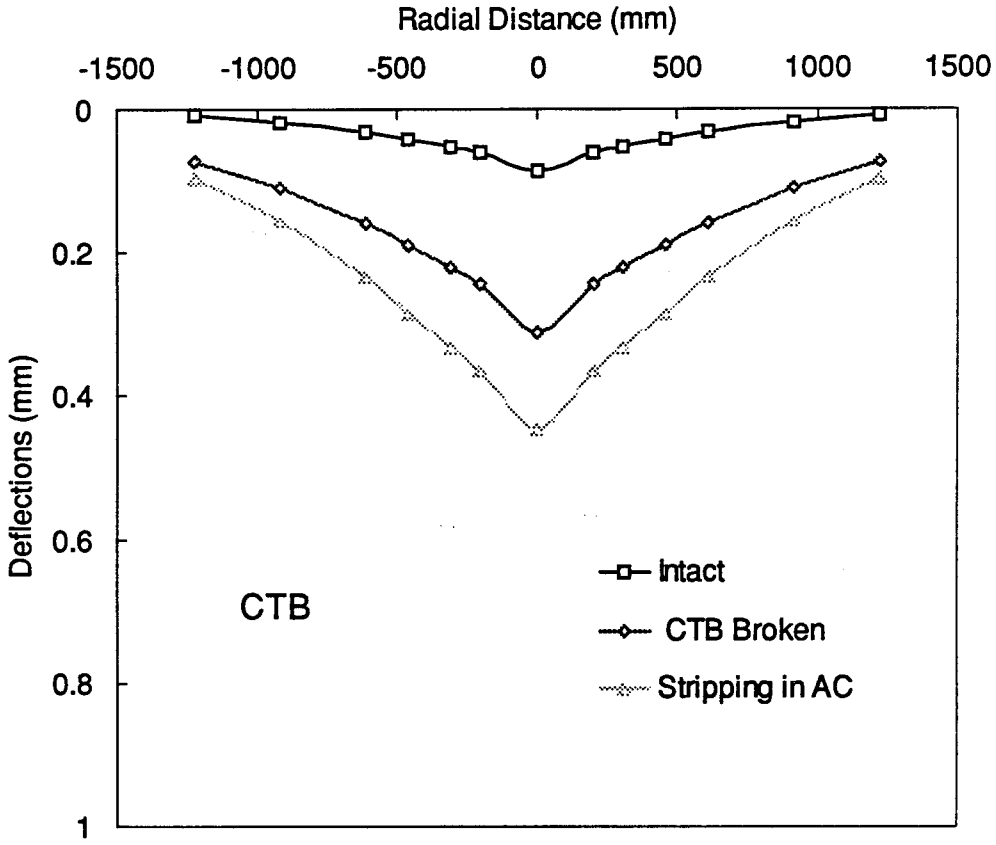

Figure 5.6: (Continued). (e) With cement-treated base (Section 21).

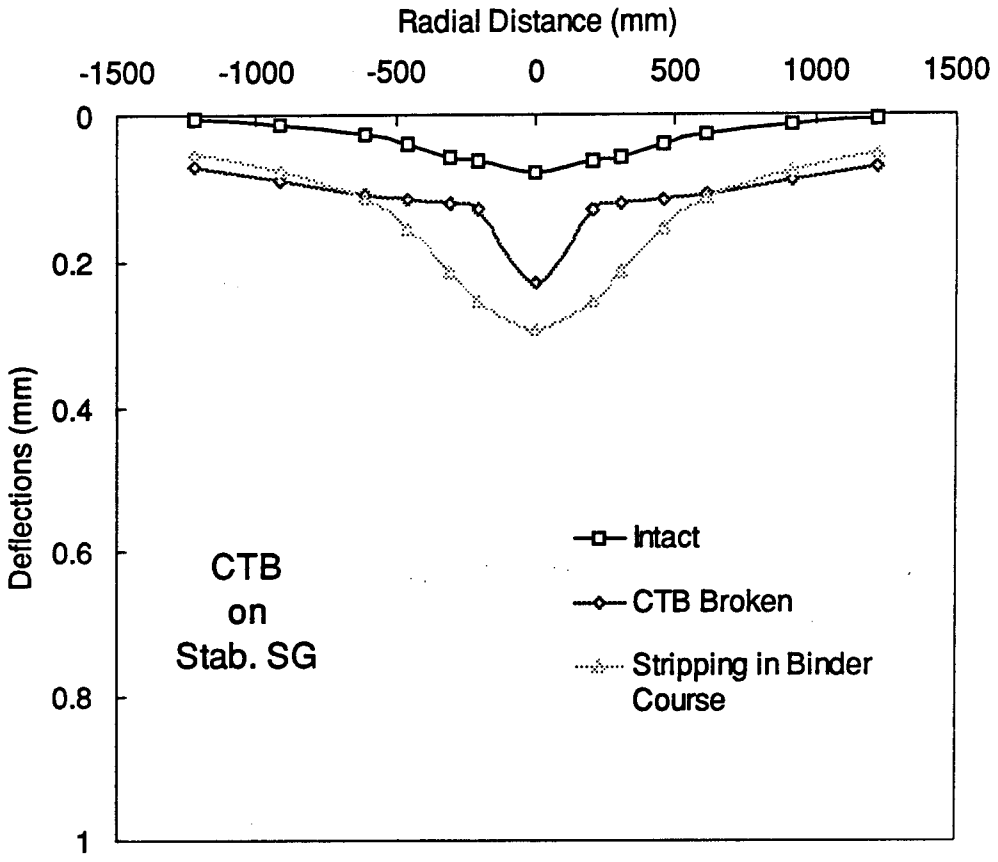

Figure 5.6: (Continued). (f) With cement-treated base on lime-stabilized subgrade (Section 19).

stabilized subgrade prevents the spread of the effects of the weakened CTB layer in the outer radial direction.

5.3.3 Summary of Findings

Through an observation of the sample field FWD deflection responses from different types of AC-surfaced pavements with different distresses, it was found that the station-to-station variation of deflection responses along the project is significant, in general. Therefore, laying out a maintenance or rehabilitation strategy based on FWD deflection responses from a limited number of arbitrarily-chosen test stations may lead to a grossly erroneous conclusion. Deflection data should be collected at locations spaced at sufficiently close intervals, and an appropriate statistical analysis or realistic engineering judgment should be made in selecting an *averaged* or *representative* response for each project section.

It was pointed out that discrepancies can often be found among visual surface condition survey records, core logs, and deflection measurements. The visual condition survey gives *overall* condition of the pavement section under evaluation, but the subsurface information cannot be accurately addressed. Coring and deflection testing would allow engineers to assess the condition of subsurface layers, but the *spatial* variation of these data could lead engineers to erroneous conclusions on the pavement condition unless the data are appropriately processed. Considering an expensive, time-consuming procedure of taking the in-situ cores and inspecting them, more closely-spaced FWD testing is a more practical solution for dealing with the spatial variation of these methods. In addition, FWD deflections are believed to represent the *structural* condition of the pavement more accurately and consistently as long as all possible systematic or operational errors are excluded. To take full advantage of the strengths FWD has, a more accurate interpretation procedure of FWD deflections for layer condition assessment is needed. Finally, it is concluded that the information from all three methods needs to be carefully combined together in order to develop the most suitable rehabilitation strategy.

The correlation study between some common pavement distresses and the deflection basin characteristics indicates that the cracked pavements generally result in deep and narrow basins while the stripped pavements yield broad, globally down-shifted basins. However, these trends are based on limited observations and need to be substantiated by a more extensive study.

6. RESULTS AND DISCUSSIONS

6.1. Deflection Analysis

The most commonly used parameter for FWD deflection analysis is the center deflection (D_0), or the maximum deflection. However, this parameter is only an indicator

of the pavement strength as a whole and is subject to significant changes by environmental and layer conditions. It is very difficult to estimate the strength of each layer by using the center deflection alone. Using the concept of load spreadability, the subgrade strength is best estimated by the outer-most sensor reading. This method, however, is not reliable because the ability of each layer to spread the load is a function of layer stiffness, distress condition, and thickness. Furthermore, it is very difficult to determine where best to place the last sensor to capture the deflection that is caused by the subgrade only.

Many attempts have been made to relate the surface deflections to the pavement structural capacity since the 1950s and have resulted in the development of a number of deflection basin parameters. These parameters were derived either from the magnitude of the measured deflections or the shape of the deflection basin. Table 6.1 shows some typical deflection basin parameters as adapted from a summary by Horak [27]. It appears that deflection basin parameters are practical and useful, as well as being good indicators of the condition of existing pavements.

6.2. Base Damage Index and Shape Factor F2

In this study, relationships among deflection basin parameters, layer moduli, and layer thicknesses were investigated. Although good relationships may be obtained based on one variable at a time, no definite trend that can apply to all cases exists. Since no single deflection basin parameter can be used to fully represent the pavement condition, combinations of deflection basin parameters were investigated.

It was discovered that the relationship between Base Damage Index (*BDI*) and Shape Factor *F*2 is uniquely defined for each value of E_{sg} (Figure 6.1) and is independent of upper layers' moduli and thicknesses. This observation was made for cases with (3-layer system) and without an aggregate base layer (2-layer system). When the base layer thickness is greater than 450 mm, the base layer thickness begins to affect these characteristic curves. Because typical (aggregate) base layer thicknesses used in North Carolina are generally less than 450 mm, only deflections obtained from pavement structures with base layer thickness less than 450 mm were considered in this study.

The *BDI* and *F*2 are defined as:

$$BDI = \delta_1 - \delta_2 \tag{6.1}$$

$$F2 = \frac{\delta_1 - \delta_3}{\delta_2} \tag{6.2}$$

where *BDI* = base damage index,
*F*2 = shape factor,
δ_1 = deflection at distance 305 mm (12 in.) from FWD load center,
δ_2 = deflection at distance 610 mm (24 in.) from FWD load center, and
δ_3 = deflection at distance 914 mm (36 in.) from FWD load center.

Table 6.1. Deflection Basin Parameters.

Deflection Parameter	Formula	Measuring Device	Reference
Area	$A = \frac{6\,(\delta_0+2\delta_{12}+2\delta_{24}+\delta_{36})}{\delta_0}$	FWD	Hoffman 1981 [28]
Base Curvature Index	$BCI = \delta_{60} - \delta_{48}$ or $BCI = \delta_{24} - \delta_{36}$	Dynaflect FWD	Peterson 1972 [29]
Base Damage Index	$BDI = \delta_{12} - \delta_{24}$	RR & FWD	
Bending Index	$BI = \delta_0 / a$	BB	Hveem 1954 [25]
Deflection Ratio	$DR = \delta_r / \delta_0$	FWD	Claessen 1976[30]
Load Spreadability Index	$LSI = (\delta_5 / \delta_3) \times F$	FWD	Wimsatt 1995 [31]
Maximum Deflection	δ_0	BB Dynaflect	Shrivner 1968 [26]
Radius of Curvature	$R = \frac{r^{2\,*}}{[2\,\delta_0\,(\delta_0 / \delta_r - 1)]}$	CM & BB	Dehlen 1962 [32]
Radius of Influence	$RI = x / \delta_0$	BB	Ford 1962 [33]
Shape Factors	$F_1 = (\delta_0 - \delta_{24}) / \delta_{12}$ $F_2 = (\delta_{12} - \delta_{36}) / \delta_{24}$	FWD	Hoffman 1981 [28]
Slope of Deflection	$SD = \tan^{-1} [(\delta_0 - \delta_r) / r]$	BB	Kung 1967 [34]
Spreadability	$S = \frac{25\,(\delta_0+\delta_{12}+\delta_{24}+\delta_{36})}{\delta_0}$	Dynaflect RR FWD	Vaswani 1971 [35]
Structural Strength Index	$SSI = A_X / (X_{min} \times E_{min})$	FWD	Jung 1992 [2]
Structural Integrity Index	$SII = A_X / (X_S \times E_m)$	FWD	Jung 1992 [2]
Surface Curvature Index	$SCI = \delta_0 - \delta_{12}$	BB RR Dynaflect FWD	Shrivner 1968 [26]
Tangent Slope	$TS = (\delta_0 - d_x) / x$	FWD	Stock 1984 [36]

δ_r	Surface Deflection	BB	Benkelman Beam
r	Distance from the Load (inch)	RR	Road Rater
a	1/4 of Deflection Basin Length	FWD	Falling Weight Deflectometer
x	Distance from Point of Maximum Deflection to Tangent Point	CM	Curvaturemeter
		*	r = 127mm
d	Deflection at the Tangent Point		
F	Minimum of δ_2 / δ_1 , δ_3 / δ_2 , ... , or δ_7 / δ_6		
Ax	Area under the surface modulus profile to Xs or to the min. value (E_{min}) at $X=X_{min}$		
E_m	Estimated subgrade modulus		
X_S	Radial distance from the test load		

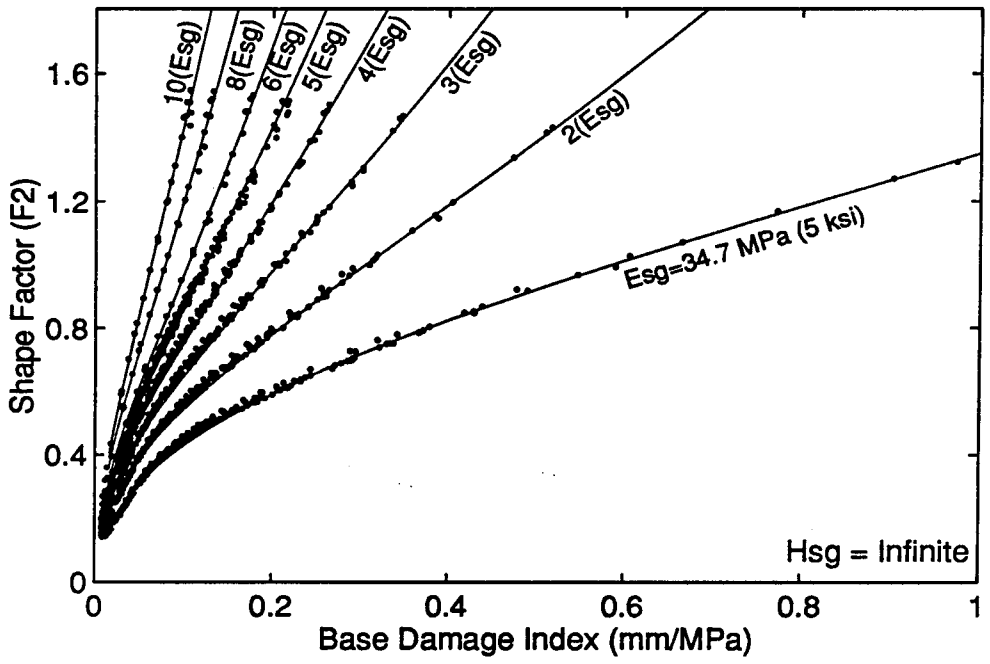

Figure 6.1: Relationships among BDI, $F2$, and E_{sg} established from synthetic deflections.

The *BDI-F2* relationship may be described using the following best-fit equation:

$$F2 = k_1(BDI)^{\frac{1}{2}} + k_2\cosh(BDI) + k_3\sinh(BDI) + k_4(BDI)^{\frac{1}{3}} \quad (6.3)$$

where k_1, k_2, k_3, and k_4 are functions of E_{sg} values and their values are presented in Table 6.2.

Table 6.2. Regression constants for relationships of *BDI*, *F2*, and E_{sg}.

E_{sg} (Mpa)	k_1	k_2	k_3	k_4
34.7	-0.410557	-0.143895	0.488900	1.409563
69.4	-3.224040	-0.324248	2.304153	3.571277
104.1	-6.214920	-0.477978	4.650247	5.660256
138.8	-8.786507	-0.578722	7.165237	7.311214
173.5	-11.738942	-0.699277	10.036685	9.195131
208.2	-14.200368	-0.770842	12.942009	10.638629
277.6	-16.965501	-0.824336	17.656740	12.125318
347.0	-11.446806	-0.526029	17.067607	8.366930

This finding is significant because E_{sg} can now be determined solely based on two deflection basin parameters, *BDI* and *F2*. Deflection behavior of a pavement system is affected by many system variables, including layer modulus and thickness. The unique *BDI-F2* relationship for a specific E_{sg} with varying upper layer moduli and thicknesses suggests that the effect of E_{sg} on deflections can be separated out from the effects of all other system variables using the *BDI-F2* relationship. That is, if the upper layer conditions change and E_{sg} remains the same, deflection measurements and thus the deflection basin parameters will change accordingly, but the *BDI* and *F2* values will fall on the same characteristic curve. Of course, in reality E_{sg} changes when the upper layer conditions change due to the stress-state dependency of soils, and this effect will be demonstrated later in the next chapter using field data.

The success of the *BDI-F2* relationship in predicting E_{sg} was investigated using well-established relationships in the multi-layered elastic theory. Under normal circumstance, the value of δ_2 will fall between the values of δ_1 and δ_3. Thus, δ_2 may be reasonably assumed as the mean value of δ_1 and δ_3, and the following equation can be obtained from Equations 6.1 and 6.2:

$$F2 = \left(\frac{2}{\delta_2}\right)BDI \quad (6.4)$$

Further, the surface deflection of a single layer system at a distance r from applied load can be described as:

$$\delta_r = \frac{P(1-\nu^2)}{E_{sg}} f(r) \tag{6.5}$$

where δ_r = surface deflection at offset r from the applied load,
P = applied load,
υ = Poisson's ratio, and
$f(r)$ = function of r, the distance from the applied load.

Combining Equations 6.4 and 6.5 yields:

$$F2 = \frac{2E_{sg}}{P(1-\nu^2)f(r)} BDI \tag{6.6}$$

For constant values of P, υ, and r, E_{sg} is uniquely defined by *BDI* and *F2*. Although Figure 6.1 is developed from the dynamic analysis, the above simplified analysis helps us understand the reason behind the unique *BDI-F2* relationship for a given E_{sg}.

Once E_{sg} is estimated, this value can be used in the condition evaluation of upper layers of a pavement system. It needs to be noted that this method accounts for dynamic effects because the data in Figure 6.1 is generated using the dynamic analysis.

6.2.1 Effects of Distress Conditions

FWD tests are often performed on damaged pavements where rehabilitation is required. Therefore, it is desirable to investigate the effects of distresses on the *BDI-F2* characteristic curves. Deflections computed from pavements with hidden cracks were compared with those computed from intact pavements. Figures 6.2 and 6.3 present the *BDI-F2* relationships that were computed for both intact and distressed pavements. The simulated distress conditions have been described in Figure 5.2. Vertical cracks were placed at every 152 mm intervals starting at a distance of 102 mm from the loading center. Stripping was simulated by a reduction of the AC modulus in the AC layer. As can be seen, within the large variations of layer thicknesses, moduli, and distress conditions, the *BDI-F2* characteristic curves remain the same. Again, the only significant parameter that affects these curves is the E_{sg}. This behavior allows us to obtain the subgrade modulus, whether the pavement is distressed or intact, using only the two deflection basin parameters, *BDI* and *F2*, as described in the previous section.

6.2.2 Effects of Depth to a Stiff Layer

The *BDI-F2* relationship developed in this study is valid only for an infinite stiff layer depth. In this section, effects of shallow depth to a stiff layer on the *BDI-F2* relationship are studied. A pavement model consisting of a thickness of 113 mm AC layer and a subgrade was analyzed with different depths to a stiff layer. The depths are 0.76 m,

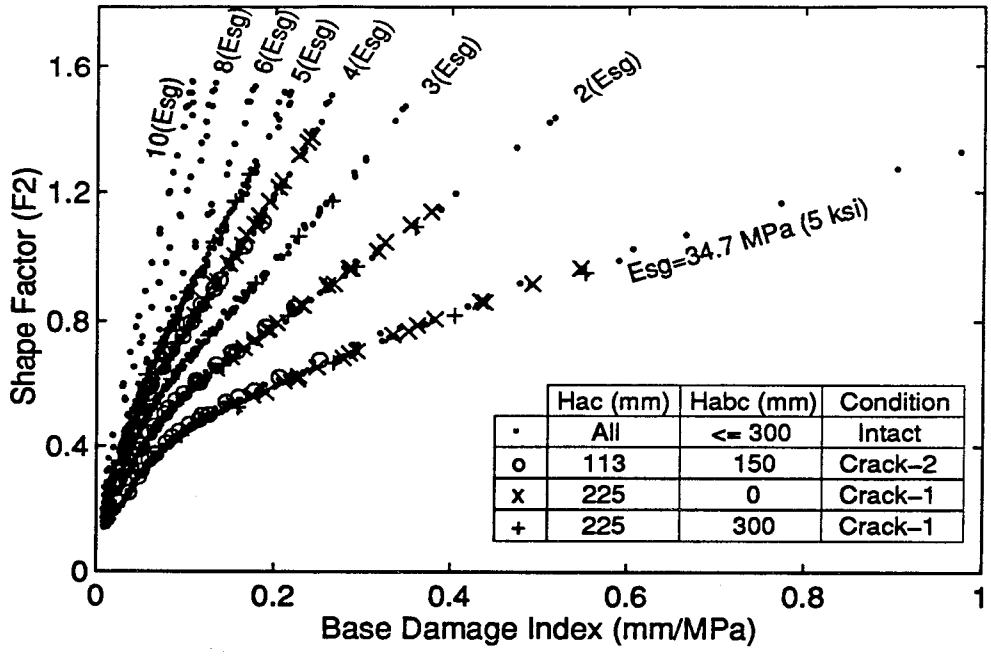

Figure 6.2: Relationships among BDI, $F2$, and E_{sg} with various cracked conditions.

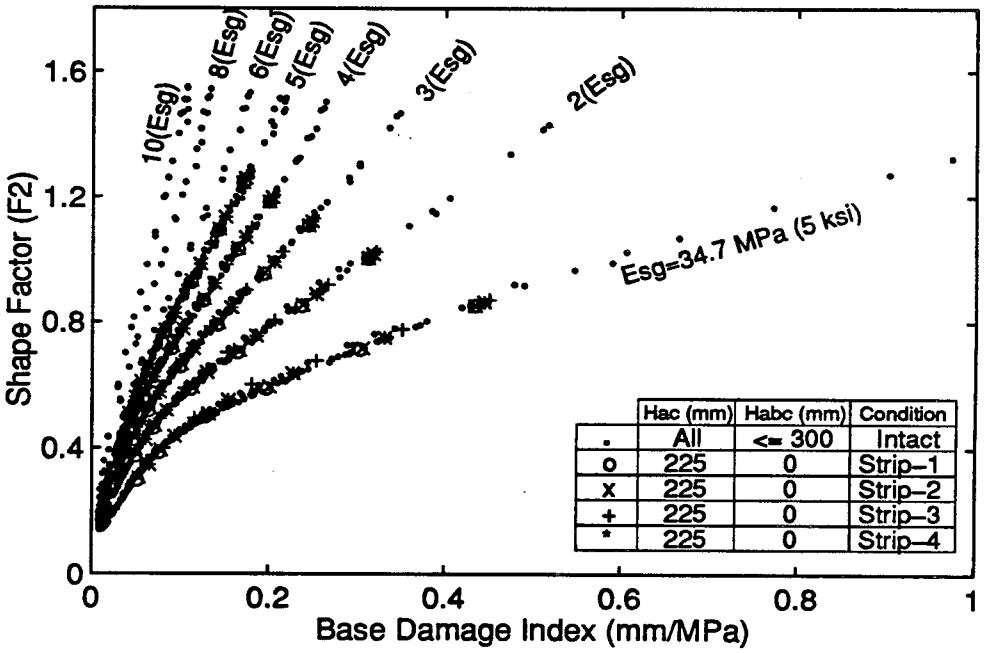

Figure 6.3: Relationships among BDI, $F2$, and E_{sg} with various stripped conditions.

1.52 m, 3.05 m, and 6.1 m. The analysis procedure is the same as that used to carry out the intact pavement analysis.

Figure 6.4 presents the *BDI-F2* relationships obtained from these analyses. It can be seen that *BDI* and *F2* values are essentially the same when the depth to a stiff layer is larger than 3.05 m. Variation begins when this depth is smaller than 3.05 m. The effect can be demonstrated using a deflection basin. For example, assuming point A in Figure 6.4 represents a measured deflection basin, then the estimated E_{sg} will be 83 MPa (12 ksi) if the depth to a stiff layer is larger than 3.05 m. On the other hand, the estimated E_{sg} will be 69 and 38 MPa (10 and 5.5 ksi) if the depths to a stiff layer are 1.52 and 0.76 m, respectively. It can be seen that the shallower the depth to a stiff layer, the larger the effect of this depth on the resulting E_{sg}. Therefore, it is important to estimate the depth to a stiff layer to obtain a correct E_{sg} value from the *BDI-F2* relationship.

The MODULUS program uses a method that is based on the concept of "line of influence" which states that the majority of the measured surface deflection at any offset is a result of the deflection below a certain depth in the pavement. If a stiff layer exists at some depth, then no surface deflection will occur beyond the offset at which the stress zone and the stiff layer intercept. The method to predict the apparent depth to a stiff layer is based on the hypothesis that the position of zero surface deflection should be strongly related to the depth in the pavement at which no deflection occurs (i.e., a stiff layer).

Several agencies including the Swedish National Road Administration and the U.S. Army Corps of Engineers have independently evaluated these depth to a stiff layer estimates, and they concluded that when true bedrock exists the MODULUS estimates were reasonable. In this study, FWD deflections obtained from the field will be processed by the MODULUS program to estimate the depth to a stiff layer. Estimated E_{sg} from field measurements will be used only when the depth to a stiff layer is larger than 3.05 m compared to that estimated by the MODULUS program.

6.3. Maximum Deflection and AREA

The deflection basin parameter, *AREA*, is a relative indicator of the strength of the pavement layer to the subgrade layer according to the study made by Hoffman and Thompson [28]. The *AREA* was defined as:

$$AREA = \frac{6(\delta_0 + 2\delta_1 + 2\delta_2 + \delta_3)}{\delta_0} \tag{6.7}$$

where *AREA* is the deflection basin area in inches, δ_0 is the center deflection, and δ_1, δ_2, and δ_3 are as defined in Equation 6.2. It was found that the *AREA* and D_0 values form distinct relationships as a function of AC layer thickness (H_{ac}), AC layer modulus (E_{ac}), and E_{sg} for a two-layer system (Figure 6.5). Therefore, E_{ac} can be determined if E_{sg},

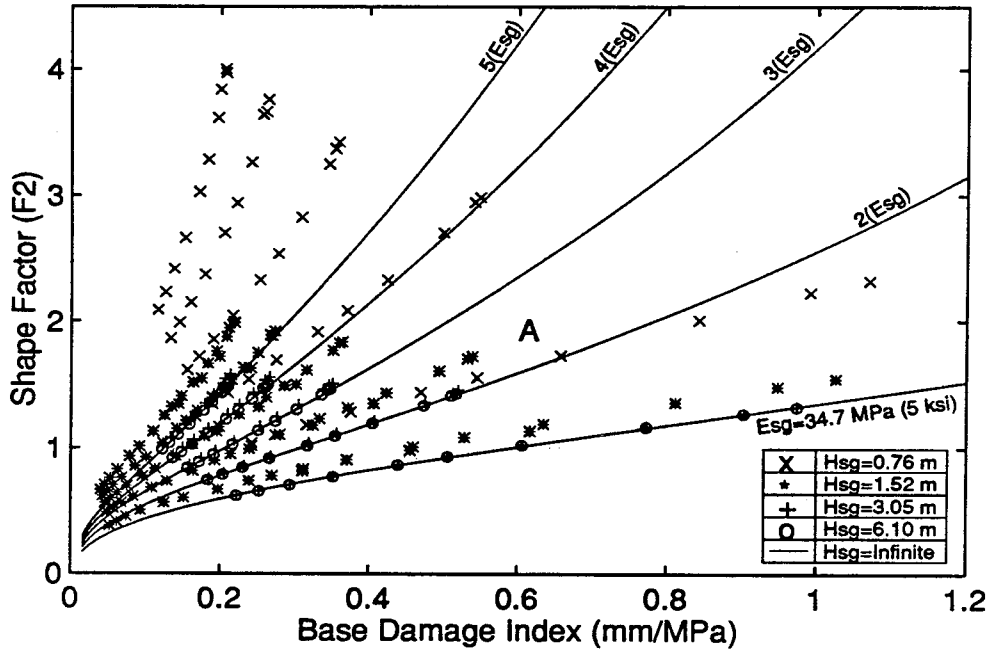

Figure 6.4: Effect of depth to rigid layer on BDI and $F2$ values.

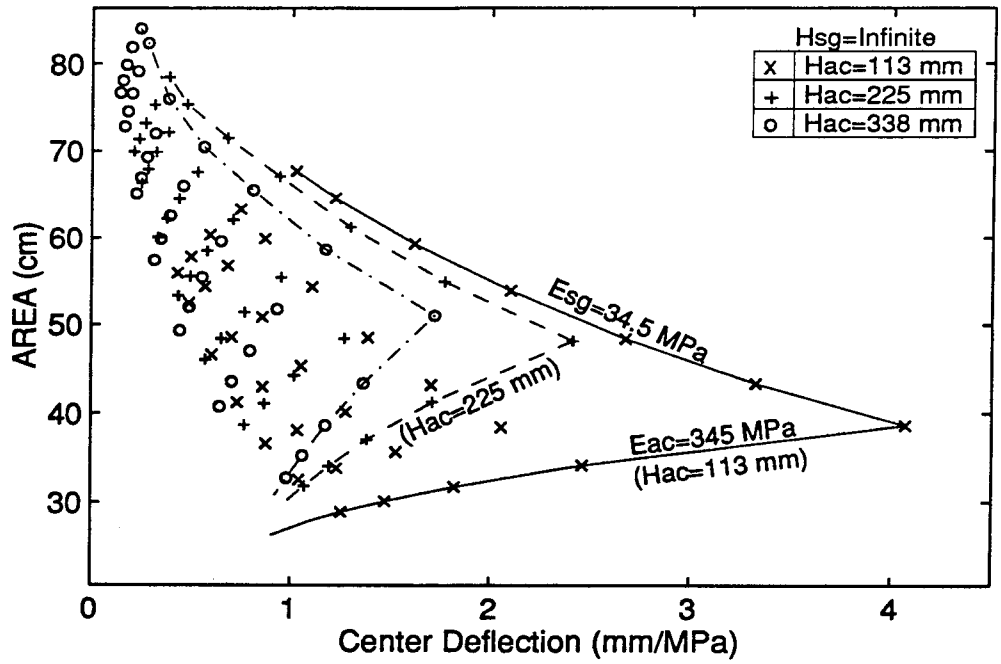

Figure 6.5: Relationships among D_0, $AREA$, H_{ac}, and E_{sg} of two-layer pavements.

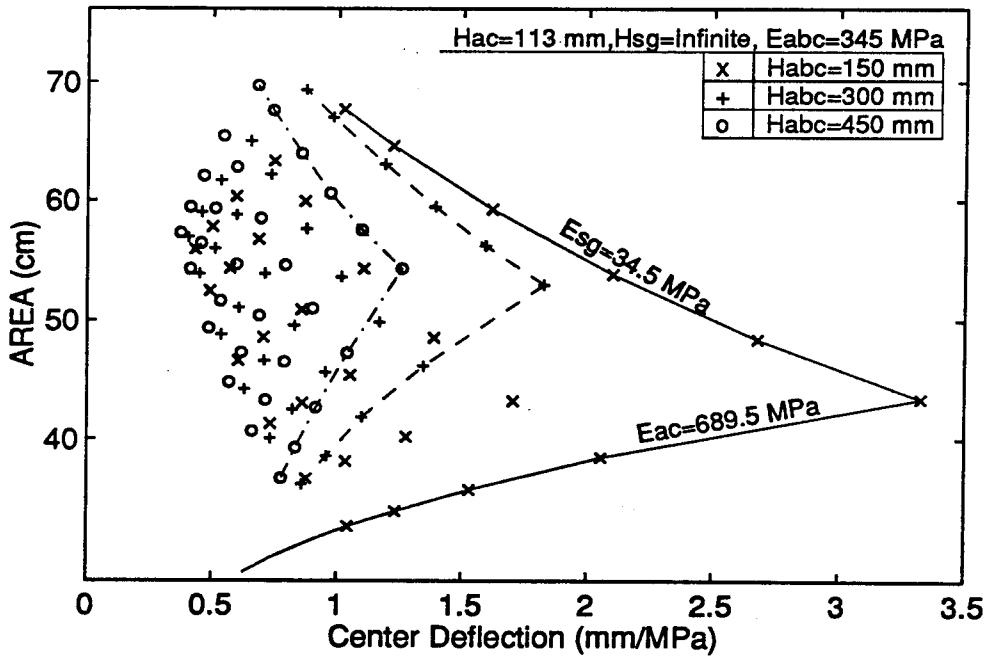

Figure 6.6: Effects of aggregate base layer thicknesses on D_0 and $AREA$.

D_0, *AREA*, and H_{ac} are known. Similar characteristics can be observed for a three-layer system; in this case, the base layer's thickness and modulus are needed in the estimation of the AC layer modulus. Figures 6.6 and 6.7 present how the thickness and modulus of the aggregate base layer influence the D_0-*AREA* relationships. It can be seen (Figure 6.6) that H_{abc} has large effects on D_0-*AREA* when E_{sg} and E_{ac} are small. On the other hand, E_{abc} seems to have a small effect on the D_0-*AREA* relationship (Figure 6.7) as compared with those effects caused by H_{abc}. This will make the estimation of E_{abc} difficult.

6.4. Shape Factor F2 and AREA

One disadvantage of the "effective moduli" concept is that it cannot determine whether an AC layer is damaged or not, although a low backcalculated AC modulus may indicate a possible damaged condition. This problem is due to the fact that a low AC modulus may be a result of a high AC temperature, not a damaged condition. Theoretically, responses of a pavement under a test load with intact and cracked (discontinuous) conditions will be different. Using FEM analysis, the difference in responses between these two conditions can be studied.

Figure 6.8 presents the *F2-AREA* relationships calculated from intact and cracked pavement models using the same pavement structure. The reference point is the intact condition with an AC modulus of 2758 MPa (400 ksi). Two different cracked conditions were analyzed: cracks in the top half and cracks in the bottom half of the AC layer. Cracks were placed at every 152 mm starting at a distance of 102 mm from the loading center. Additional analyses were made on the intact pavement model with reduced AC moduli of 1379 and 689 MPa (200 and 100 ksi).

As can be seen from Figure 6.8, deflections obtained from the intact pavements with three different AC moduli form a distinct *F2-AREA* relationship as shown in dashed line. Therefore, deflections computed from the cracked pavement models should fall somewhere along this dashed line if the "effective moduli" approach is valid. It can be seen that instead of falling on the dashed line, the *F2* and *AREA* obtained from the cracked pavement models deviate away from this line. This demonstrates that a damaged AC pavement may be detected using the *F2-AREA* relationship.

It is also shown that *F2-AREA* of the pavement model with cracks in the top half of the AC layer deviate to the upper-right of the dashed line, while the *F2-AREA* computed from a model with cracks in the bottom half of the AC layer deviate to the lower-left of the dashed line. This behavior can not be explained using analytical equations since the load-displacement relationships of a layered system are extremely complicated with dynamic analysis and can only be solved by numerical approximations. Results from these FEM analyses were encouraging with regard to using *F2-AREA* for pavement condition assessment.

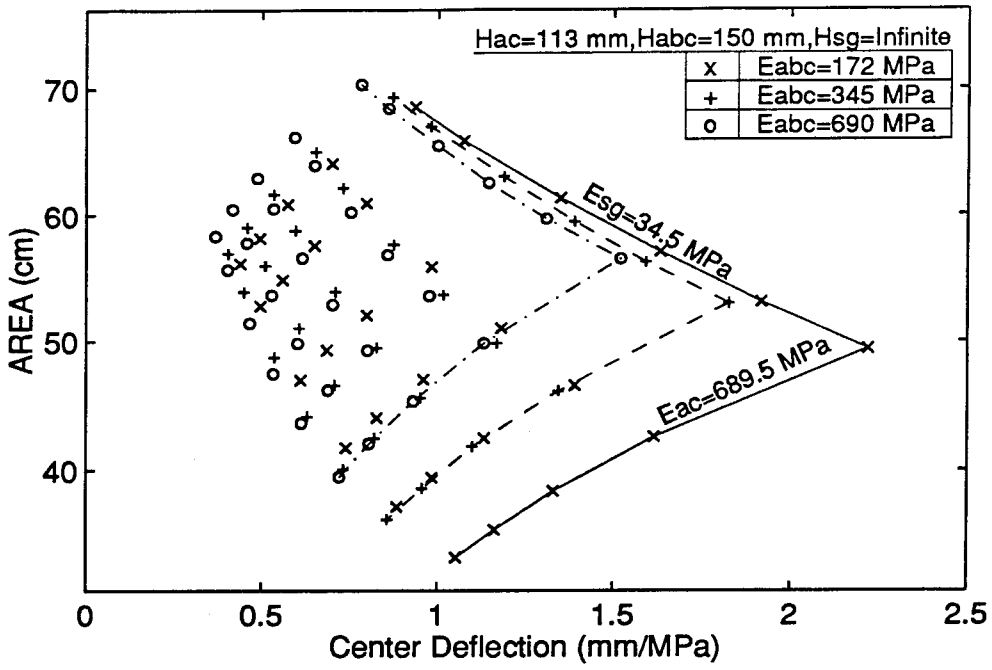

Figure 6.7: Effects of the aggregate base layer moduli on D_0 and $AREA$.

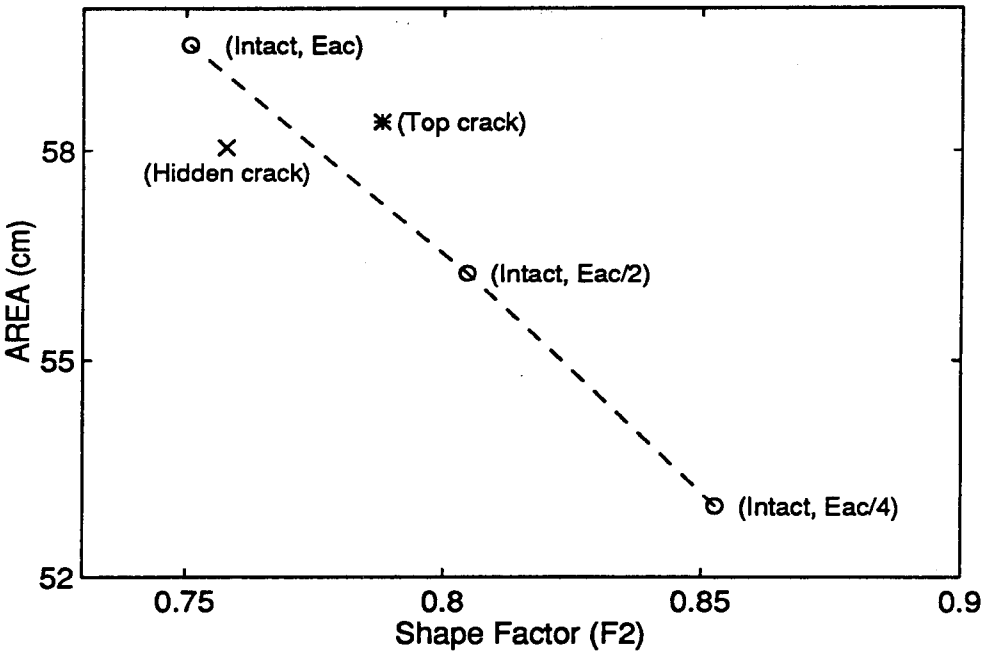

Figure 6.8: Effects of layer conditions on $F2$-$AREA$ relationship.

When deflections obtained from the intact models were processed, it was found that there exists an "envelope" in the *F2-AREA* relationships for a given AC layer thickness, regardless of the conditions underneath (Figure 6.9). That is, *F2* and *AREA* values are present within the envelope for the given combinations of layer moduli and aggregate base layer thicknesses (Table 5.1).

Therefore, a different *F2-AREA* envelope may be obtained for each AC thickness. Figure 6.10 shows the *F2-AREA* envelopes for AC thicknesses of 112, 225, 338, and 450 mm computed from synthetic deflections. As described earlier, the *F2-AREA* values will fall on the left-lower side of the envelope if deflections from an intact pavement are used.

Presented in Figure 6.11 are the results computed from FWD deflections measured from intact pavements (Table 5.2). Each symbol represents deflections measured from a given pavement at the same location at a different time of day during the four trips. It can be seen that *F2-AREA* are all well under the envelope within the large variations of the AC temperatures. It should be noted that there are different AC thicknesses in these sections, with or without an aggregate base layer. Different envelopes obtained from synthetic data should be applied to the same pavement layer thicknesses in the field to insure equal comparison. Due to the limited number of data sets available, observations were made based on interpolation of the FEM computed deflections. It can be seen that NC 54 and NC 24 have very close *F2-AREA* values except those obtained the from the summer trip (with AREA values between 45 and 60). Cores obtained from these sites revealed that the AC thicknesses were 254 and 229 mm, while the design thicknesses were 267 and 184 mm for NC 54 and NC 24, respectively. These *F2-AREA* relationships were found to match closely with the envelope obtained from the intact pavement model with an AC thickness of 225 mm. The AC thicknesses of US 264 and US 17 are 114 and 305 mm (core), respectively. When comparing the AC thickness, it is not surprising to see that US 17 has the envelope toward the lower-left, while US 264 has the envelope pointed in the upper-right direction.

Deflections measured from different sections at US Highway 421 (Tables 5.5 to 5.12) were incorporated to study the *F2-AREA* relationships. Various distresses were observed at the time of the FWD test. Fatigue cracking and stripping were the two major distresses according to core data and distress surveys. These conditions make them good candidates for the damaged pavement study. Figure 6.12 presents the *F2-AREA* relationships for sections 1, 23, 3, and 16 which contained an aggregate base layer. As can be seen, field measurements deviate significantly from envelope A, which represents an intact pavement with an AC thickness of 112 mm and a depth to a stiff layer of 1.52 m. It is noted that depth to a stiff layer also plays an important role in the *F2-AREA* relationship.

Attempts were made to correlate the AC core conditions with *F2-AREA*. For example, locations 0 and 6 of section 23, marked as 1 and 2, were full-depth patched, while location 9 of section 3 (marked as 3) was overlayed with severe stripping in the binder course according to the core data. On the other hand, location 8 of section 1 and

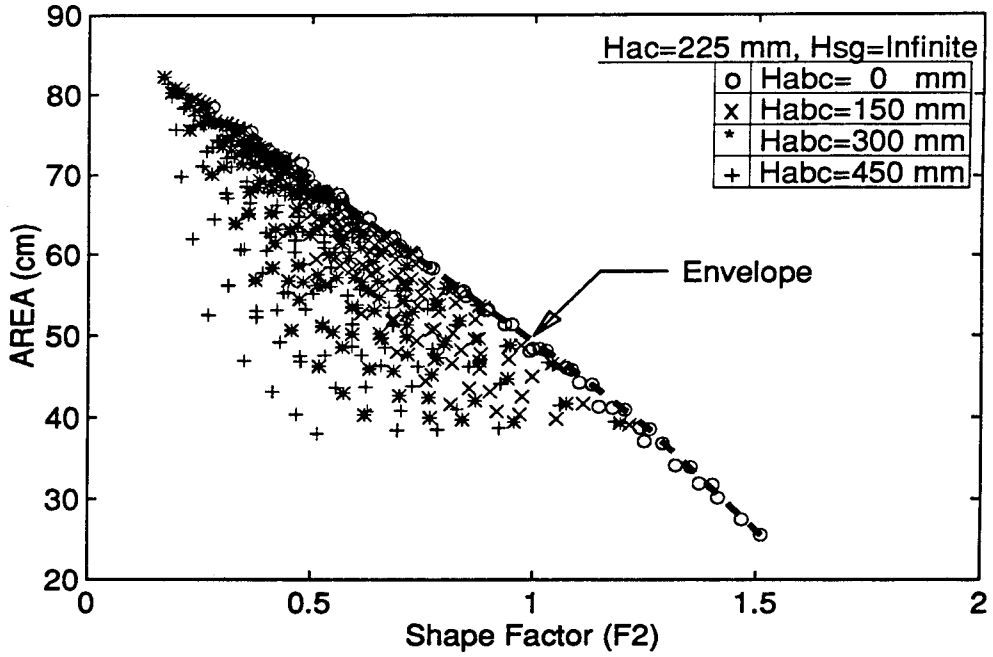

Figure 6.9: Relationship of *F2-AREA* for pavements with H_{ac}=225 mm and various H_{abc} values.

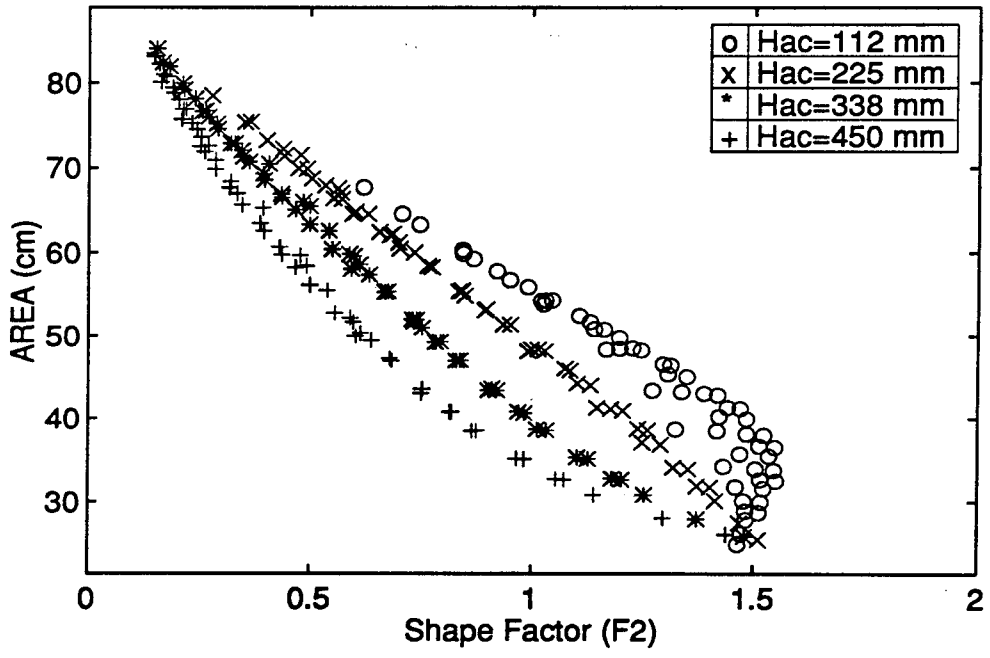

Figure 6.10: Relationship of *F2-AREA* for different pavement models.

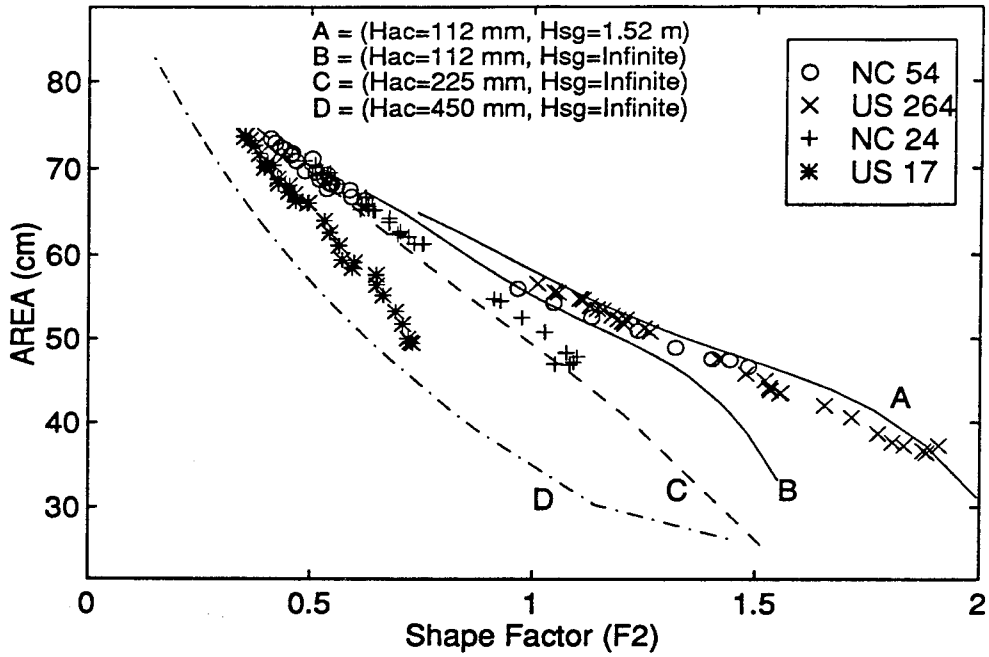

Figure 6.11: *F2-AREA* relationship obtained from intact pavements.

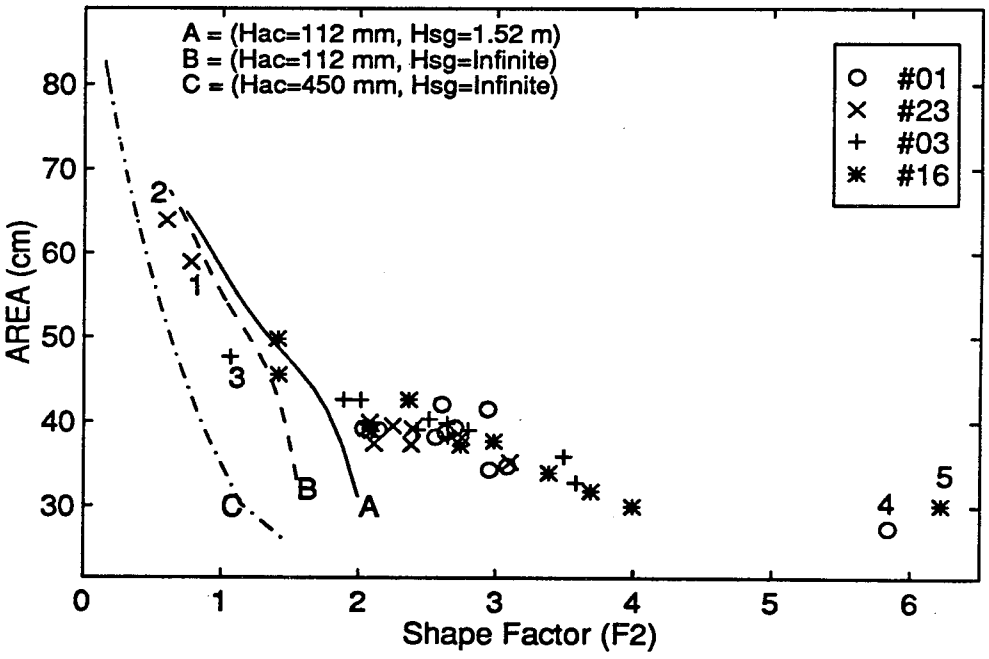

Figure 6.12: *F2-AREA* relationship obtained from US 421 pavement sections with an aggregate base course.

location 8 of section 16 (marked as 4 and 5, respectively) appeared to have good conditions. This seems to contradict what was observed previously. It should be remembered, however, that the core represents only a very small portion of a pavement as compared to the entire region covered by the FWD sensors. Distress surveys from these sections have shown that a large number of these sections were under medium to severe fatigue cracking. The entire pavement of section 3 was even overlayed to reduce the damage acceleration to the pavement. Overall, these sections can be identified as damaged pavements when comparing the *F2-AREA* values with a desired envelope derived from FEM analysis.

Similar observations can be made for sections 7, 20, 9, and 22 as shown in Figure 6.13. The B envelope should be considered as the controlled envelope because it has an AC thickness of 225 mm which is close to the design AC thickness of 229 mm for these sections. Core retrieved from location 1 of section 7 (marked as 1) was logged in good condition, while location 3 (marked as 2) was stated to have severe stripping in the base. The distinctive point (marked as 3) represents location 8 of section 20 which was logged as having stripping at each layer interface and in HB. Again, it seems reasonable to judge a pavement condition using *F2-AREA* relationships, although there are a few conditions from the core logs that cannot be explained.

As demonstrated previously, the presence of damage in an AC layer may be detected using the *F2-AREA* relationship determined from the FWD deflections. Overall, this method shows encouraging results, although the specific type of distress (e.g., stripping or cracking) can not be identified. This is due to the fact that a pavement system is complex owing to the large number of factors involved, their interactions, and the randomness of the distresses with regard to location, severity, and extent. The FEM models incorporated in this study are still the fundamental ones which will play an important role in the result. Nevertheless, better understanding of the behavior of broken pavements under the FWD test will result as experience is accumulated and analysis techniques are improved.

7. DEFLECTION ANALYSIS PROCEDURES

7.1. Proposed Procedure

As described in the previous chapter, the subgrade modulus can be determined solely by the two deflection basin parameters *BDI* and *F2*. This approach is valid for both pavements without an aggregate base layer (two-layer) and with an aggregate base layer (three-layer). It should be noted that depth to a stiff layer was found to have a big influence on this method. Different charts should be developed for each depth to a stiff layer to obtain a correct subgrade modulus. However, only the infinite depth to a stiff layer has been incorporated in the forward modeling of this study. Once E_{sg} is determined, it can be used as an input variable to determine upper layer moduli.

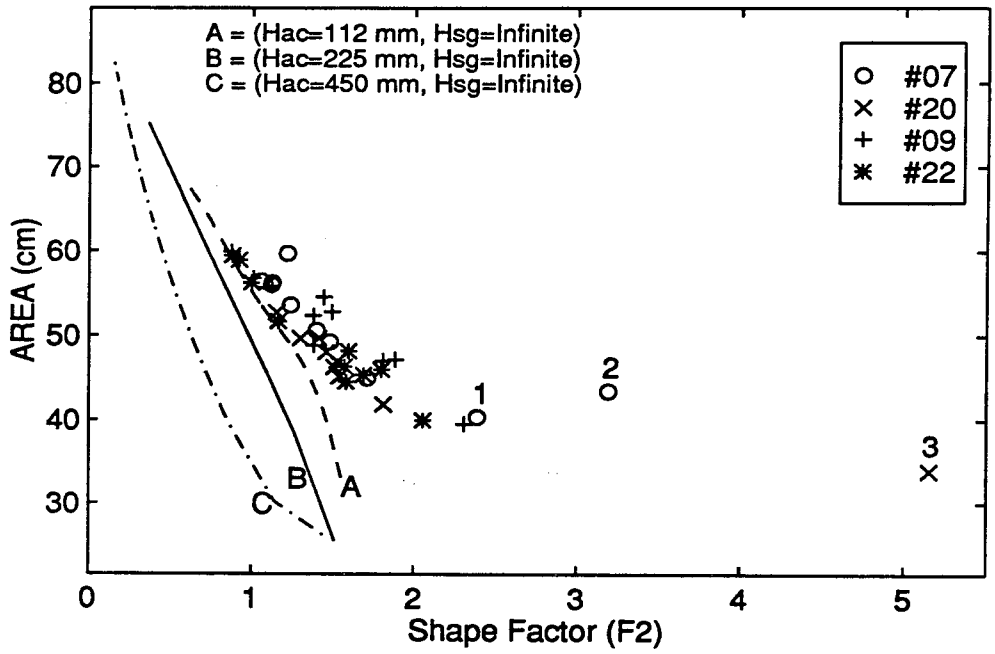

Figure 6.13: *F2-AREA* relationship obtained from US 421 pavement sections with full-depth AC layer.

The subgrade modulus can be used together with H_{ac}, D_0, and *AREA* to estimate E_{ac} for a two-layer system (see Figure 7.1). The same procedure is used for a three-layer system. An additional procedure is required to estimate the modulus of the aggregate base layer. The previous chapter demonstrated that E_{abc} has relatively small effects on D_0-*AREA* relationships; that is, E_{abc} is insensitive to the values of D_0 and *AREA*. This causes difficulties in determining E_{abc} values using D_0-*AREA* relationships. Another deflection basin parameter, Base Curvature Index (*BCI*), was incorporated to overcome this problem. *BCI* is defined as:

$$BCI = \delta_2 - \delta_3 \tag{7.1}$$

where *BCI* = Base Curvature Index,
δ_2 = deflection at a distance of 610 mm from load center, and
δ_3 = deflection at a distance of 914 mm from load center.

BCI was employed because it incorporates the deflections measured at distances of 610 and 914 mm from the test load which accounts for the condition of the base layer. This will provide additional information to the prediction model to better secure E_{abc} values. Figure 7.2 shows the prediction procedure for a three-layer system.

The procedures described above are somewhat of an "effective moduli" approach because no condition evaluation is involved. Additional steps need to be taken to identify whether a pavement is damaged or not. The *F2-AREA* relationship suggested in the previous chapter can be used for AC condition assessment. For example, if a data point of *F2-AREA* of a deflection basin is located above the described envelope, the AC layer of this particular pavement section may be damaged. On the other hand, if the data point is below the envelope, then the asphalt layer may be in good condition. Therefore, *F2-AREA* can be used in addition to the relationships of *BDI-F2*, D_0-*AREA*, and *BCI* for layer condition assessment of a pavement.

7.2. Artificial Neural Networks

The proposed procedures can be implemented using the ANN technique to automatically estimate pavement layer moduli. An ANN system is a collection of simple processors (generally called neurons or units) that are interconnected to form a mathematical representation of the mapping or relationship that may be embedded in any set of data. The structure of ANNs allows them to be global approximators even in the absence of knowledge about the mathematical form of the mapping between an input signal and the corresponding output signal. A multi-layered, feedforward-type network is the most common class of ANNs used for this type of function mapping. A typical multi-layered network consists of an input layer, an output layer, and one or two intermediate layers (Figure 7.3). The input signal is presented to the network through the units in the input layer. This signal is then propagated through the intermediate units to the output units via the interconnections in the network. The strength of a signal passing through a unit undergoes a nonlinear transformation as shown in Figure 7.3. Further, the strength of

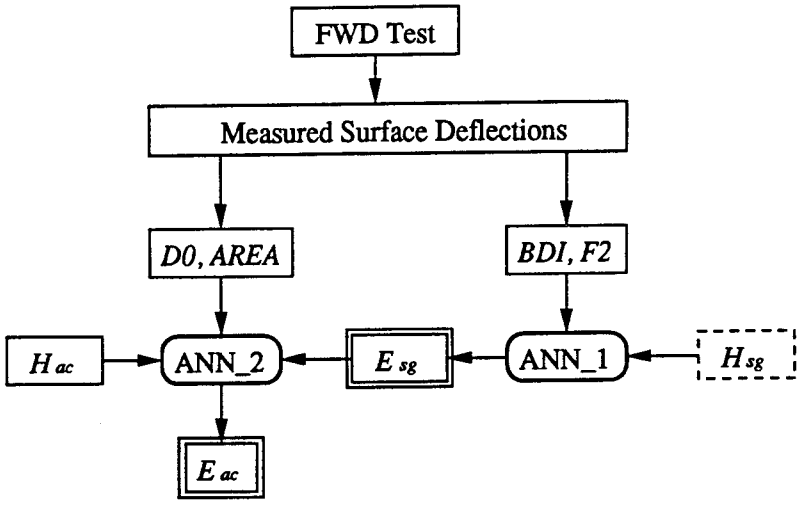

Figure 7.1: Flow chart representing prediction procedure for two-layer pavement systems.

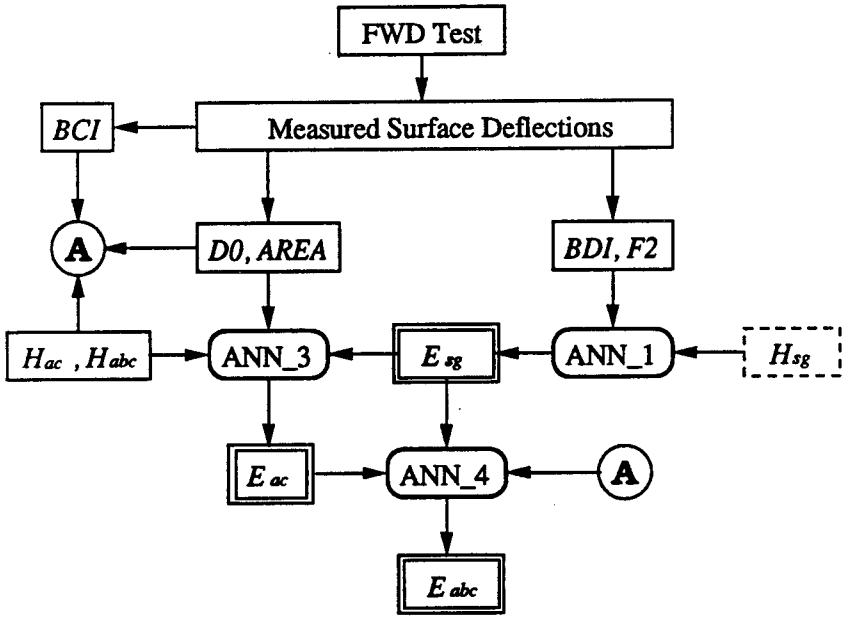

Figure 7.2: Flow chart representing the prediction procedure for three-layer pavement systems.

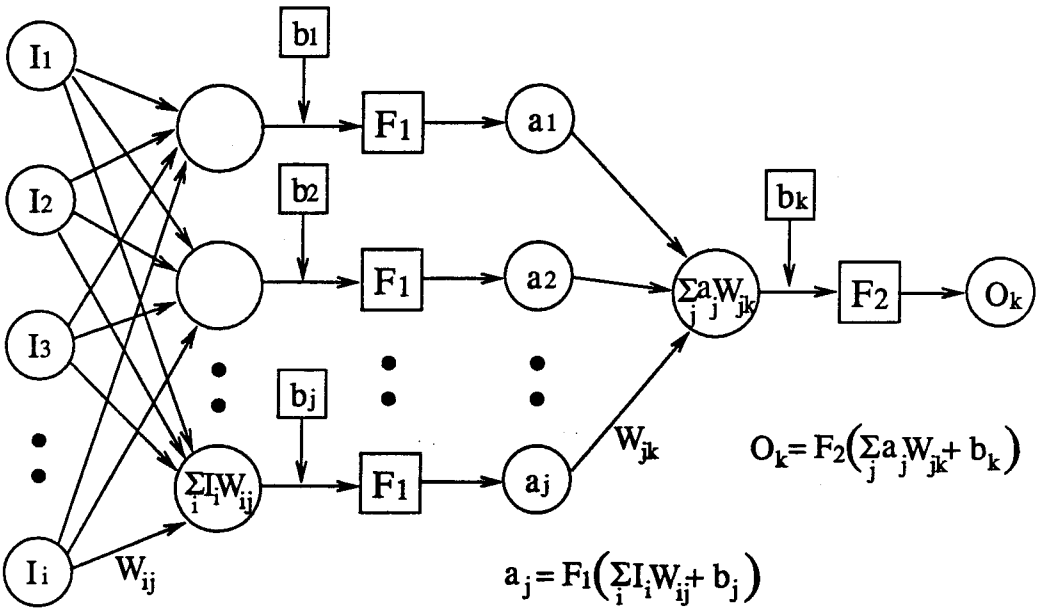

Figure 7.3: Schematic diagram of the Artificial Neural Networks

the propagated signal is adjusted throughout the network by the connection strengths (generally called connection weights). These connection weights are updated, in an iterative manner, until the predicted output signals are as close as possible to the actual signals corresponding to those input signals. A representative sample data set that includes a set of input signals and their corresponding output signals is used during this weight updating process. This process is called training. The weight updating procedure used in this study is a modified version of backpropagation algorithm [37].

An approximation of the mapping between the input and the output signals is encoded in the connection weights of a trained network. This trained network is then able to propagate a new input signal through the network and predict the resulting output signal. In this mode of operation, the network is used as an approximate function of the mapping between the input and the output signals.

In the feed-forward type framework, the ANN is trained to capture the mapping between the deflection basin (input signal) and the corresponding pavement characteristics (output signal). Data representing many instances of pavement characteristics and the resulting deflection basins are used to train the network. The trained network, when presented with an observed deflection basin, is then able to predict the most likely set of pavement characteristics that yield the given deflection basin.

7.3. ANN Training and Testing

The Neural Network Toolbox in the MATLAB program [38] was employed to carry out the training and prediction of layer moduli. The prediction procedures described in Figures 7.1 and 7.2 for two-layer and three-layer pavement systems were implemented using MATLAB code. The network sizes and information on the training and testing cases are presented in Table 7.1. Synthetic deflections calculated by ABAQUS were used in these ANNs. Once the networks were trained, the corresponding weights were saved for future prediction use.

Table 7.1. Training and testing information on the ANNs.

	ANN_1	ANN_2	ANN_3	ANN_4
Input Units	*BDI* *F2*	D_0, *AREA* H_{ac}, E_{sg}	D_0, *AREA* H_{ac}, H_{abc}, E_{sg}	D_0, *AREA*, *BCI* H_{ac}, H_{abc}, E_{sg}, E_{ac}
Hidden Units	4	5	4	5
Output Units	E_{sg}	E_{ac}	E_{ac}	E_{abc}
Training Cases	1400	200	1400	1400
Testing Cases	20	20	30	30
Testing RMSE[a]	6.6%	11.6%	21%	34%

[a]Root-Mean-Square-Error

Figures 7.4 and 7.5 show the prediction performance of the ANN_1 and ANN_2 when tested using synthetic deflections that were not included in training. Twenty examples were used to test ANN_1 and ANN_2 while thirty examples were used to test ANN_3 and ANN_4 (Figures 7.6 and 7.7). The relatively large testing root-mean-square-errors (RMSEs) shown in Table 7.1 are mainly due to the limited number of data sets given in the training process. The prediction accuracy can be increased by adding more data sets to the training networks and randomizing the discrete data points.

7.4. Pre-test Using Field FWD Data

FWD deflections measured from the pavement sections listed in Table 5.2 were used to test the proposed procedures. Deflections were first normalized by FWD load amplitudes, and then the deflection basin parameters, *BDI*, *F2*, *BCI*, *AREA*, and D_0, were computed. These parameters, together with the layer thicknesses, were then given to the trained networks to estimate layer moduli.

7.4.1 Subgrade Modulus Prediction

The computed *BDI* and *F2* were input to the ANN_1 which was trained to predict E_{sg} as described in the previous section. The predicted E_{sg} values are presented in Figure 7.8. It can be seen that the estimated E_{sg} values seem to be very high for US 421 and US 264 pavements. This is because these sections have relatively shallow depths to a stiff layer as shown in Table 5.2. As noted earlier, the *BDI-F2* relationships were developed based on deflection data calculated from a number of pavements with the assumption of infinite depth to a stiff layer. Therefore, the predicted E_{sg} for pavements with shallow depth to a stiff layer will not be correct.

Although the magnitudes of E_{sg} are incorrect, some valuable observations on stress-state dependency of soils can be made by following the trends shown in Figure 7.8. The individual data point in Figure 7.8 represents the predicted E_{sg} value at a specific time of day in each season for each pavement site. Therefore, for each season 7 to 10 data points were gathered representing FWD tests performed within a day. These data points were plotted such that earlier time data is positioned to the left side of the group. Thus, knowing the typical pavement temperature variation with respect to time of day, one can interpret that data points toward the right hand side of each seasonal group represent higher temperatures. For sections US 421, NC 54, and US 264, the E_{sg} values decrease as the pavement temperature increases, i.e., as AC layer modulus decreases. Also, for these sections, E_{sg} values for summer are lower than those for other seasons, indicating the stress-softening effect of the soils in these sections. A reverse trend can be found in Figure 7.8 from NC 24 and US 17 pavements. These opposite trends can be explained by different soil types for these sections as shown in Table 5.2. The soil types for NC 24 and US 17 are A-2-3 and A-3, which represent sandy soil, whereas the soil type for US 421, NC 54, and US 264 is clayey. Well known stress-softening and stress-hardening behavior

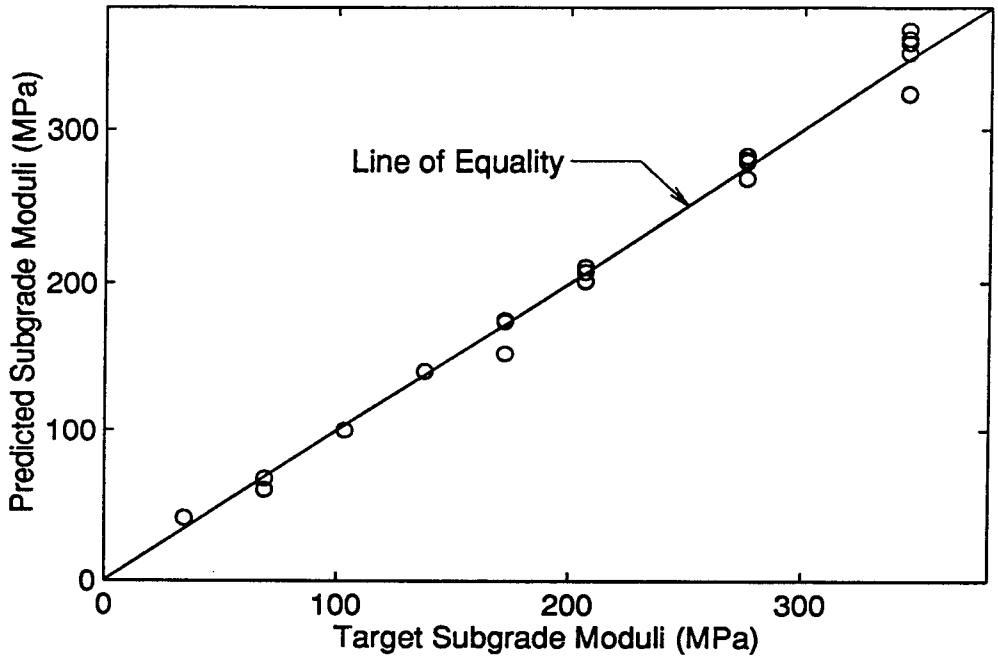

Figure 7.4: Prediction performance of ANN_1 for subgrade modulus.

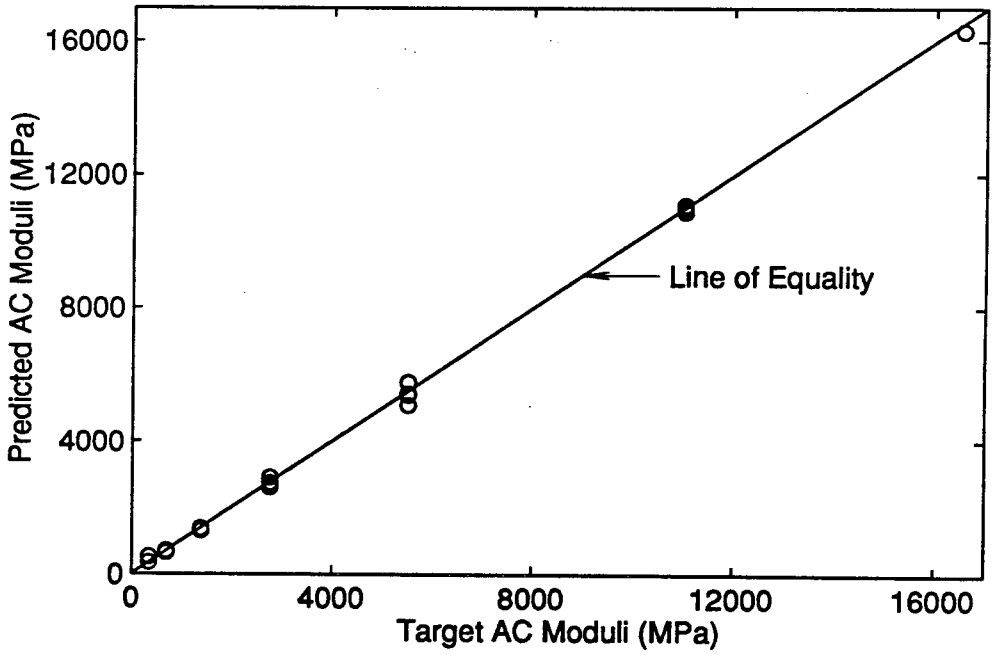

Figure 7.5: Prediction performance of ANN_2 for AC modulus.

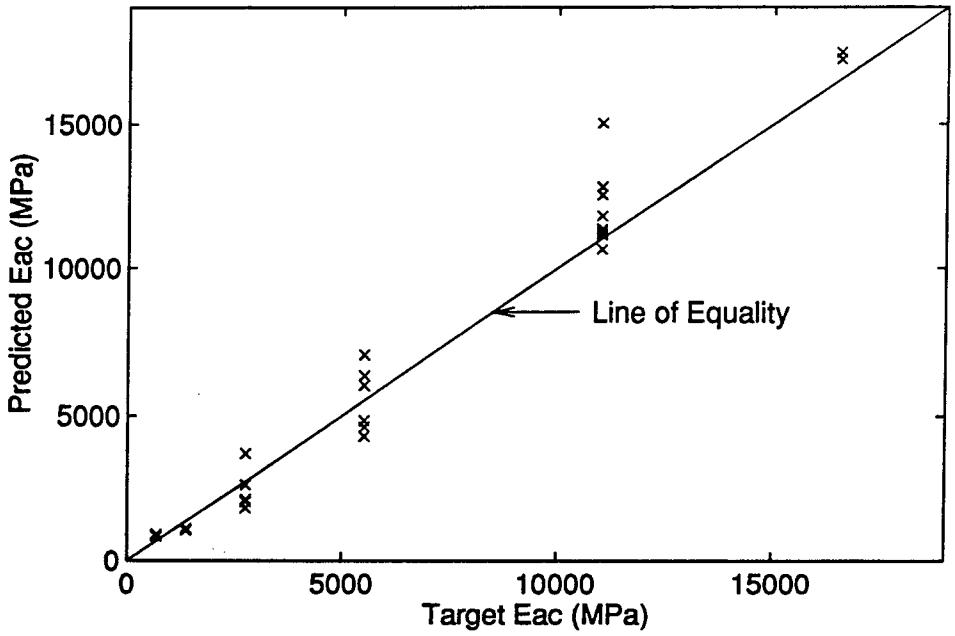

Figure 7.6: Prediction performance of ANN_3 for AC modulus (3-layer system).

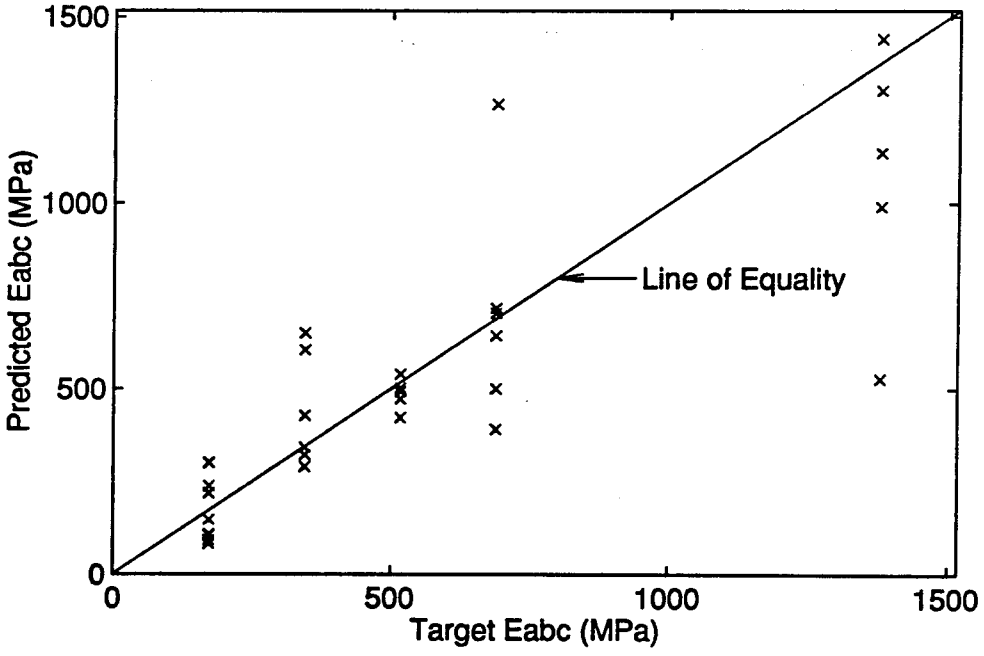

Figure 7.7: Prediction performance of ANN_4 for ABC modulus.

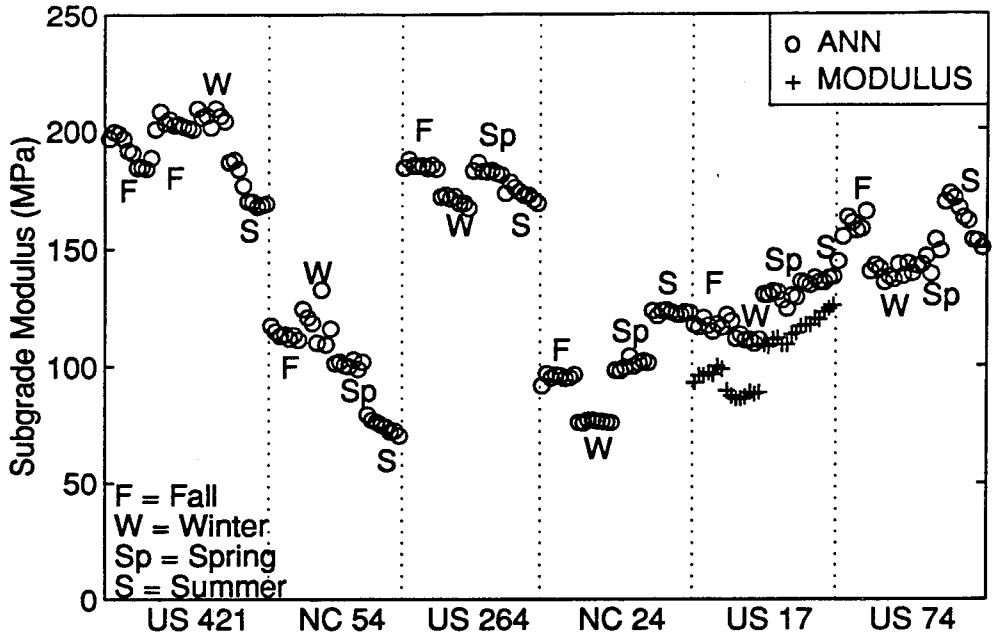

Figure 7.8: Subgrade moduli predicted by the ANN-based method for the five pavements and the MODULUS estimated E_{sg} for the US 17 pavement.

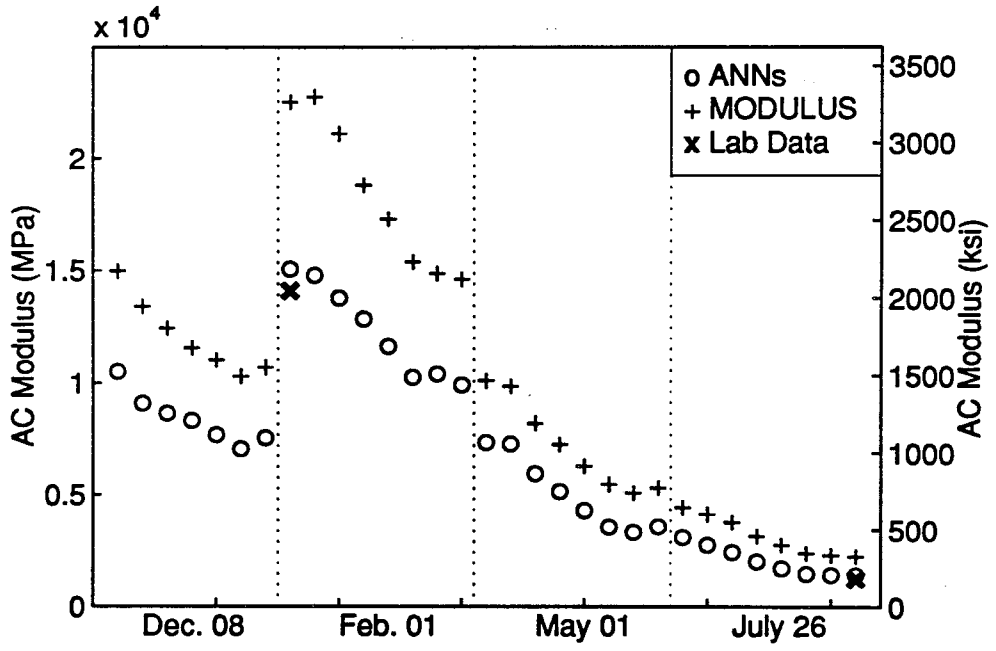

Figure 7.9: AC moduli obtained by the ANN-based method and by the MODULUS program for FWD deflections measured from US 17, NC.

of clayey soils and sandy soils can explain the trends described above. The predicted E_{sg} values for US 74 (Figure 7.8) are not compared here because the soil type of this section is not available.

7.4.2 Two-layer Pavement

Since the US 17 section has a fairly deep stiff layer of which deflections can be approximated as an infinite depth to a stiff layer using dynamic analysis, the predicted moduli values can be regarded as valid. Therefore, the US 17 data were further processed to compare with backcalculated moduli values using the MODULUS program. It is shown in Figure 7.8 that the subgrade moduli obtained by the MODULUS program are consistently lower than those obtained by the ANN. This agrees with the conclusion made by other researchers that the subgrade modulus is usually underestimated when dynamic effects occurring in the measurements are not taken into account in the analysis.

The predicted E_{sg}, together with D_0, *AREA*, and H_{ac}, of the US 17 pavement were then input to ANN_2 to predict E_{ac}. Figure 7.9 presents the AC moduli predicted by both methods. The MODULUS program consistently predicted higher AC moduli than those predicted by ANN_2. This is a result of underestimation of subgrade moduli which is compensated by overestimation of AC moduli.

It can be seen that the MODULUS program predicted unreasonably high AC moduli during February. According to the previous record [23], the mid-depth AC temperatures of this pavement were measured as 7.0°C and 42.6°C (44.6°F and 108.7°F) for the first FWD drop in February and the last FWD drop in July, respectively. According to the laboratory dynamic modulus test results performed on field cores [22], AC moduli for these temperatures and for the FWD loading frequency are estimated to be 1.41×10^4 MPa and 1,241 MPa (presented by the symbol **X** in Figure 7.9), respectively. Although cores were obtained from a different site, the resulting dynamic moduli are unlikely to vary by the large difference shown in Figure 7.9 for the MODULUS results. Good agreement was found when comparing these laboratory determined dynamic moduli with the AC moduli predicted by the ANN, demonstrating the importance of using dynamic analysis for processing FWD data.

7.4.3 Three-layer Pavement

Layer moduli prediction of a three-layer pavement system can be carried out in a manner similar to that used to predict a two-layer system. US Highway 74 was used to demonstrate this prediction procedure. The depth to a stiff layer of this section was estimated to be 6.8 m using the MODULUS program. Therefore, E_{sg} predicted from *BDI-F2* can be treated as valid. This pavement was one of the studied sections for the temperature correction project; therefore, the same FWD setup and testing procedures were used as described in the previous section. The calculated *BDI*, *F2*, D_0, *AREA*, and

BCI were processed through ANN_1, ANN_3, and ANN_4 to estimate E_{sg}, E_{ac}, and E_{abc}.

Figure 7.10 presents the layer moduli estimated by the ANNs and the MODULUS program. As can be seen in Figure 7.10(a), E_{sg} estimated by the dynamic analysis-based ANN method is consistently higher than that estimated by the MODULUS program. This agrees with the results presented earlier. The ANN-predicted E_{ac}, however, also shows higher magnitude than that predicted by the MODULUS program. This seems to contradict the findings shown previously. It should be noted that this section is a three-layer pavement, and the modulus of the aggregate base layer also plays an important role in predicting the layer moduli.

Again, according to the previous record [23], the mid-depth AC temperatures of this pavement were measured as -1^{o}C and 40^{o}C (30^{o}F and 104^{o}F) for the first FWD drop in January and the last FWD drop in August, respectively. Based on the laboratory dynamic modulus test results performed on field cores [22], the AC moduli for these temperatures and for the FWD loading frequency are estimated to be 1.51x10^{4} MPa and 1,448 MPa (presented by the symbol **X** in Figure 7.10(b)), respectively. Although the ANN-predicted E_{ac} for the first FWD drop of January trip is lower than the value estimated from the laboratory determined dynamic modulus, it is much closer to the estimated dynamic modulus as compared to the value predicted by the MODULUS program. The ANN-predicted E_{abc}, however, shows a lower value than that estimated by the MODULUS program.

Although questions may arise due to the fact that the testing performances are not good enough for ANN_3 and ANN_4, this result demonstrates the potential use of the deflection basin parameters and ANNs for evaluating in-situ pavement conditions. It needs to be noted that the prediction performance of ANNs can always be improved by feeding more representative information to the network as well as adjusting the network sizes. It is believed that better prediction will result when the data base used to train the network is complete.

7.4.4 Damage Condition

Because pavement sections studied in the temperature correction projects did not have any noticeable distresses, additional FWD tests were performed on US 1 near Vass, North Carolina during this research study. Detailed information on this test section was described in Table 5.3. As described in Section 6.4, the damage condition of a pavement may be identified using the *F2-AREA* relationship.

Figure 7.11 presents the *F2-AREA* relationships obtained from the FWD deflections measured from the US 1 pavement. Numbers represent deflections obtained before the overlay, while letters represent those obtained after the overlay (e.g., the number 1 and the letter a both represent the deflections obtained from test location 1,

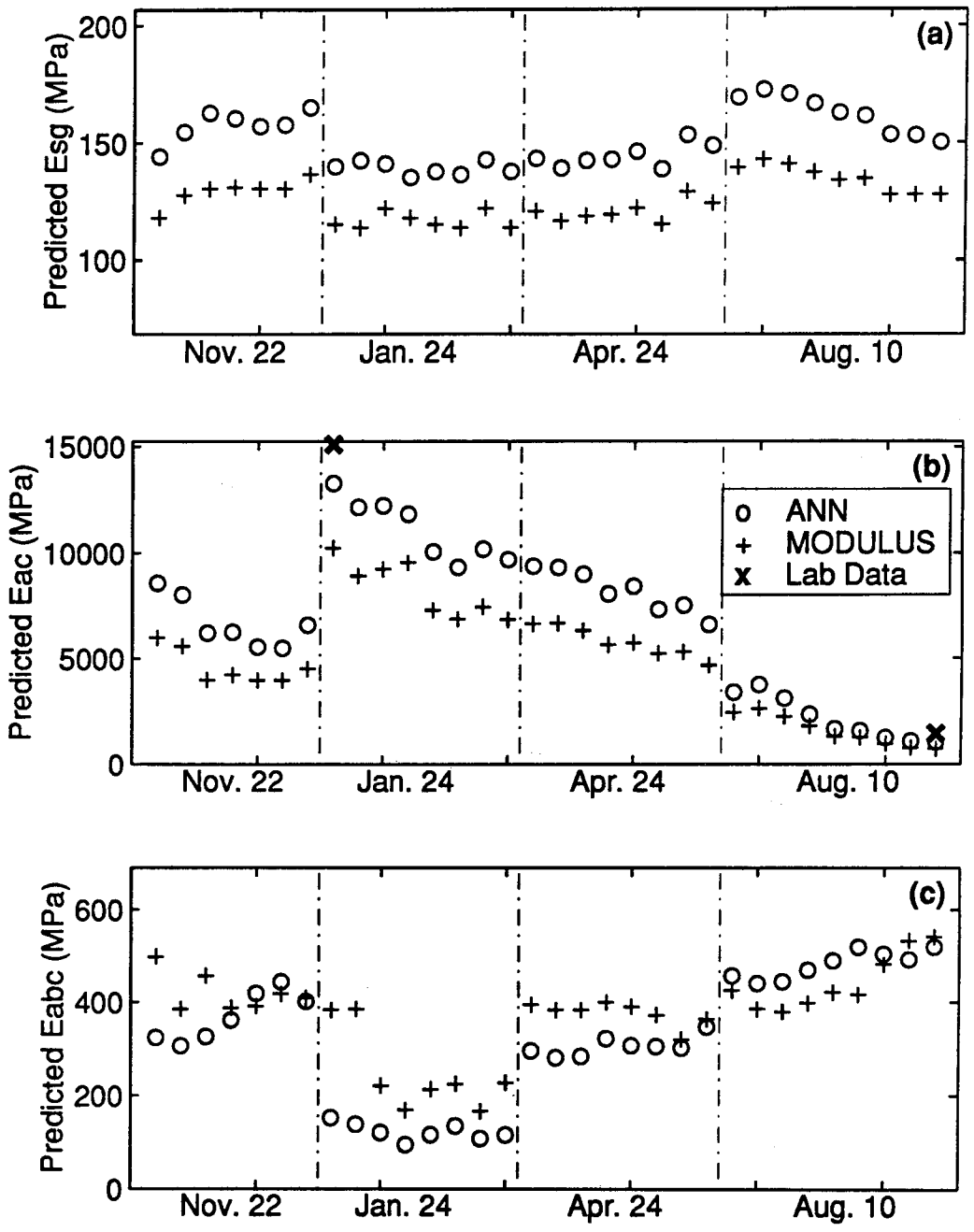

Figure 7.10: Layer moduli obtained by the ANN-based method and by the MODULUS program for FWD deflections obtained from US 74, NC.

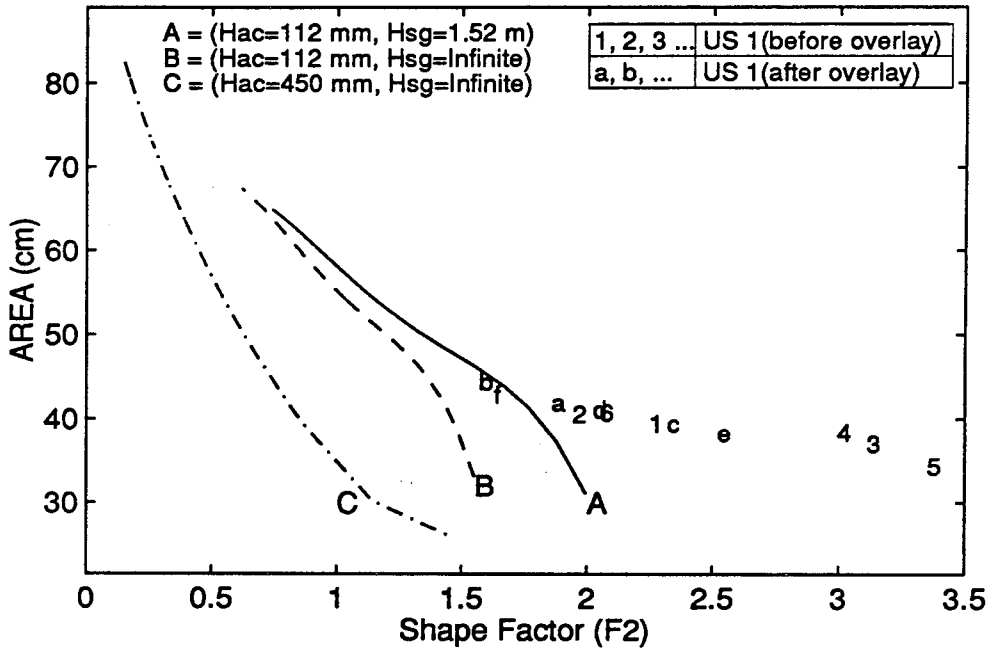

Figure 7.11: *F2-AREA* relationship obtained from US 1 (before and after the overlay).

etc.). It can be seen that those points obtained before the overlay deviate more from the envelope A than those obtained after the overlay, indicating a strength increase after the overlay. Locations 1 and 2 were visually determined to be in intact condition before the overlay. As can be seen in Figure 7.11, locations 1 and 2 are closer to the envelope A. Location 4 had severe fatigue cracking before the overlay and is shown to deviate far more from the envelope. Location 5, however, was identified as mildly cracked and shows the greatest deviation in the figure. The depth to a stiff layer at location 5 estimated by the MODULUS program shows a shallow depth as compared to the other locations. Since shallower depth to a stiff layer will cause the envelope to move to the upper-right direction, the position of location 5 in the figure will need a separate envelope with which to compare. A similar situation exists for location 3. Location 6 was identified as being in a severely cracked condition, and in the figure it shows less deviation from the envelope. No explanation can be found at present for what caused this to happen. Overall, the *F2-AREA* relationship can identify the AC layer condition quite well.

As demonstrated in this section, the *F2-AREA* relationship can be used to identify whether a pavement is damaged or not. However, caution should be used when comparing the measured *F2* and *AREA* with those obtained from the intact pavement models. The AC layer thickness and depth to a stiff layer appear to have some impact on the *F2-AREA* relationships. Different envelopes should be used for different pavement structures when this approach is used. Envelopes can be established using FEM forward calculations, and this procedure can be implemented using ANNs.

7.5. Summary

Unlike the majority of the existing backcalculation programs that iteratively adjust the layer moduli to match the measured deflections, the proposed method first determines the subgrade modulus by means of two deflection basin parameters, *BDI* and *F2*, and then applies the estimated subgrade modulus and other parameters as input variables to a trained ANN to estimate the upper layers' moduli. In contrast to other programs that require the input of seed values for layer moduli, this method does not require initial estimates as input. Because most of the computation time is spent upfront during data generation and training of the networks, this approach is computationally efficient. Therefore, this proposed method is applicable for routine tasks and field use.

8. CONCLUSIONS AND RECOMMENDATIONS

In this study, synthetic deflections were obtained using FEM forward calculations. Various pavement conditions were studied, including intact, hidden crack, and stripping in the AC layer. Infinite depth to a stiff layer was assumed and linear elastic material was employed in all FEM models. Dynamic analysis and a two-dimensional axisymmetric model were employed to carry out the analysis. Synthetic deflections were then studied together with known pavement conditions. A deflection basin parameter approach was

taken for the development of pavement evaluation procedures. Field FWD deflections were further incorporated to validate the proposed procedures. These procedures can also be implemented using computer programs and Artificial Neural Networks.

8.1. Conclusions

Within the limits of this study, the following conclusions can be drawn:

1. The deflection basin parameters, *BDI* and *F2*, can be used to determine the elastic modulus of the subgrade of a pavement. The AC layer moduli can then be estimated by using the predicted subgrade layer moduli along with other deflection basin parameters. These estimation procedures are automated by using ANNs.
2. The E_{sg} prediction procedure based on the *BDI-F2* relationship seems to predict stress-softening and stress-hardening effects of different soils quite well.
3. Results from this study confirm that moduli of the subgrade are generally underestimated when dynamic FWD deflections are analyzed using static analysis-based programs. Better estimation of the layer moduli can be achieved by employing dynamic analysis to process the FWD measurements.
4. The pavement condition, whether it is damaged or not, may be detected using the deflection basin parameters *F2* and *AREA*. However, no specific type of distress can be identified using the current method.
5. The prediction procedure as implemented through ANNs is ideally suited for field applications. Most of the computation time is spent upfront during the training of the network, and these trained networks can then be used for prediction with very small computation requirements.

8.2. Recommendations

This study has been limited to the investigation of pavements with infinite depth to a stiff layer. Therefore, the effects of depth to a stiff layer need to be studied to complete these evaluation procedures. More field measurements are needed to further verify the proposed procedures. Additional research is needed to investigate the effects of stress-dependency of unbound materials on the proposed procedures. Simulation of various distress types using FEM should also be improved in future studies. Further research should be done to extend the proposed procedures to pavements with an aggregate base layer thicker than 450 mm or with a cement-treated base.

9. IMPLEMENTATION AND TECHNOLOGY TRANSFER

The final deflection analysis procedure recommended for implementation by NCDOT is described in details under Section 3. Proposed Deflection Analysis Procedure of Part I of this report (pages 4 to 6). A MATLAB program that can take the field FWD

deflections directly as input and then estimate the pavement layer moduli has been developed in this study and is available to NCDOT for implementation. However, the MATLAB program and the Neural Network Toolbox developed by MathWorks, Inc., are needed to run this program. This MATLAB program is platform independent, e.g., analysis can be done on a PC, a MAC, or various types of workstations, as long as the MATLAB program is available. This program can also be converted to an executable file using the Compiler Toolbox from MathWorks, Inc., which will make the analysis easy and practical for all levels of users.

It must be noted that the following restrictions apply to the use of this procedure:

1. The depth to a stiff layer of the pavement being evaluated must be infinity or relatively deep (deeper than 4 m) because the procedure was developed from a data base using infinity as the depth to a stiff layer.
2. This procedure is valid for full-depth AC pavements (2-layer) and 3-layer pavement systems with an aggregate base layer thickness that does not exceed 450 mm. It is not to be used for analyzing deflections obtained from pavements with a cement-treated base layer.
3. The prediction accuracy needs to be improved by incorporating a larger data base of deflection basins in the training process. This is particularly true for the 3-layer pavement system.

The following guidelines are given for field data collection to use the recommended procedure:

1. The recommended procedure was developed based on the FWD data collection procedure currently used by the NCDOT. Therefore, there is no need of modifying the current NCDOT FWD test procedure to use the recommended procedure.
2. It is recommnended to analyze deflection basins from different locations individually instead of analyzing only selected representative basins. The analysis results from the individual deflection basins of the same pavement section can be evaluated together to assess the overall condition of the pavement and to determine appropriate rehabilitation and maintenance strategies.
3. It is recommended that cores be obtained according to the current NCDOT practice. The thicknesses and condition of the cores need be compared with the input data and prediction results. The findings from this comparison will be an excellent feedback to improve the prediction reliability of the recommended deflection analysis procedure for the future uses.
4. Since the procedure is valid only for pavements with a deep stiff layer, it is important to check the depth of a stiff layer. When this data is not available in original construction records or too time consuming to identify, MODULUS 5.0 program can be used to obtain approximate information on the depth of a stiff layer.

References

1. Yoder, E. J. and M. W. Witczak, *Principles of Pavement Design*, Second Edition, John Wiley & Sons, Inc., 1975.
2. Jung, F. W. and D. F. E. Stolle, "Nondestructive Testing with Falling Weight Deflectometer on Whole and Broken Asphalt Concrete Pavements," In *Transportation Research Record 1377*, TRB, National Research Concil, Washington, D.C., 1992, pp. 183-192.
3. Hossain, M. and L. A. Scofield, "Interpretation of Backcalculated Layer Moduli of Crack-and-Seat Pavement from Falling Weight Deflectometer Data," In *Transportation Research Record 1377*, TRB, National Research Concil, Washington, D.C., 1992, pp. 167-171.
4. Uddin, W., R. B. Hackett, A. Joseph, Z. Pan, and A. B. Crawley, "Three-Dimensional Finite-Element Analysis of Jointed Concrete Pavement with Discontinuities," In *Transportation Research Record 1482*, TRB, National Research Concil, Washington, D.C., 1995, pp. 26-32.
5. Chang, D-W., Y. V. Kang, J. M. Roesset, and K. H. Stokoe II, "Effect of Depth to Bedrock on Deflection Basins Obtained with Dynaflect and Falling Weight Deflectometer Tests," In *Transportation Research Record 1355*, TRB, National Research Concil, Washington, D.C., 1992, pp. 8-16.
6. Thompson, M. R., "ILLI-PAVE Based NDT Analysis Procedures," In *Nondestructive Testing of Pavements and Backcalculation of Moduli (A. J. Bush III and G. Y. Baladi, Eds.)*, ASTM STP 1026. ASTM, Philadelphia, 1989, pp. 229-244.
7. Hibbitt, Karlsson and Sorensen, Inc., *ABAQUS Finite Element Computer Program*, Version 5.5, 1995.
8. Chen, D-H., M. Zaman, J. Laguros, and A. Soltani, "Assessment of Computer Programs for Analysis of Flexible Pavement Structure," In *Transportation Research Record 1482*, TRB, National Research Concil, Washington, D.C., 1995, pp. 123-133.
9. Zaghloul, S. M., and T. D. White, "Use of a Three-Dimensional, Dynamic Finite Element Program for Analysis of Flexible Pavement," In *Transportation Research Record 1388*, TRB, National Research Concil, Washington, D.C., 1993, pp. 60-69.
10. Kuo, C-M., K. T. Hall, and M. I. Darter, "Three-Dimensional Finite Element Model for Analysis of Concrete Pavement Support," In *Transportation Research Record 1505*, TRB, National Research Concil, Washington, D.C., 1995, pp. 119-127.
11. Mallela, J., and K. P. George, "Three-Dimensional Dynamic Response Model for Rigid Pavements," In *Transportation Research Record 1448*, TRB, National Research Concil, Washington, D.C., 1994, pp. 92-99.
12. Zaghloul, S. M., T. D. White, and T. Kuczek, "Evaluation of Heavy Load Damage Effect on Concrete Pavements Using Three-Dimensional, Nonlinear Dynamic

Analysis," In *Transportation Research Record 1449*, TRB, National Research Concil, Washington, D.C., 1994, pp. 123-133.

13. Lee, Yung-Chien, *Flexible Pavement Condition Assessment Using Deflection Data*, Dissertation, North Carolina State University, Raleigh, NC, 1997.
14. Davies, T. G., and M. S. Mamlouk, "Theoretical Response of Multilayer Pavement Systems to Dynamic Nondestructive Testing," In *Transportation Research Record 1022*, TRB, National Research Concil, Washington, D.C., 1985, pp. 1-7.
15. Roesset, J. M. and K-Y. Shao, "Dynamic Interpretation of Dynaflect and Falling Weight Deflectometer Tests," In *Transportation Research Record 1022*, TRB, National Research Concil, Washington, D.C., 1985, pp. 7-16.
16. Sebaaly, B. E., M. S. Mamlouk, and T. G. Davies, "Dynamic Analysis of Falling Weight Deflectometer Data," In *Transportation Research Record 1070*, TRB, National Research Concil, Washington, D.C., 1986, pp. 63-68.
17. Nazarian, S., and K. M. Boddapati, "Pavement-Falling Weight Deflectometer Interaction Using Dynamic Finite-Element Analysis," In *Transportation Research Record 1482*, TRB, National Research Concil, Washington, D.C., 1995, pp. 33-43.
18. Uddin, W., D. Zhang, and F. Fernandez, "Finite Element Simulation of Pavement Discontinuities and Dynamic Load Response," In *Transportation Research Record 1448*, TRB, National Research Concil, Washington, D.C., 1994, pp. 100-106.
19. Cho, Y-H., B. F. McCullough, and J. Weissmann, "Considerations on Finite-Element Method Application in Pavement Structural Analysis," In *Transportation Research Record 1539*, TRB, National Research Concil, Washington, D.C., 1996, pp. 96-101.
20. Hibbitt, Karlsson and Sorensen, Inc., *ABAQUS User's Manual*, Version 5.5, 1995.
21. Seed, H. B., and I. M. Idriss, *Soil Moduli and Damping Factors for Dynamic Response Analyses*, Report No. ERRC 70-10, Earthquake Engineering Research Center, College of Engineering, U. of California, Berkekey, California, Dec., 1970.
22. Kim, Y. R., B. O. Hibbs, Y-C. Lee, and E. H. Inge, Jr., *Asphalt Paving Material Properties Affected by Temperature*. Center for Transportation Engineering Studies, North Carolina State University, Raleigh, March 1994.
23. Kim, Y. R., S. Park, and L. Shao, *Statewide Calibration of Asphalt Temperature Study from 1992 and 1993*. Draft Final Report Submitted to the North Carolina Department of Transportation, North Carolina State University, Raleigh, Oct. 1996.
24. Khosla, N.P., N. Kim, S. Satish, and Y.R. Kim, "A Comparative Study of Performance of Different Designs for Flexible Pavements," Paper submitted to the 8th International Conference on Asphalt Pavements, 1996.
25. Hveem, F. N., "Pavement Deflection and Fatigue Failures," In *Highway Research Board Bulletin 114*, 1955, pp. 43-73.

26. Shrivner, F.H., Moore, W.M., McFarland, W.F., and Carey, G.R. *A system approach to the flexible pavement design problem.* Res. Report no. 32-11, Texas Transportation Institute, College Station, TX, 1968.

27. Horak, E., "The Use of Surface Deflection Basin Measurements in the Mechanistic Analysis of Flexible Pavements," Proc., Sixth International Conference on the Structural Design of Asphalt Pavements, U. of Michigan, Ann Arbor, 1987, pp. 990-1001.

28. Hoffman, M. S. and Thompson, M. R., *Mechanistic Interpretation of Nondestructiv Pavement Testing Deflections*, Univ. of Ill. at Urbana-Champaign, Transportation Engineering Series 32, Illinois Cooperative Highway and Transportation Research Program Series 188, June 1981.

29. Peterson, G. and Shephard, L.W., *Deflection Analysis of Flexible Pavements*, Final Report, Material and Testing Division, Utah State Dept. of Highways, UT., 1972.

30. Claessen, A. I. M., C. P. Valkering, and R. Ditmarsch, "Pavement Evaluation with the Falling Weight Deflectometer," Proc., AAPT, Vol. 45, 1976, pp. 122-157.

31. Wimsatt, A. J., M. R. Murphy, and S. R. Lambert, "The Load Spreadability Index: A Method for Analyzing Falling Weight Deflectometer Deflection Data," Informal report obtained from Pavement Section, Design Division, Texas Department of Transportation, 1995.

32. Dehlen, G. L., "Flexure of a Road Surfacing, Its Relation to Fatigue Cracking, and Factors Determining Its Severity," In *Highway Research Board Bulletin 321*, 1962, pp. 26-39.

33. Ford, M. C. and J. R. Bissett, "Flexible Pavement Performance Studies in Arkansas," In *Highway Research Board Bulletin 321*, 1962, pp. 1-15.

34. Kung, K-Y, "A New Method in Correlation Study of Pavement Deflection and Cracking," Proc., Second International Conference on the Structural Design of Asphalt Pavements, U. of Michigan, Ann Arbor, 1967, pp. 1037-1046.

35. Vaswani, N. K., "Method for separately evaluating structural performance of subgrades and overlying flexible pavements," In *Highway Research Record 362*, Highway Research Board, 1971, pp. 48-62.

36. Stock, A. F. and J. Yu, "Use of Surface Deflection for Pavement Design and Evaluation," In *Transportation Research Record 954*, TRB, National Reseach Concil, Washington D.C., 1984, pp. 64-69.

37. Rumelhart, D. E., J. L. McClelland, and the PDP Research Group, *Parallel distributed processing - Volume 1: Foundation*, MIT Press, Cambridge, Mass., 1986.

38. *Neural Network Toolbox*, User's Guide, The MathWorks, Inc., May 1995.

39. Kim, Y. R. and Y-C. Lee, "Interrelationships Among Stiffness of Asphalt-Aggregate Mixtures," In Journal of Association of Asphalt Paving Technologies, Vol. 64, 1995, pp. 575-609.

40. Holland, J. H., *Adaptation in natural and artificial systems*, University of Michigan Press, Ann Arbor, 1975.

41. Goldberg, D. E., *Genetic algorithms in search, optimization and machine learning*, Addison-Wesley, Reading, Mass., 1989.

42. AASHTO Guide for Design of Pavement Structures Washington, D. C., 1986.

43. Baltzer, S. and J. M. Jansen. "Temperature Correction of Asphalt-Moduli for FWD-Measurements," Proc. 4th International Conference on Bearing Capacity of Roads and Airfields, Vol. 1, Minneapolis, MN, 1994.

44. Inge, E. H. and Y. R. Kim, "Prediction of Effective Asphaltic Layer Temperature," *Transportation Research Record*, 1473, TRB, Washington, D. C., 1995, pp. 93-100.

45. Shao, L., S. W. Park and Y. R. Kim, "A Simplified Procedure for Prediction of Asphalt Pavement Subsurface Temperatures Based on Heat Transfer Theories," *Transportation Research Record* (in press).

46. Ullidtz, P. *Pavement Analysis*. Elsevier, New York, 1987.

47. Johnson, A. M. and R. L. Baus, "Alternative Method for Temperature Correction of Backcalculated Equivalent Pavement Moduli," *Transportation Research Record*, 1355, Transportation Research Board, Washington, D. C., 1992.

48. Kim, Y. R., B. O. Hibbs, and Y-C. Lee. "Temperature Correction of Deflections and Backcalculated Moduli," *Transportation Research Record*, 1473, TRB, Washington, D. C, 1995, pp. 55-62.

49. AASHTO Guide for Design of Pavement Structures Washington, D. C., 1993.

50. Park, S. W. and Y. R. Kim, "Temperature Correction of Backcalculated Moduli and Deflections Using Linear Viscoelasticity and Time-Temperature Superposition," *Transportation Research Record* (in press).

APPENDICES

Appendix A Case Study - Viscoelastic Analysis Using ABAQUS

Asphalt concrete is the key component that dominates the performance of flexible pavements. Behavior of the asphalt concrete material in flexible pavements cannot be completely described by commonly available pavement analysis programs which are based on the multi-layered linear elastic theory. To better understand the behavior of a flexible pavement under repeated traffic load, it is preferable to use appropriate material models (i.e., viscoelastic model for asphalt concrete mixture) for pavement structural analysis.

The objective of this study is to investigate the suitability of using a viscoelastic material model for pavement structural analysis using ABAQUS. Relaxation moduli of asphalt concrete mixtures were first determined from the laboratory. A series of cyclic controlled-load/deformation tests were carried out. Finite element analyses of these tests were performed using ABAQUS. Much agreement was found between the laboratory measured responses and the calculated values. A flexible pavement structure with field FWD history measurements was further analyzed using both elastic and viscoelastic material models. The results show that viscoelastic model can better describe the behavior of a flexible pavement than the elastic model. From this finding, better estimation of the in-service pavement performance under repeated traffic loads may result.

A.1 Formulations

Asphalt concrete is a viscoelastic particulate composite comprised of aggregate particles (rigid, elastic) and an asphalt binder (viscoelastic). Therefore, its current stress is a function of the current strain and strain rate and/or past values of strain rate. A typical creep and recovery test for viscoelastic material characterization is presented in Figure A.1. It can be seen that a viscoelastic material responds with its elastic deformation immediately when a load is applied and then creeps under the constant load. A portion of the elastic deformation recovers immediately when the load is removed, and then relaxation follows. Unlike elastic materials, the response of a viscoelastic material under load is a function of time.

Asphalt concrete is also known as a thermo-rheological material whose response under load depends upon temperature in addition to the time-dependent behavior described above. For a non-aging, linear viscoelastic medium, the uniaxial stress and strain relationship can be described by the following convolution integrals:

$$\sigma(t) = \int_0^t E(t-\tau)\frac{d\varepsilon(\tau)}{d\tau}d\tau \qquad \text{(A.1)}$$

$$\varepsilon(t) = \int_0^t D(t-\tau)\frac{d\sigma(\tau)}{d\tau}d\tau \qquad \text{(A.2)}$$

where $\sigma(t)$ = stress at time t,

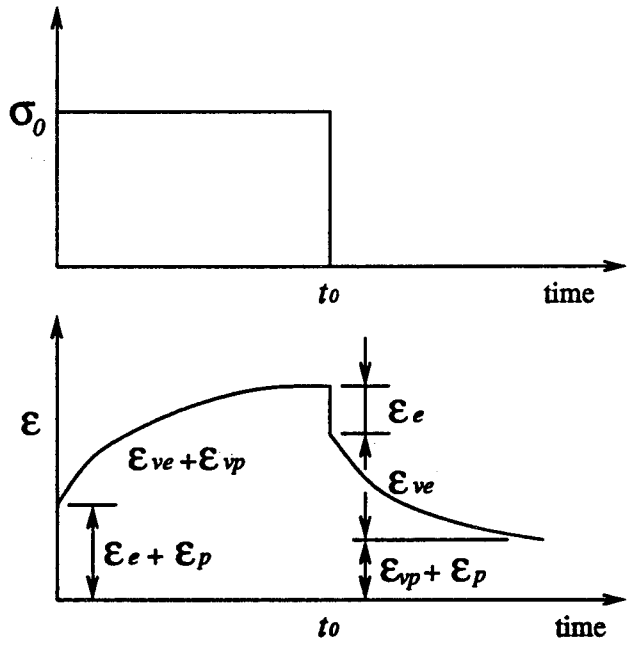

Figure A.1: Creep and recovery test of a viscoelastic material.

$\varepsilon(t)$ = strain at time t,
$D(t)$ = creep compliance as a function of time, t,
$E(t)$ = relaxation modulus as a function of time, t, and
τ= the integration parameter.

Thus, the behavior of a linear viscoelastic material can be characterized by either its creep compliance or relaxation modulus. In general, the properties of asphalt concrete mixtures can be determined in the laboratory and are affected by many factors such as: viscosity of asphalt cement, aggregate gradation, temperature, etc. It has been demonstrated by Kim and Lee [39] that an asphalt-aggregate mixture is a thermo-rheologically simple material; that is, a master creep compliance curve can be constructed by horizontally shifting creep curves at different temperatures to a reference temperature curve along the log time axis. The master creep compliance (or master relaxation modulus) function can present the viscoelasticity of the material in a more complete manner by obtaining short-time and long-time deformation behavior from lower and higher temperatures (so-called time-temperature correspondence).

ABAQUS provides two ways of describing the viscoelastic material behavior, time domain analysis and frequency domain analysis. It is convenient to use the time domain representation because all the measurements obtained in the laboratory are described as a function of time. The viscoelastic model described in ABAQUS is

$$\tau(t) = G\left[\gamma(t) + \int_0^t g(t-s)\frac{d\gamma(s)}{ds}ds\right] \tag{A.3}$$

where $\tau(t)$ = shear stress at time t,
$\gamma(t)$ = shear strain at time t,
$g(t)$ = shear relaxation modulus as a function of time, t,
G = long term elastic shear modulus, and
s = the integration parameter.

For the relaxation test, g is the constant strain. Thus,

$$\tau(t) = G\left[1 + g(t)\right]\gamma \tag{A.4}$$

The time dependent t-g relationship measured in the relaxation test is often characterized by the time dependent relaxation modulus $G_R(t)$:

$$\tau(t) = G_R(t)\gamma \tag{A.5}$$

Comparing Equations A.4 and A.5, we obtain the result that

$$g(t) = \left[\frac{G_R(t)}{G} - 1\right] \tag{A.6}$$

Material parameters needed for the ABAQUS viscoelastic model are the shear modulus and bulk modulus, whereas the modulus obtained from the laboratory is typically measured in a uniaxial test mode. An analytical procedure is needed to convert the uniaxial relaxation modulus to the shear modulus and bulk modulus. Assuming the material is isotropic and non-aging, the relationships among relaxation modulus, shear modulus, and bulk modulus can be represented as,

$$\tilde{K} = \frac{\tilde{E}}{3(1-2\tilde{\nu})}, \quad \tilde{G} = \frac{\tilde{E}}{2(1+\tilde{\nu})} \tag{A.7}$$

where $\tilde{K}$ = Carson transform of the bulk relaxation modulus,

$\tilde{G}$ = Carson transform of the shear relaxation modulus,

$\tilde{E}$ = Carson transform of the uniaxial relaxation modulus, and

$\tilde{\nu}$ = Carson transform of Poisson's ratio.

Assuming Poisson's ratio does not change with time, the Carson transform of the Poisson's ratio ($\tilde{\nu}$) becomes a constant (ν). Therefore, the shear and bulk relaxation moduli can be estimated from the uniaxial relaxation modulus in the following relationships:

$$K(t) = \frac{E(t)}{3(1-2\nu)}, \quad G(t) = \frac{E(t)}{2(1+\nu)} \tag{A.8}$$

It is convenient to present the relaxation modulus in Prony series format for time history analysis. The Prony series expression of the relaxation modulus is

$$G_R(t) = G + \sum_{i=1}^{N} G_i^p \, e^{(-t/\tau_i^p)} \tag{A.9}$$

where G = long term shear modulus, and

N, G_i^p, and τ_i^p (i =1, 2, ..., N) are material constants.

A MATLAB program was written to quickly obtain the coefficients of the Prony series expression of the relaxation modulus. Figure A.2 demonstrates the Prony series fitted data and the measured relation modulus. As can be seen, the Prony series fits the measured data very well. The coefficients of the Prony series are then given to the ABAQUS input data deck to describe the viscoelastic material behavior.

A.2 Analysis of Cyclic Loading Test

Laboratory measurements from two types of asphalt concrete mixtures, AAD and AAM, were used to evaluate the viscoelastic material model in ABAQUS. Two types of tests, controlled-load and controlled-deformation mode, were conducted in this task. The tests were performed by applying a constant magnitude of 10 Hz cyclic load/deformation to 102-mm (4-inch) diameter by 203-mm (8-inch) height specimens. Three levels of load and deformation were conducted on each mixture as described in Table A.1.

Table A.1: Load and deformation levels used for cyclic loading tests.

Mixture Type	Controlled-Load (kN)	Controlled-Deformation (mm)
AAD	0.267	0.1270
	0.489	0.1778
	0.978	0.2794
AAM	0.5	0.1270
	1.1	0.1778
	2.0	0.2794

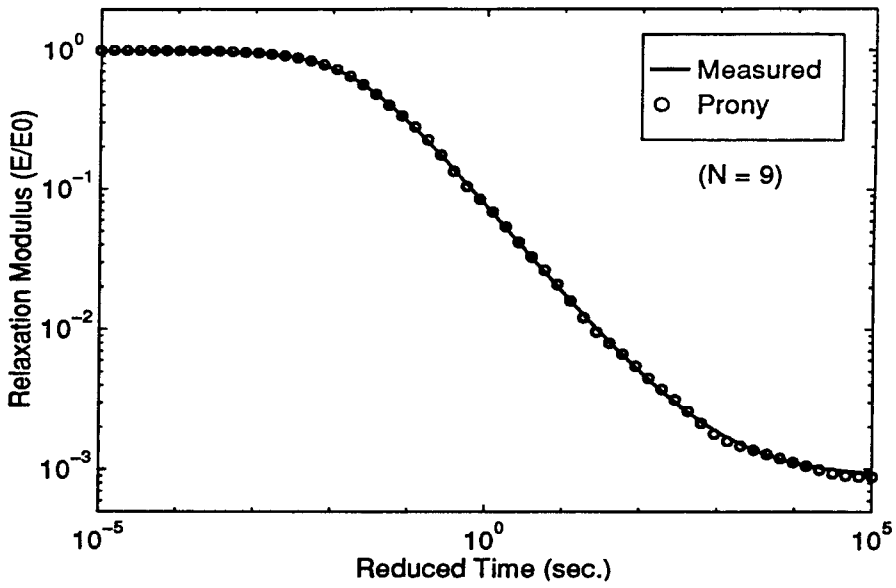

Figure A.2: Measured relaxation modulus and its Prony series data.

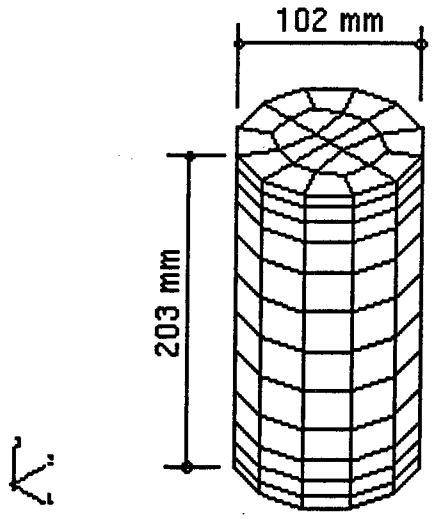

Figure A.3: 3-D finite element mesh of the testing specimen.

Three-dimensional elements were used to model the specimen as presented in Figure A.3. The cyclic controlled-load test was modeled by applying the actual loading history data measured in the laboratory to the top elements of the model, while the cyclic controlled-deformation test was modeled by applying the actual deformation data measured in the laboratory to the model through the BOUNDARY option in the DYNAMIC analysis procedure in ABAQUS. Dynamic analysis with a viscoelastic material model was used for all test cases. The Prony series expressions of the shear and bulk relaxation moduli were calculated from the measured relaxation modulus in uniaxial mode for both mixtures according to Equations A.7 to A.9 described previously.

Figure A.4 presents the measured and calculated deformations from the three load levels of the controlled-load test mode of the AAM mixture. Much agreement was found to exist between the measured and predicted values, except for in the case of the highest load level. This is probably due to the the fact that the given load (2 kN) has exceeded the linear range of the viscoelastic model. Similar results were discovered for the AAD mixture. Good agreement between the measured and predicted stresses was found for both mixtures for controlled-deformation tests as shown in Figure A.5. There is a discrepancy between the peak values for the AAM mixture. This may, again, be due to the fact that the resulting load has exceeded the linear range of the material. In general, ABAQUS produces good results as long as the applied load to the specimen is within the linear range of that material.

A.3 Analysis of Flexible Pavements

To evaluate how much improvement the viscoelastic model can make in predicting pavement responses, further studies were carried out. Two analyses were conducted on a pavement structure (same finite element mesh, loading, and boundary conditions) with the material model of the asphalt concrete layer being elasticity and viscoelasticity. Actual FWD measurements obtained from the flexible pavement section of US 70 near Clayton, North Carolina were used for this task. This pavement section consists of a 140 mm (5.5 in.) thick AC layer, a 280 mm (11 in.) thick granular aggregate base course, and a subgrade with a fixed thickness of 1219 mm (48 in.). Further information about this section and FWD tests performed can be found elsewhere [22]. This pavement was modeled using ABAQUS 2-D, axisymmetric finite elements. An interface element was employed in the outer-most elements to simulate the infinite extend in the lateral direction of the pavement. FWD loading history data was applied to the finite element model by assuming the load was uniformly distributed over a circular plate with a radius of 150 mm (5.91 in.). This history data is presented in Figure A.6.

For elastic analysis, layer moduli were obtained by the MODULUS backcalculation program, except the AC modulus which was based on the AC

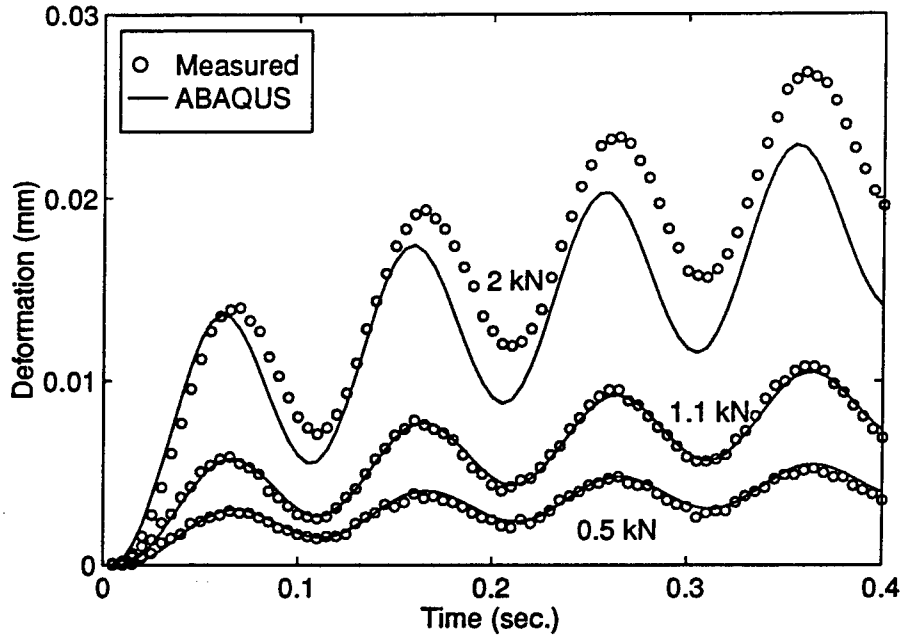

Figure A.4: Measured and calculated deflections of the cyclic controlled-load tests for AAM mixture.

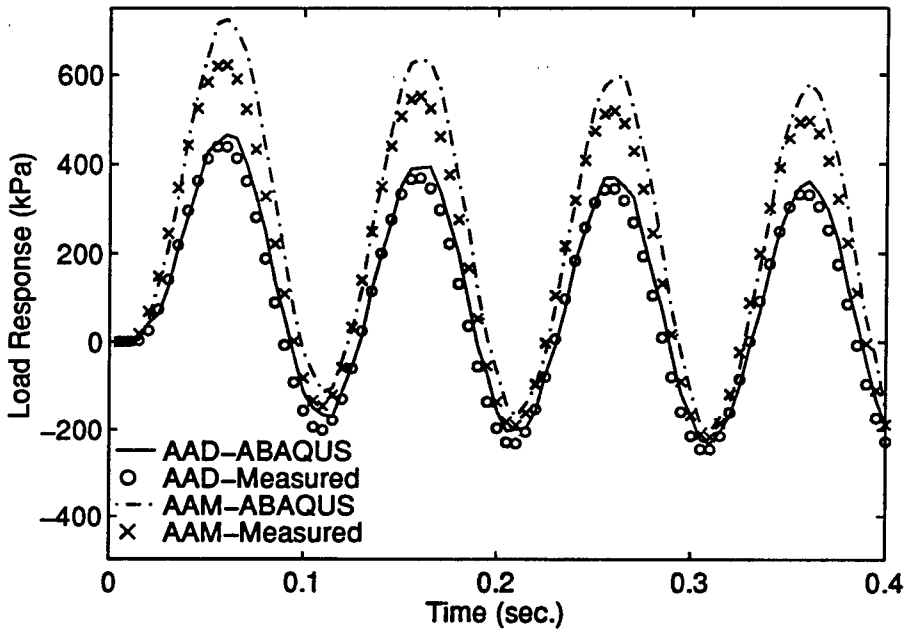

Figure A.5: Measured and calculated pressure of the cyclic controlled-strain tests (at 0.127 mm deformation) for AAD and AAM mixtures.

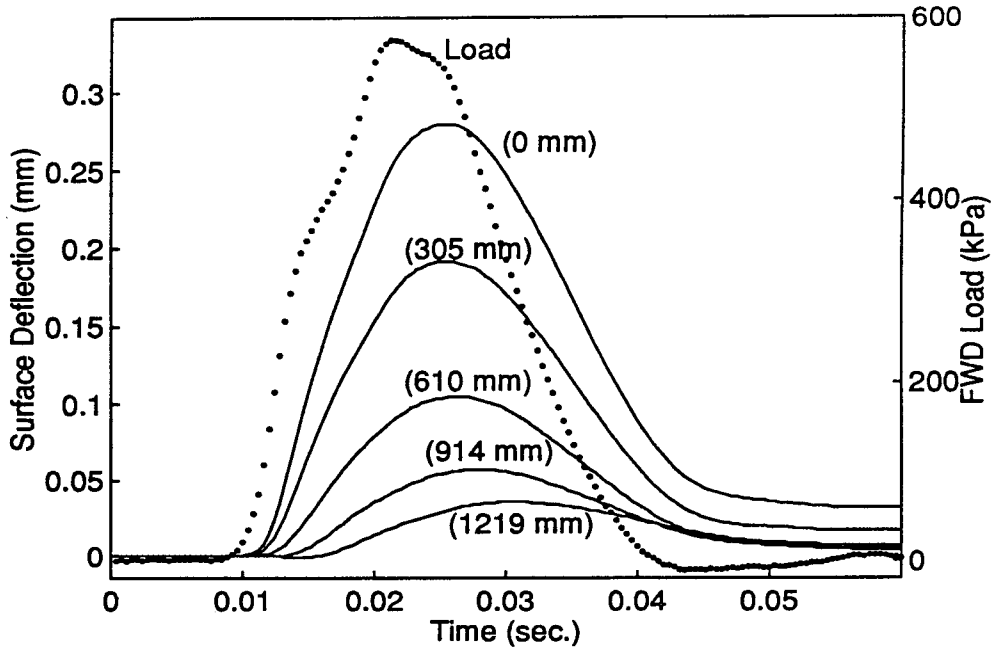

Figure A.6: FWD history data measured from US 70 near Clayton, NC (Oct. 1992).

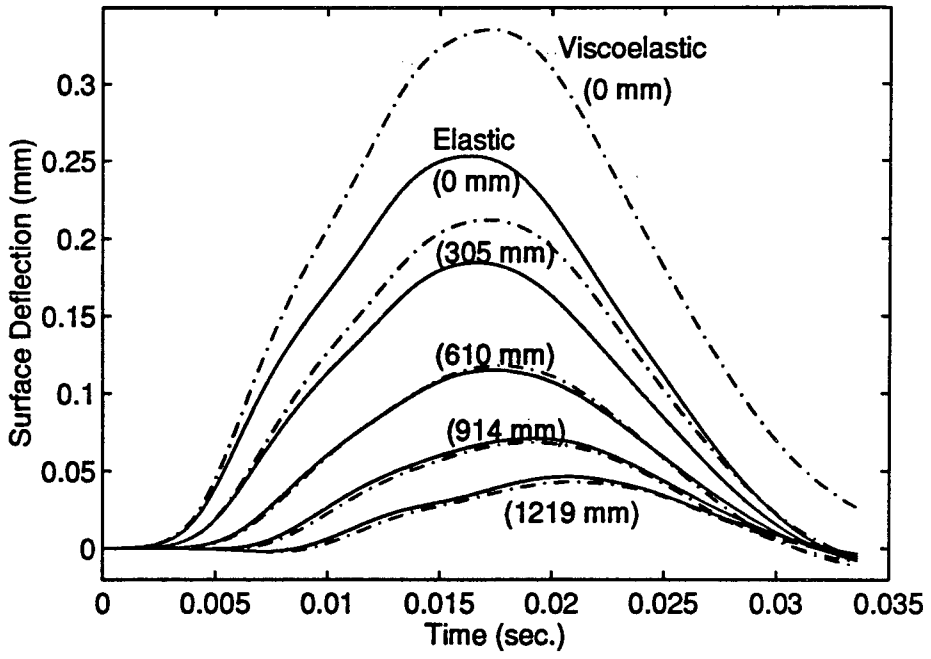

Figure A.7: Comparison of elastic and viscoelastic deflections under an FWD load calculated by ABAQUS.

temperature at the time of the FWD test and the loading frequency. For viscoelastic analysis, the relaxation modulus of the asphalt concrete mixture was obtained from laboratory tests using the same type of mixture that was used in the field [38]. This relaxation modulus was then incorporated into ABAQUS by means of the Prony series expression.

Results of these two analyses are presented in Figure A.7. As can be seen, the deflection of the first sensor computed from the viscoelastic analysis does not return to its original position when the load is removed, while the deflection caused by the elastic analysis does return to zero. This is to be expected because of the time-dependent characteristic (relaxation) of the viscoelasticity. The same phenomenon is observed in the field measurements as presented in Figure A.6. The discrepancy in peak deflections between these two cases is due to the difference in the material parameters used by the two models. Another important point to be made is that no significant difference can be found between the two cases for the deflections obtained after the fourth sensor (a radial distance of 614 mm from the loading center). This indicates that the surface deflections measured at a radial distance larger than 614 mm from the load are not affected by the AC layer. This phenomenon agrees with the layered elastic theory.

A.4 Temperature Consideration

Another important factor that affects the properties of the viscoelastic material is the temperature. For thermo-rheologically simple materials, a master curve can be constructed at a reference temperature. In order to compute deflections under an FWD load and compare them against the measured values, it is necessary to obtain the relaxation modulus at an "effective" pavement temperature at the time of the FWD test. ABAQUS provides an option to use the time-temperature shift function for the determination of the relaxation modulus from the master curve. The shift function is defined by the Williams-Landell-Ferry (WLF) approximation as follows:

$$\log(A) = -\frac{C_1(\theta - \theta_0)}{C_2 + (\theta - \theta_0)} \qquad \text{(A.10)}$$

where θ = temperature,

θ_0 = reference temperature,

A = shift factor function of the temperature , and

C_1, C_2 = calibration factors at the reference temperature.

The laboratory master curve was constructed at the reference temperature of 25°C (77°F). The measured mid-depth temperature of the asphalt concrete layer at the time of the FWD test was 21.7°C (71°F) for this particular case. The constants of the WLF function were obtained using the laboratory data as presented in Figure A.8. Using the laboratory master curve and the shift factor at 21.7° (71°F), the relaxation modulus at that temperature was determined.

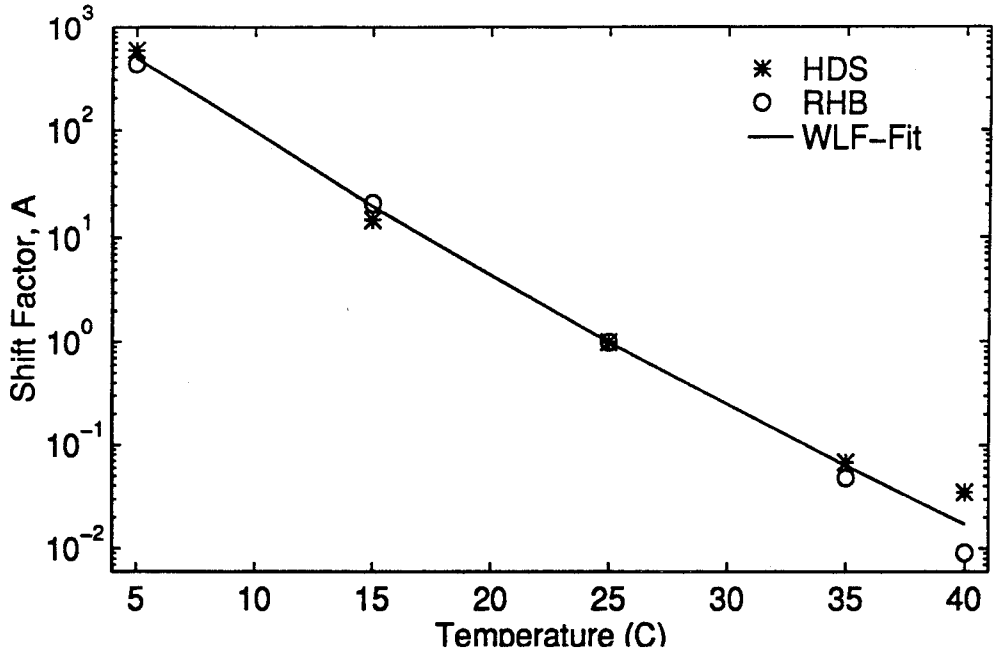

Figure A.8: WLF approximations and the measured shift factors at various temperatures.

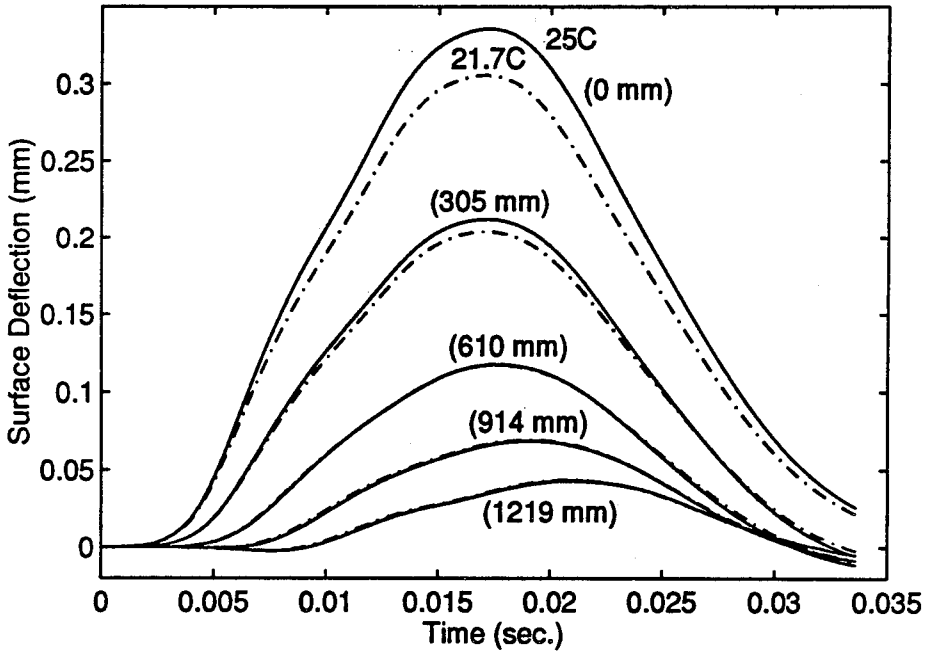

Figure A.9: Comparison of the calculated deflections at different temperatures using viscoelastic analysis with WLF shift function.

The time-temperature shift option was further incorporated in the same pavement model analyzed earlier with the WLF constants and the mid-depth pavement temperature. Similar deflection curves, though smaller in magnitude were observed (Figure A.9) when compared with the values computed without using the WLF model (25°C). This is to be expected because lower pavement temperature will yield higher modulus, and thus result in smaller deflections under the same loading condition.

A.5 Summary

This study demonstrates that ABAQUS is capable of analyzing the behavior of a viscoelastic material using the constitutive model provided in ABAQUS. Comparisons of the laboratory data and the ABAQUS calculated responses under cyclic loading tests show much good agreement except when the applied load is large. This discrepancy may be due to the fact that the applied load has exceeded the assumption of a valid linear viscoelastic model. In particular, the master relaxation modulus is constructed using the superposition method. By comparing the actual FWD history data and the calculated deflections, we have seen that the use of a viscoelastic model for flexible pavement analysis can describe the actual pavement responses more closely than those deflections carried out by a pure linear elastic material model. The temperature effect of a viscoelastic material can be incorporated using the WLF approximations.

As presented in this study, the use of appropriate material models in pavement analysis can describe the actual responses more closely under traffic loads. However, pavement materials are usually complex, and the "real" field material properties are very difficult to obtain. In addition, responses due to one factor, such as Young's modulus, can be easily overshadowed by other factors, such as temperature, moisture, distress conditions, or human error. As a result, the most accurate analysis method is not necessarily the most appropriate method for the evaluation of in-service pavement conditions.

Appendix B Case Study - ANN and GA Techniques

The primary goal of this study is to investigate the potential alternatives of backward search techniques in predicting the layer properties of a pavement system based on FWD deflection information.

Backcalculation programs are commonly used to process NDT deflections for the estimation of in-situ pavement layer properties. This task is often accomplished by matching a theoretically calculated deflection basin to the measured deflections. One of two approaches is often employed in the backcalculation programs: (1) a gradient search approach in which pavement layer moduli are iteratively adjusted until the theoretical and measured deflection basins agree within a preset allowable tolerance and (2) a data base approach that uses a combination of pattern searching and interpolation to calculate a theoretical deflection basin from exemplars within a predefined data base of basins.

There are limitations in operating these backcalculation programs in addition to the issues of realistic material models used in the multi-layered theory. First, a set of initial values is needed to run these programs, and these values have a great impact on the results. Thus, experience with these programs is almost essential in order to find reasonable answers. Secondly, computation time is generally significant, although it may be reduced with today's high performance computers. Thirdly, non-unique solutions can occur and may mislead the repair strategies. Thus, an appropriate backcalculation method should be able to work around these limitations or provide a way to prevent them from happening.

In addition to the two approaches mentioned above, other techniques are also available. Two techniques, artificial neural networks (ANNs) and genetic algorithm (GA), are investigated in this study. Backpropagation type ANNs are used to develop a nonlinear mapping between the material properties of pavement layers and the surface deflections. This is achieved by presenting many instances of the deflection information and the corresponding layer properties which must be predicted to the ANNs. After the ANN has learned the mapping, it is tested for prediction accuracy using a test data set that was not used during the development of the model.

Unlike the gradient search techniques, GA is a newer non-gradient based optimization technique that carries out global search in more efficient ways. The goodness-of-fit techniques are generally more accurate but may consume relatively more time than the ANN-based techniques. However, ANN-based techniques are only global approximators and therefore may not be as accurate as the optimization-based techniques. In this study, comprehensive analyses are carried out to evaluate the relative merits and shortcomings of these two methods. One of the primary outcomes of this task will be to provide a comprehensive comparison of these techniques with respect to their speed and accuracy in the deflection analysis of pavements.

B.1 Artificial Neural Networks

An ANN system is a collection of simple processors (generally called neurons or units) that are interconnected to form a mathematical representation of the mapping or relationship that may be embedded in any set of data. The structure of ANNs allows them to be global approximators even in the absence of knowledge about the mathematical form of the mapping between an input signal and the corresponding output signal. A multi-layered, feed-forward type network is the most common class of ANNs used for this type of mapping function. A typical multi-layered network consists of an input layer, an output layer, and one or two intermediate layers (Figure B.1). The input signal is presented to the network through the units in the input layer. This signal is then propagated through the intermediate units to the output units via the interconnections in the network. The strength of a signal passing through a unit undergoes a nonlinear transformation as shown in Figure B.1. In addition, the strength of the propagated signal is adjusted throughout the network by the connection strengths (generally called connection weights). These connection weights are updated, in an iterative manner, until the predicted output signals are as close as possible to the actual signals corresponding to those input signals. A representative sample data set that includes a set of input signals and their corresponding output signals is used during this weight updating process. This process is called training. The weight updating procedure used in this study is a modified version of backpropagation algorithm [37].

An approximation of the mapping between the input and the output signals is encoded in the connection weights of a trained network. This trained network is then able to propagate a new input signal through the network and predict the resulting output signal. In this mode of operation, the network is used as an approximate function of the mapping between the input and the output signals.

In the feed-forward type framework, the ANN is trained to capture the mapping between the deflection basin (input signal) and the corresponding pavement characteristics (output signal). Data representing many instances of pavement characteristics and the resulting deflection basins are used to train the network. The trained network, when presented with an observed deflection basin, is then able to predict the most likely set of pavement characteristics that yields the given deflection basin.

B.2 Genetic Algorithm Optimization Technique

A genetic algorithm (GA) is a non-gradient-based, probabilistic global search procedure that is designed according to the survival-of-the-fittest phenomenon prevalent in natural evolution [40,41]. A typical GA consists of the following key operations (see Figure B.2): selection (analogous to natural selection), cross-over (analogous to mating in nature), and mutation (analogous to gene mutation). A GA begins with a population of random strings of numbers (namely, pavement parameters) where each string represents a potential solution to the error minimization problem. The resulting deflection basin for

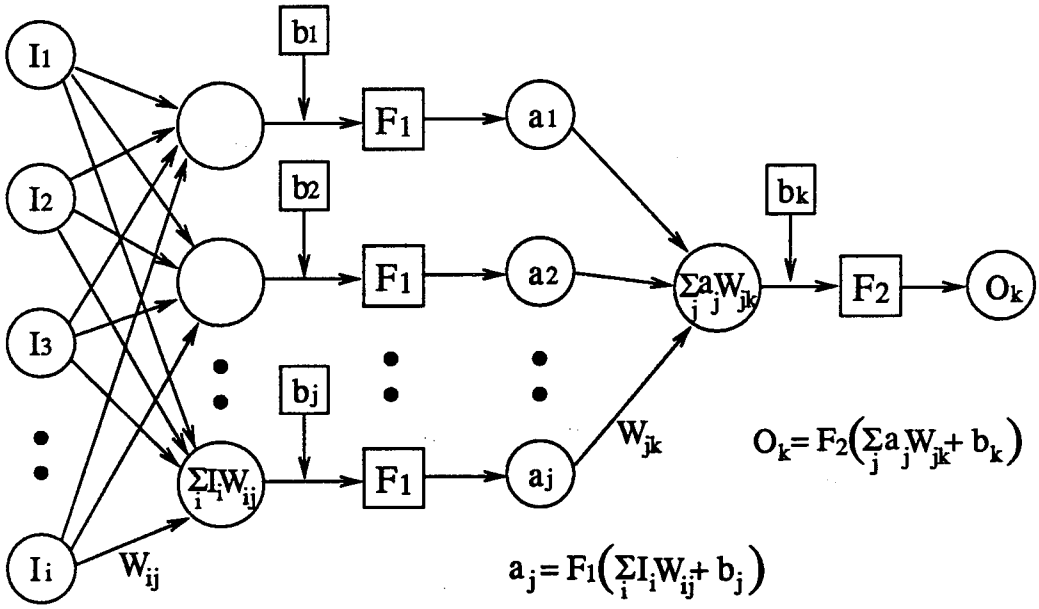

Figure B.1: Schematic diagram of the Artificial Neural Networks

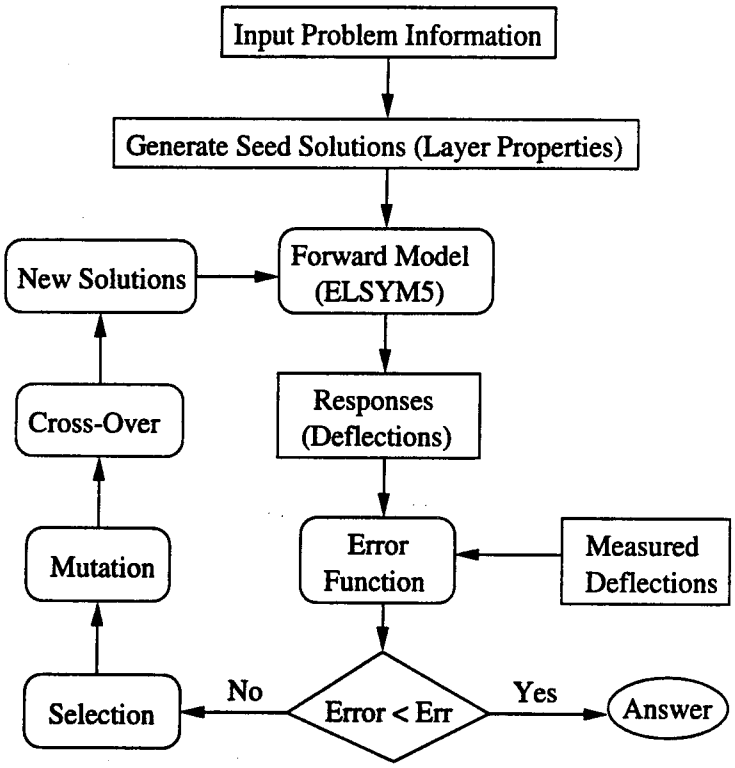

Figure B.2: Schematic diagram of the Genetic Algorithm technique.

each string (i.e., a set of pavement parameters) is then computed using a forward model and the corresponding error is recorded. During the selection operation, a mating population is selected such that strings with lower error values are given a higher chance of survival. The cross-over operation is then carried out to exchange, in a random manner, the information embedded in the strings in the mating population. The mutation operation is carried out, again in a random manner, to change arbitrarily the information at randomly selected locations. This sequence of operations is repeated iteratively until the population converges to the string (i.e., the set of pavement parameters) that minimizes the error.

The GA described above does not require any gradient information during the error minimization process. Thus, any numerical model that computes the deflection basin can be incorporated in an interchangeable manner into the algorithm. Unlike standard gradient search methods this algorithm carries out global search, and the quality of the solution does not depend on a starting solution. This feature may be useful and important in practical situations where no previous information about the pavement section under study is available. In the context of backcalculation of pavement parameters, the algorithm is set up to determine the set of pavement parameters that minimizes the error between the predicted and the actual deflections at all discrete radial offsets. This is accomplished by minimizing the maximum error occurring at all radial offsets. The accuracy of the GA-based method can be controlled by varying the error tolerance used to determine convergence.

B.3 Calculation of Deflection Basins

The Elastic Layered System computer program, ELSYM5, is used to generate the synthetic deflection basins for this study. The ELSYM5 is based on multi-layered linear elastic theory which is one of the most popular methods used by pavement engineers today. Pavement structures are usually composed of two or more layers with the highest quality and strength at the top. This theory assumes that material properties of each layer are isotropic and homogeneous, that there is full friction between interfaces, and that material properties are represented by Poisson's ratio and an elastic modulus. Detailed descriptions on the multilayered linear elastic theory can be found elsewhere [1].

A three-layer pavement structure (asphalt concrete surface layer, aggregate base layer, and subgrade) was used for this study. A 40 kN (9,000 lb. force) uniformly-distributed load was applied over an area with a radius of 150 mm (5.91 inches) to match the FWD testing. The elastic modulus and thickness of each layer were randomly selected within reasonable ranges. Poisson's ratios for AC surface layer, aggregate base, and subgrade were assumed as 0.3, 0.35, and 0.4 respectively. Surface deflection locations were selected at 0, 203, 305, 457, 610, 914, and 1219 mm (0, 8, 12, 18, 24, 36, 48 inches) offset from the center of the loading plate. The computed deflection values were then saved along with the input material properties in pairs for further study.

B.4 Application Scenarios

This case study was carried out to investigate the feasibility of using ANN and GA techniques in predicting pavement layer properties. Synthetic surface deflection data was generated using the multi-layered elastic-based program, ELSYM5, with known layer material properties under idealized FWD load of a three-layer pavement system. These data sets (deflections and material properties) served as the basis for the applications of ANN. A set of deflections was selected from the synthetic data for GA analysis.

Several scenarios were applied in the prediction of pavement characteristics, namely, layer moduli and thicknesses. In all cases, the resulting deflection basin corresponding to a given pavement condition was obtained assuming linear elastic behavior in each layer of the pavement. The deflection basin was represented by seven discrete radial offsets (typical FWD setting). A series of scenarios was defined with increasing prediction requirements from the backcalculation technique. These scenarios are summarized in Table B.1 which shows the ranges of each parameter used in each scenario.

A network was trained to capture the input-output mapping for each scenario defined above. For each scenario, the training cases were generated by applying the forward model (ELSYM5) to estimate the deflection basins corresponding to several sets of pavement parameters chosen randomly within the ranges of each parameter (as specified in Table B.1). The network configuration (i.e., number of units in each layer) and the training characteristics (i.e., number of training cases and computation time) for the scenarios are summarized in Table B.2. The training errors and the number of iterations for each network are also presented.

Table B.1: Ranges of parameters for the five scenarios.

	Case A	Case B	Case C	Case D	Case E
E_{ac}, MPa	1723 - 16547	1723 - 16547	1723 - 16547	1723 - 16547	1723 - 16547
E_{abc}, MPa	207 - 552	207 - 552	207 - 552	207 - 552	207 - 552
E_{sg}, MPa	27 - 193	27 - 193	27 - 193	27 - 193	27 - 193
H_{ac}, cm	14 (fixed)	10 - 46	14 (fixed)	10 - 46	10 - 46
H_{abc}, cm	28 (fixed)	10 - 56	28 (fixed)	10 - 56	10 - 56
H_{sg}, cm	∞	∞	100 - 760	100 - 760	100 - 760

A general framework for the GA-based method was set up to estimate the pavement parameters for any of the above scenarios. Within this framework, the method estimates the necessary pavement parameters that result in a deflection basin within a specified level of acceptable deviation from a target deflection basin. The GA method was applied only to the scenarios for which the ANN-based method failed to give reasonable results. As will be described later, the ANN-based method performed reasonably well in all scenarios except scenario E. In this scenario, six pavement parameters (the moduli and thicknesses of all three layers) were to be estimated. Therefore, each string in the GA consisted of six real valued numbers representing the six unknown pavement parameters.

The population consisted of 120 strings. Other essential GA-specific parameters are tabulated in Table B.3. The error tolerance for the maximum allowable deviation of deflection at any radial offset was set at 2%.

Table B.2. ANN testing summary.

	Case A	Case B	Case C	Case D	Case E
# of Cases	5000	5800	5000	5000	12667
Error (SSE)	0.5607	7.1148	33.2127	32.3036	366.113
Iterations	325	325	325	800	1450
Training Time (sec./iter.)[a]	10	13	15	55	63
Input Units	7 Defl.	7 Defl. H_{ac}, H_{abc}	7 Defl.	7 Defl. H_{ac}, H_{abc}	7 Defl.
Output Units	E_{ac}, E_{abc} E_{sg}	E_{ac}, E_{abc} E_{sg}	E_{ac}, E_{abc} E_{sg}, H_{sg}	E_{ac}, E_{abc} E_{sg}, H_{sg}	E_{ac}, E_{abc}, E_{sg} H_{ac}, H_{abc}, H_{sg}
Structure[b]	7x10x3x3	9x11x3x3	7x11x4x4	9x12x4x4	7x12x6x6

[a]Based on a Pentium 120 MHz machine.
[B]Structure = (input units) x (hidden units) x (hidden units) x (output units).

Table B.3. GA specific data.

No. of strings in population	120
Cross-Over probability	100%
Mutation rate (genes/iteration)	5-20%
Error tolerance	2%
Maximum of iterations	60
CPU time (sec./iteration)	76

B.5 Results and Discussions

First, the prediction performance of each network was evaluated by applying the network to predict the pavement parameters for a set of deflection basins. A common error measure was used to represent the prediction performance for each scenario and compare their relative performances. The error measure is based on the root mean square of the difference between the predicted and the actual values of individual pavement parameters. Table B.4 shows the performance of each network when tested on new input signals that were not included in the training. The number of test cases, the average prediction error for each pavement parameter, and the overall average prediction error are summarized in this table.

Table B.4. ANN testing summary.

	Case A	Case B	Case C	Case D	Case E
Test Cases	1000	1200	1000	1000	1562
Overall *RMSE*[a]	0.0039	0.0499	0.0392	0.084	0.1196
E_{ac} *RMSE*	0.0101	0.0765	0.0316	0.0459	0.0764
E_{abc} *RMSE*	0.0053	0.0364	0.0229	0.0601	0.1373
E_{sg} *RMSE*	0.0052	0.0170	0.0437	0.1103	0.1309
H_{ac} *RMSE*	--	--	--	--	0.0400
H_{abc} *RMSE*	--	--	--	--	0.1624
H_{sg} *RMSE*	--	--	0.1094	0.1017	0.1265

[a]Root-Mean-Square-Error

The prediction performances of each network are also shown graphically in Figures B.3 to B.7. Each figure compares the network predicted and the actual values of a pavement parameter. These results indicate that the networks corresponding to cases A, B, C, and D are able to predict relatively accurately the values of the moduli of the three layers. Networks for cases C and D are also able to predict the subgrade thickness to within reasonable accuracy. The network corresponding to case E, which is designed to predict the moduli as well as the thickness of all layers, did not perform well in predicting most of the parameters. The overall prediction performance of this network, which is the worst of all the cases, is not unexpected since this network has to predict two additional parameters, namely, the thickness of the AC and the ABC layers. The performance of this network may be improved by changing the network configuration (i.e., number of intermediate units) and/or by enhancing the network training through more training cases and lower error levels. Further investigation is necessary and is currently underway.

The application of the GA-based backcalculation method was limited to only scenario E in which six pavement parameters were to be determined. Table B.5 shows the target deflection basin and the pavement parameters as predicted by the GA-based method. The deflection basins corresponding to the estimated pavement parameters and the resulting error at each radial offset (which are within the specified 2% error tolerance) are also shown in Table B.5. Although the deflection basin is within 2% deviation, the estimated parameters result in a mean error of about 28% with the maximum error of about 77% corresponding to the modulus of the ABC layer. This result is compared with the ANN predicted parameters in the same table. In this case the mean error was also about 28% with the maximum error of about 65% again corresponding to the modulus of the ABC layer.

Several reasons may account for the poor prediction performance in scenario E. As mentioned previously, the network training process may be improved, or the error tolerance for the GA-based search may be tightened. These improvements may result in better prediction performance if the relationship between the pavement parameters and the resulting deflection basins is indeed unique; i.e., if it is a one-to-one relationship. This may depend on the type of forward model used to predict the deflection basin. Simple models may not be able to characterize and capture variations in some parameters, and as a result

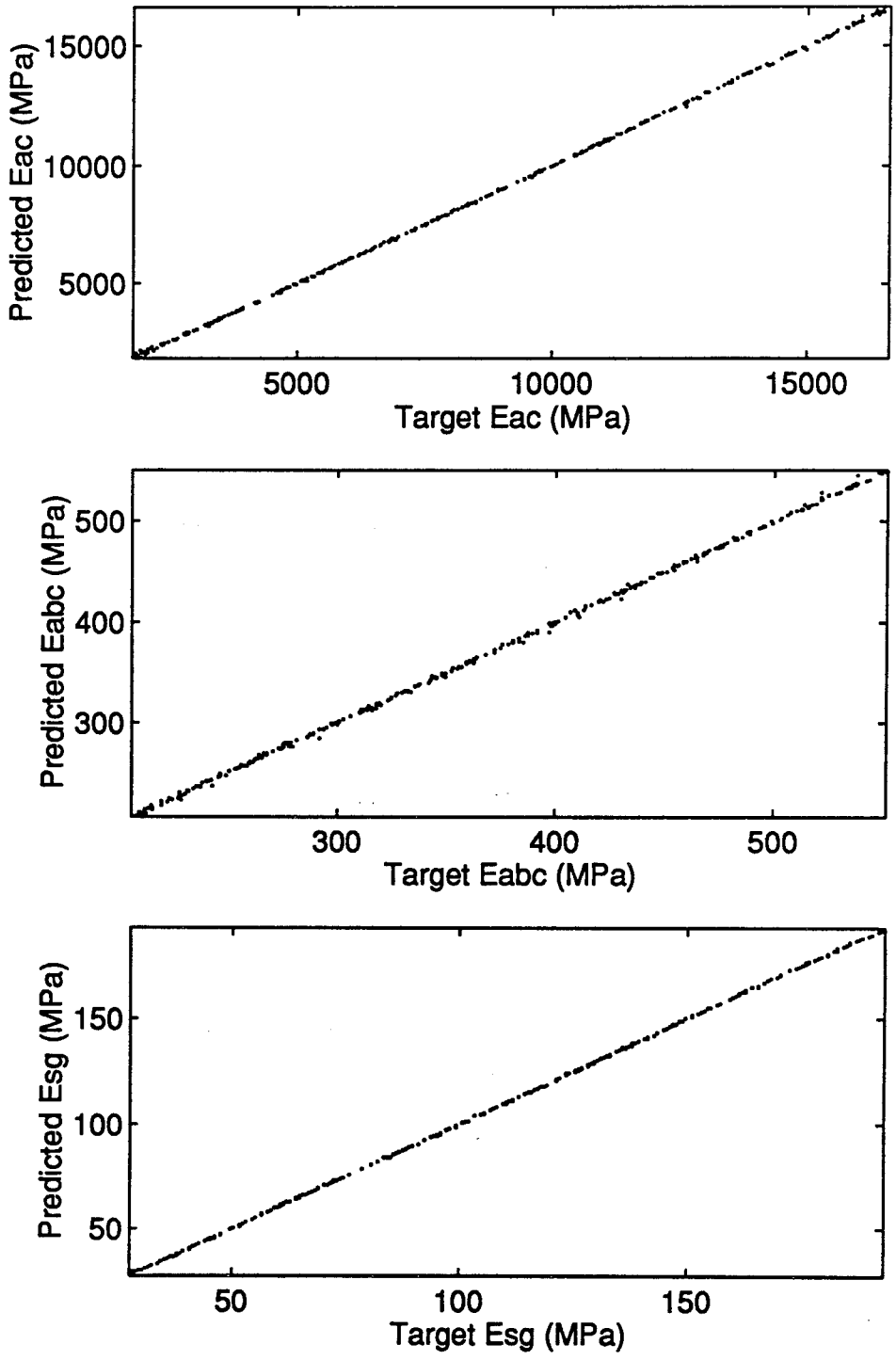

Figure B.3: Summary of testing results for scenario A.

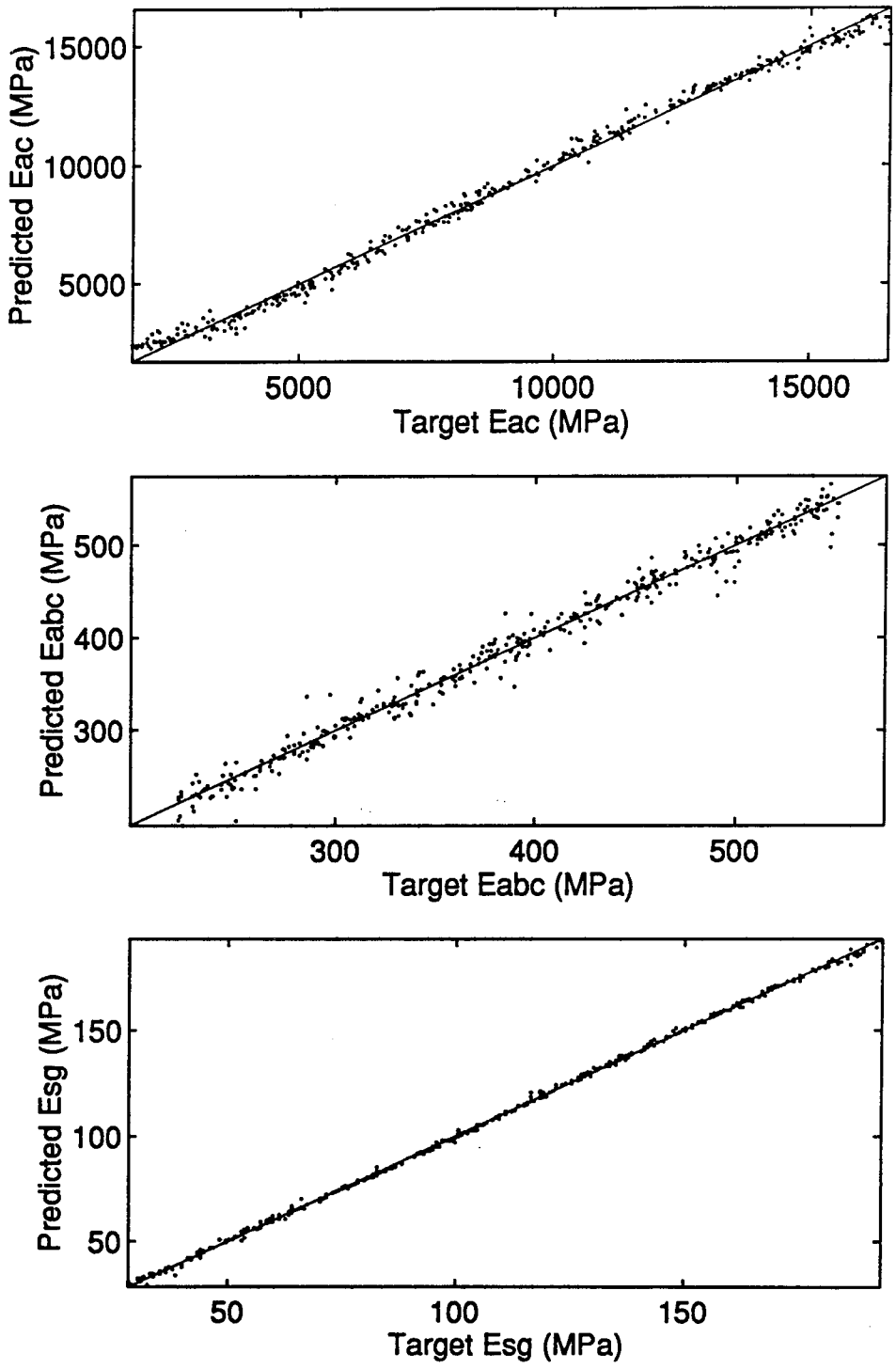

Figure B.4: Summary of testing results for scenario B.

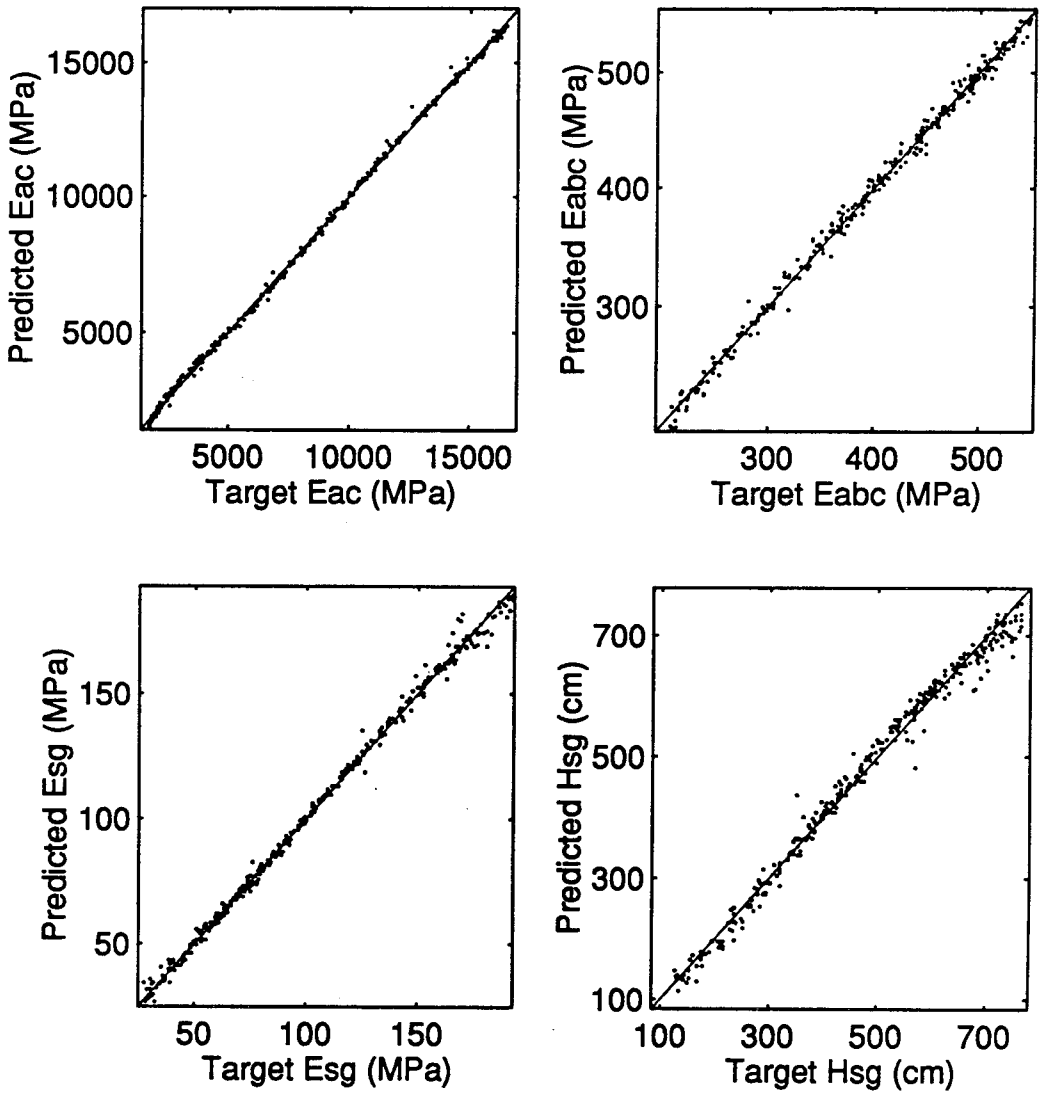

Figure B.5: Summary of testing results for scenario C.

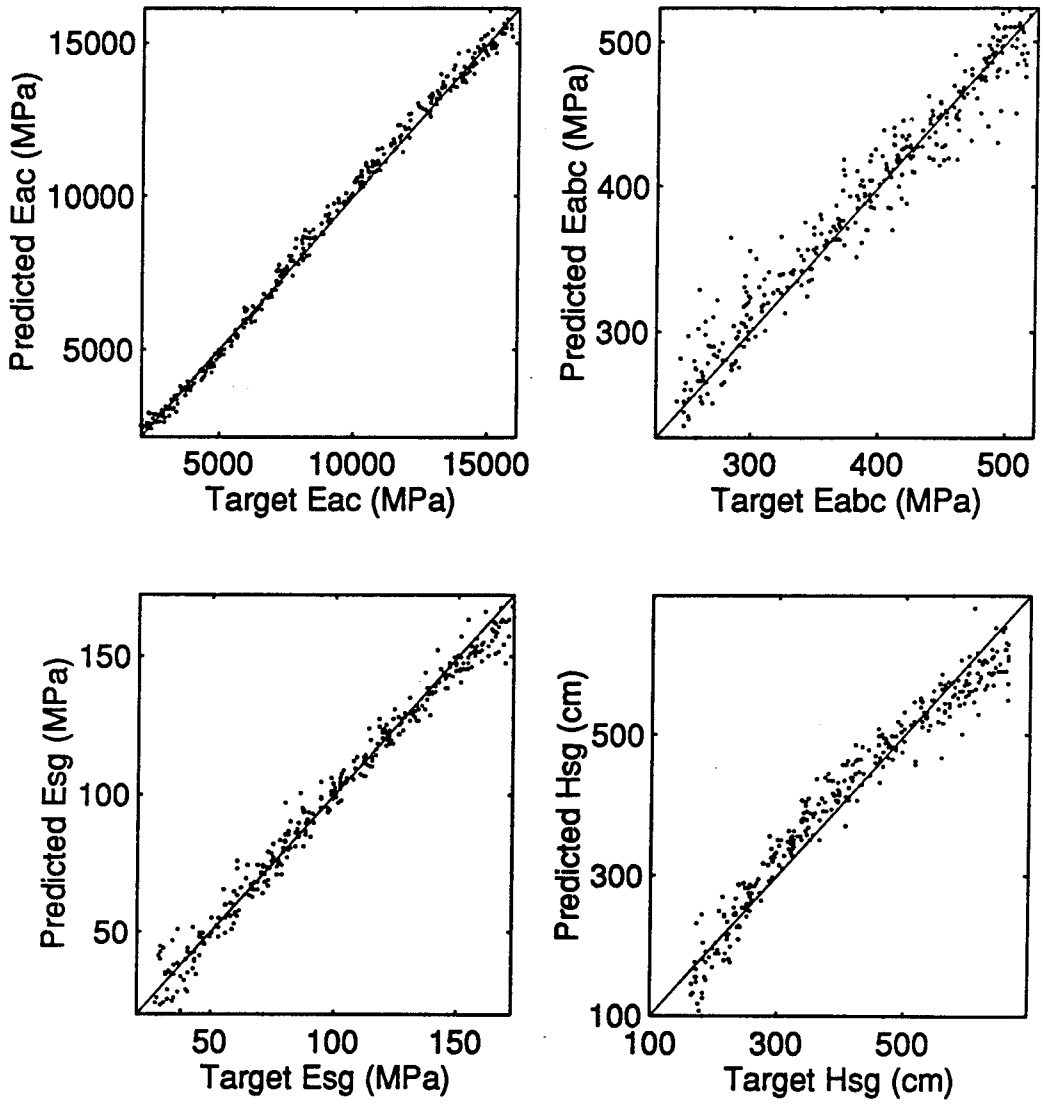

Figure B.6: Summary of testing results for scenario D.

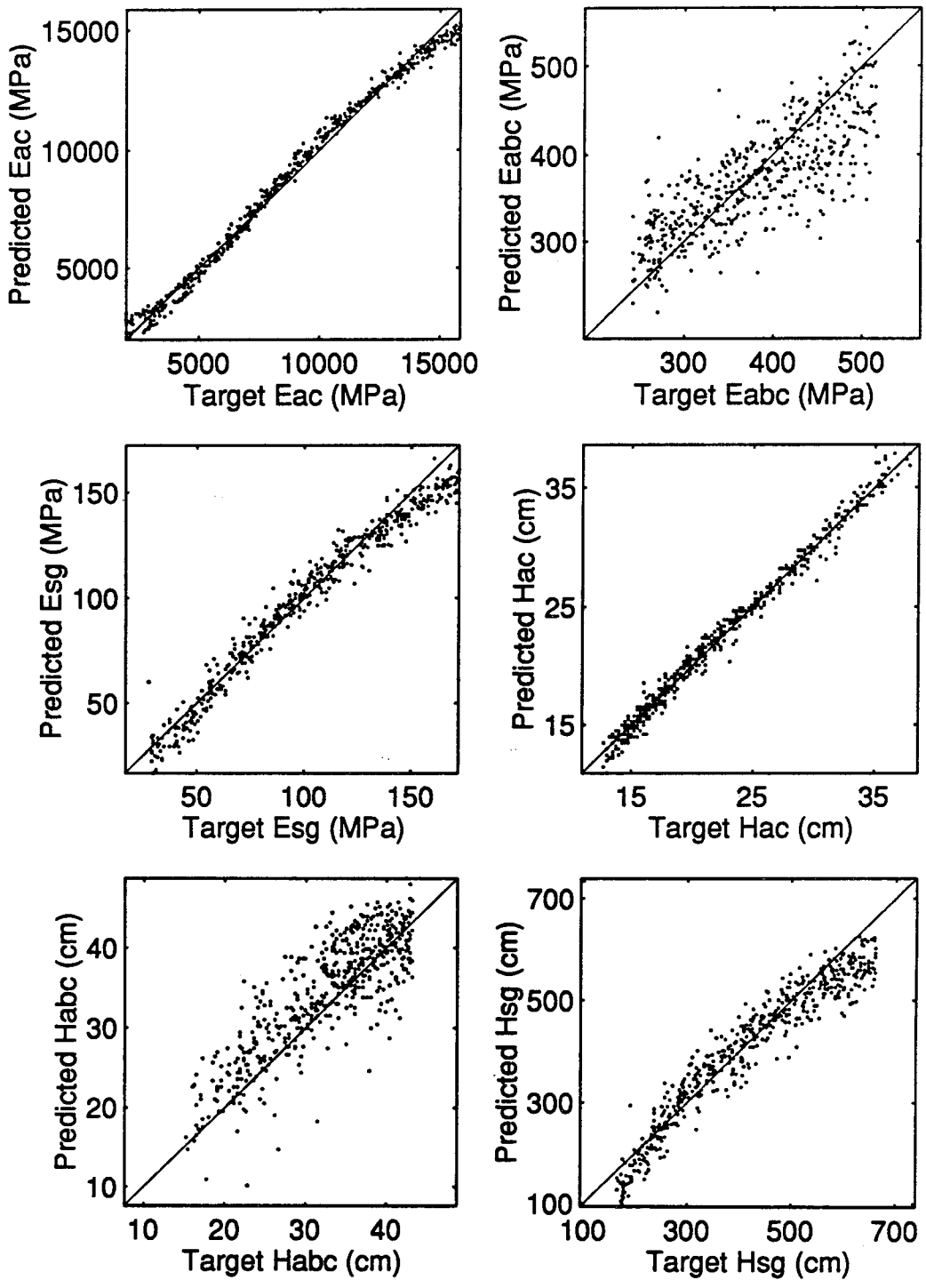

Figure B.7: Summary of testing results for scenario E.

will show little sensitivity to those parameters. For example, the two sets of pavement parameters shown in Table B.6, although quite different from each other with a maximum deviation of about 43% corresponding to the ABC layer modulus, lead to almost identical deflection basins with a maximum deviation of only about 0.1%. This observation points to the non-uniqueness of the forward mapping implied by the forward model.

Table B.5. Comparison of GA and ANN analysis results for one set of target values.

		Predicted		Error	
	Target	GA	ANN	GA	ANN
E_{ac}, (MPa)	12837	10363	12355	0.195	0.04
E_{abc}, (MPa)	255	452	420	0.773	0.647
E_{sg}, (MPa)	46	37	19	0.188	0.574
H_{ac}, (cm)	36.7	43	42.4	0.172	0.156
H_{abc}, (cm)	42.2	50.8	47.3	0.204	0.121
H_{sg}, (cm)	724	409	384	0.130	0.181
			Mean Error	0.277	0.287
δ_0 (mm)	0.1260	0.1281	--	0.017	--
δ_1 (mm)	0.1171	0.1174	--	0.002	--
δ_2 (mm)	0.1136	0.1135	--	0.001	--
δ_3 (mm)	0.1089	0.1086	--	0.002	--
δ_4 (mm)	0.1041	0.1039	--	0.002	--
δ_5 (mm)	0.0941	0.0940	--	0.001	--
δ_6 (mm)	0.0839	0.0843	--	0.004	--

Table B.6 Example of multiple solutions of a deflection basin.

	Set A	Set B	Error
E_{ac}, (MPa)	12873	12873	0
E_{abc}, (MPa)	255	365	0.4324
E_{sg}, (MPa)	45.5	42	0.0788
H_{ac}, (cm)	36.7	40.6	0.1073
H_{abc}, (cm)	42.2	45.7	0.1102
H_{sg}, (cm)	470	442	0.0595
δ_0 (mm)	0.12596	0.12608	0.001
δ_1 (mm)	0.11709	0.11711	0.002
δ_2 (mm)	0.11354	0.11354	0
δ_3 (mm)	0.10889	0.10884	0.005
δ_4 (mm)	0.10411	0.10406	0.005
δ_5 (mm)	0.09411	0.09406	0.005
δ_6 (mm)	0.08392	0.08397	0.005

This non-unique nature of the forward mapping limits the performance of both backcalculation methods presented here. The feed-forward type ANN used to capture the mapping cannot implement a one-to-many relationship as indicated by the above

observation. Under these circumstances, the ANN will tend to predict, in general, a set of parameters that is an interpolation of the multiple sets of values. The GA-based method will converge, at best, at one of the multiple solutions even if the error tolerance is set to an extremely low value. However, any optimization based method, including a GA, offers the opportunity to search for alternative solutions in a systematic manner. Therefore, the GA-based method will be able to determine the multiple sets of pavement parameters instead of a set of interpolated (or averaged) parameter values, as implemented by the ANN-based method. Pavement engineers with specialized knowledge of in-situ material properties can then select the most reasonable set of pavement characteristics by considering supplementary information available on the pavement being analyzed.

The selection of the most appropriate backcalculation method will depend on many factors, including accuracy and efficiency, run-time turn-around time requirements, data availability, and extendibility to new and more complex forward models. The ANN-based method spends most of its computation time up front during data generation and training, with minimal run-time requirements. On the other hand, the GA-based method does not require large data sets but uses most of its computation time during the search process, and therefore results in relatively large run-time requirements.

B.6 Summary

This study presents the potential of the ANN and GA techniques to backcalculate pavement layer properties using NDT deflection data. Comparisons of these two methods can be summarized as follows:

1. The ANN-based method spends most of its computation time up front during data generation and training, with minimal run-time requirements. On the other hand, the GA-based method does not require large data sets but uses most of its computation time during the search process, and therefore results in relatively large run-time requirements.
2. The ANN method can carry out global searches even in the absence of knowledge about the mathematical form of the mapping between an input signal and the corresponding output signal. The GA method, however, requires the forward model to be included in the analysis procedure.
3. ANN is unable to solve the problems with non-unique solutions. On the contrary, GA has the ability to capture multiple solutions within the given allowable error.

Further study and investigation of the two methods are warranted to make a more conclusive comparison. The choice of the most appropriate method to use will depend, among other factors, on the scenario under investigation, the type of forward model, the run-time turn-around requirements, as well as prediction accuracy and efficiency.

Appendix C. A Phenomenological Approach for Temperature Correction of FWD Deflection Basin

C.1. Introduction

The temperature of the asphalt layer is one of the major environmental factors that affect the surface deflections of a flexible pavement. In order to assess the structural integrity of the pavement using deflection data, the data first need to be corrected against temperature effects. This correction is typically carried out by adjusting the deflection measured at an arbitrary temperature to an equivalent deflection at the standard (or reference) temperature. The effective (or average) temperature of the asphalt layer is determined through either a direct measurement or a theoretical prediction. Various models for prediction of effective asphalt temperatures have been proposed by others; e.g., AASHTO Guide (42), Baltzer and Jansen (43), Kim et al. (44), and Shao et al. (45).

Many researchers have developed models either for temperature-modulus correction or for temperature-deflection correction. For example, Ullidtz (46), Johnson and Baus (47), Baltzer and Jansen (43), and Kim et al. (48) proposed models for temperature correction of asphalt modulus, and AASHTO Guide (49) and Kim et al. (48) presented models for temperature correction of flexible pavement deflections. The majority of these models are based on a statistical analysis of data obtained from a limited range of mixture types and pavement profiles, and therefore often fail to effectively correct moduli or deflections for certain mixture types and pavement profiles. In order to ameliorate these shortcomings, Park and Kim (50), based on a mechanistic study of the mixture's thermo-rheological properties which are primarily responsible for the temperature effects on backcalculated moduli and pavement deflections, developed an analytical model that can be applied to any pavement with known thermo-rheological properties of the asphalt mixture used in it.

Even though the theoretical correction procedure developed by Park and Kim (50) yields accurate corrections with a plausible thermo-mechanistic basis and excellent generality, the procedure requires a good knowledge of the thermo-rheological properties of the mixture involved and, for a deflection correction, it additionally requires a forward deflection computation. The thermo-rheological properties (i.e., the relaxation modulus and the time-temperature shift factor) of a mixture are usually obtained through a series of laboratory creep tests, which is usually time-consuming and costly.

Existing temperature-deflection correction models can handle only the center deflection, and to the best of the authors' knowledge, no model has been published that can correct deflections other than the center one. To be practical, the deflection correction model should be able to correct the entire deflection basin, from which a temperature-independent, moduli backcalculation or deflection interpretation may be carried out.

In this study, a temperature-deflection correction model, based on a statistical analysis of available FWD deflections and measured pavement temperatures, is presented. Emphasis has been placed on discussing the characteristics of the observed temperature dependence of the deflections, and presenting the detailed steps necessary for establishing a model. The resulting model has a simple, explicit algebraic form, and only a small number of numerical constants that represent the best-fit curve of the available data are involved in the model.

C.2. Variation of FWD Deflections with Pavement Temperature

In order to study the dependence of FWD deflections on pavement temperature, a number of sites across North Carolina were selected for FWD tests and a simultaneous measurement of the pavement's effective temperatures. A total of six flexible pavement sections with different designs were considered. They were either full-depth asphalt pavement or pavement with an aggregate base course. The thickness of asphalt layer ranged from 115 mm (4.5") to 305 mm (12"). In order to cover a wide enough range of pavement temperatures, FWD tests were conducted at different times of day in all four seasons (repeatedly on the same spot). Four different load levels were applied, but only deflections under 40 kN (9 kips) load were used in the analysis. Temperatures within the pavement layers were measured at the time of FWD tests using thermocouples installed at different depths. The mid-depth temperature of the asphalt layer was taken as the *effective* (or *average*) temperature of the layer.

Figures C.1(a) to (c) show some typical variations of FWD deflections with pavement temperature measured, respectively, at the loading center, at the third sensor, and the sixth sensor locations in three selected sections. The third and the sixth sensors are located 305 mm (12") and 914 mm (36"), respectively, from the center of the loading plate. A total of seven sensors were used with the last sensor located 1219 mm (48") away from the loading center. The three sections selected have the minimum, the maximum, and an intermediate asphalt layer thickness; the asphalt thicknesses for Site 1, Site 2, and Site 3 are 115 mm (4.5"), 305 mm (12"), and 203 mm (8"), respectively.

Overall, the deflection increases with increasing temperature. This temperature dependence is most pronounced for the deflections at the loading center and gradually decreases with increasing radial offset; the deflections from the sixth sensor show virtually no particular temperature dependence. It was pointed out by Park and Kim (50) that the deflection of pavement surface depends on combinations of parameters including the thermo-rheological properties of the asphalt-aggregate mixture and the thicknesses of the pavement layers. Figures C.1(a)-(c) indicate that the section with the thickest asphalt layer (Site 2) shows the greatest temperature dependence.

When the deflection-temperature relations are plotted on a semi-logarithmic scale, the trend can be roughly characterized by a linear relationship between the logarithm of deflection and temperature, as shown in Figure C.2 (for w_1 at Site 1). The degree of the

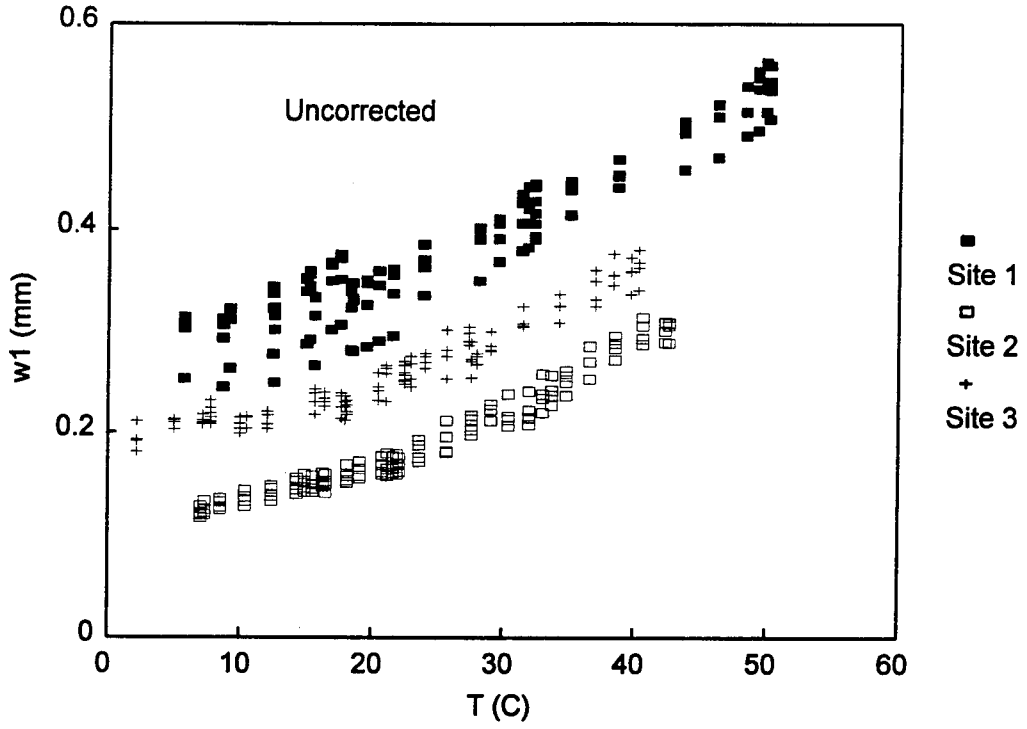

Figure C.1. Variation of FWD deflections with pavement temperature (P = 40 kN or 9 kips). (a) At loading center (R = 0 mm).

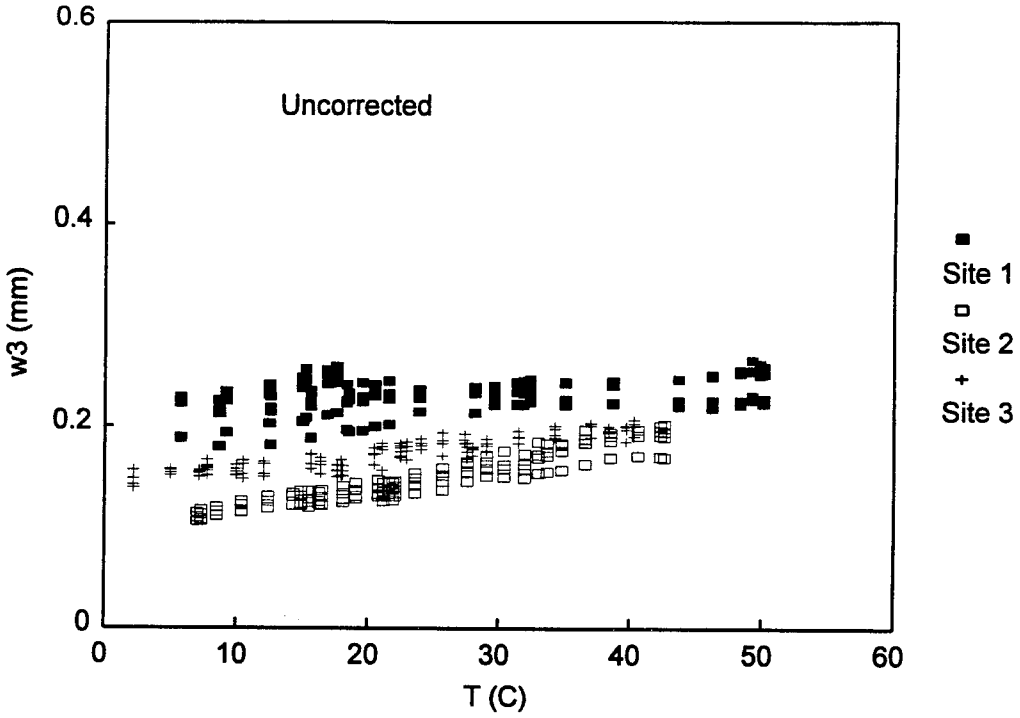

Figure C.1. (Continued). (b) At third sensor (R = 305 mm or 12").

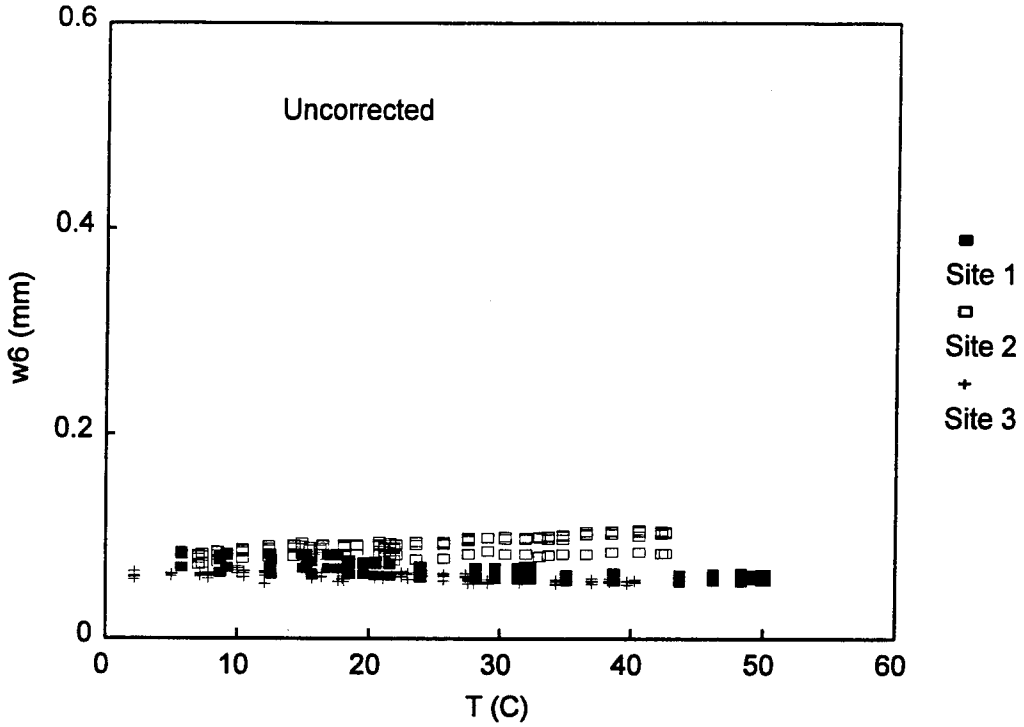

Figure C.1. (Continued). (c) At sixth sensor (R = 914 mm or 36").

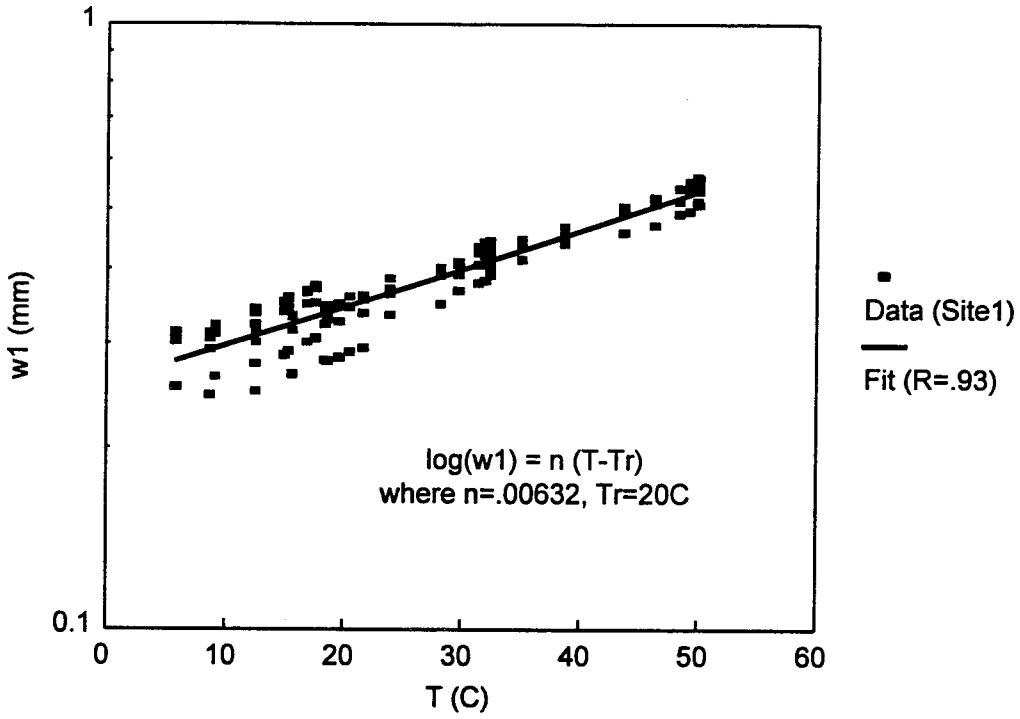

Figure C.2. Typical variation of FWD deflection with pavement temperature on a semi- logarithmic scale and its linear least squares fit (from center deflections at Site 1).

temperature dependence is represented by the slope of a straight-line fit as indicated in Figure C.2. This slope depends on the thickness of the asphalt layer and also, as discussed below, on the offset distance of the sensor. In fact, this slope on a semi-logarithmic plot of deflection vs. temperature plays a key role in our temperature correction modeling illustrated below.

C.3. Development of a Temperature-Deflection Correction Model

A deflection measured at a certain temperature can be corrected to an equivalent deflection at a reference temperature by multiplying an appropriate correction factor, i.e.,

$$w_{T_0} = \lambda_w w_T \tag{C.1}$$

where w_{T0} is the deflection corrected to the *reference* temperature T_0 and w_T is the deflection measured at temperature T. The temperature-deflection correction factor λ_w thus can be defined by:

$$\lambda_w = \frac{w_{T_0}}{w_T} \tag{C.2}$$

When one idealizes the deflection-temperature relationship by a linear relationship between log w and T (e.g., Figure C.2), it can be shown that the correction factor defined by Equation C.2 can be expressed directly in terms of the slope of the straight line. For this, let us take the following linear relationship between log w and T:

$$\log w = b + nT \tag{C.3}$$

where b is the intercept on the log w axis and n is the (positive) slope. Rewriting Equation C.3, one obtains:

$$w = 10^{b+nT} \tag{C.4}$$

Substituting Equation C.4 into Equation C.2, one finally obtains the correction factor in terms of n as follows:

$$\lambda_w = 10^{-n(T-T_0)} \tag{C.5}$$

From an observation of n-values for different test sites with different asphalt thickness, it was found that the slope n is an increasing function of asphalt layer thickness. In order to determine the analytical expression of the thickness-dependence of n, the slope n was computed for each of the seven sensor deflections for each of the six sites considered, using a linear least squares fit as illustrated in Figure C.2. The computed n-values, for all six sites for a particular sensor location, are then plotted against the asphalt thickness. Figure C.3 shows the variation of n-values with asphalt thickness for center deflections. Based on Figure C.3, even though the correlation is not very strong, it is clear that n increases with increasing asphalt thickness, in general. Since it was difficult to identify a particular functional form that can represent the n vs. h_{AC} relationship, a *linear* least squares fit was applied, and the coefficient thus obtained is indicated in Figure C.3.

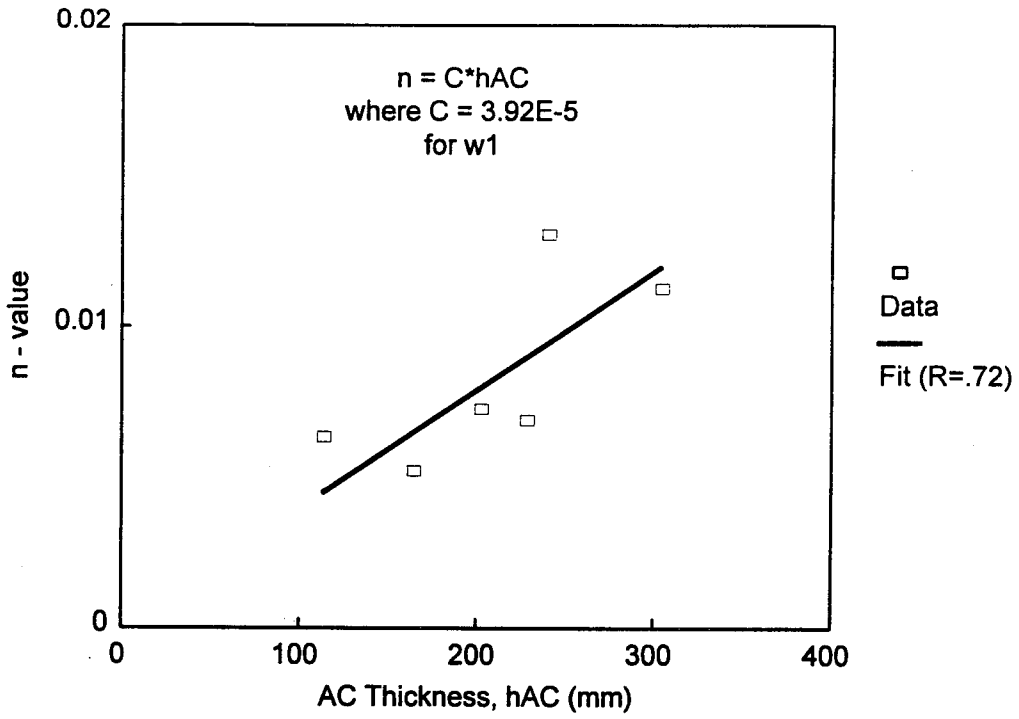

Figure C.3. Variation of n-values with asphalt layer thickness and its linear least squares fit (from center deflections at all six sites).

Physically, n should be zero for zero asphalt thickness (i.e., for absence of an asphalt layer), and thus the y-intercept of each line is set to zero. Then the relationship between n and the asphalt thickness can be expressed by:

$$n = C\,h_{AC} \tag{C.6}$$

where h_{AC} is the thickness of the asphalt layer and the coefficient C is the slope of the line shown in Figure C.3. Remember the n vs. h_{AC} relationship and the C-value given in Figure C.3 are for center deflections. Similar steps were taken for the remaining six sensor deflections. The resulting C-values are plotted against offset distance in Figure C.4. The following expression was obtained from a quadratic least squares fit to these data:

$$C = 3.90\times10^{-5} - 6.08\times10^{-8}R + 2.39\times10^{-11}R^2 \tag{C.7}$$

where R is the radial offset distance (in *mm*) of the sensor in consideration. As indicated in Figure C.4, the seven sensors are located respectively at R = 0, 203, 305, 457, 610, 914, and 1219 mm from the center of the loading plate. Since Equation C.7 is developed based on deflection data obtained from this particular sensor arrangement, it should be safe to add a constraint that Equation C.7 is valid only for $R \leq 1219$ mm (48"). However, as seen from Figure C.1(c), deflections from outer sensors at sufficiently large offset distances are virtually independent of temperature; therefore, one may reasonably assume that C = 0 for $R > 1219$ mm, or equivalently, take $\lambda_w = 1$ in Equation C.1. For pavements with an unusually thick asphalt layer, however, this assumption may not be appropriate, and the necessary temperature corrections should be made based on proper engineering judgment and experience.

Substituting Equation C.7 into Equation C.6, and then into Equation C.5, one obtains the following expression for the temperature-deflection correction factor:

$$\lambda_w = 10^{-(3.90\times10^{-5} - 6.08\times10^{-8}R + 2.39\times10^{-11}R^2)\,h_{AC}\,(T-T_0)} \tag{C.8}$$

It can be seen that the correction factor λ_w is a function of pavement temperature T, asphalt thickness h_{AC}, and sensor offset distance R. The units used in deriving Equation C.8 are *mm* for deflection and offset distance and *°C* for temperature. Appropriate conversion factors should be applied to Equation C.8 for units other than those adopted here.

Some sample correction factors for a range of pavement temperatures (0°C - 60°C), different asphalt thicknesses (100, 200, and 300 mm), and different sensor locations (for w_1, w_3, and w_6, respectively) are plotted in Figures C.5(a)-(c) for a reference temperature of 20°C. Again, it is evident that the greater the asphalt thickness and the smaller the offset distance, the greater the temperature correction that will be required.

C.4. Test of the Model

First, let us apply our model, Equation C.8, to correct the deflections shown in Figures C.1(a)-(c). Substituting the respective values of T, h_{AC}, and R associated with each data (of uncorrected deflections) into Equation C.8 and then into Equation C.1, one can obtain a corrected deflection corresponding to the data. The corrected deflections thus

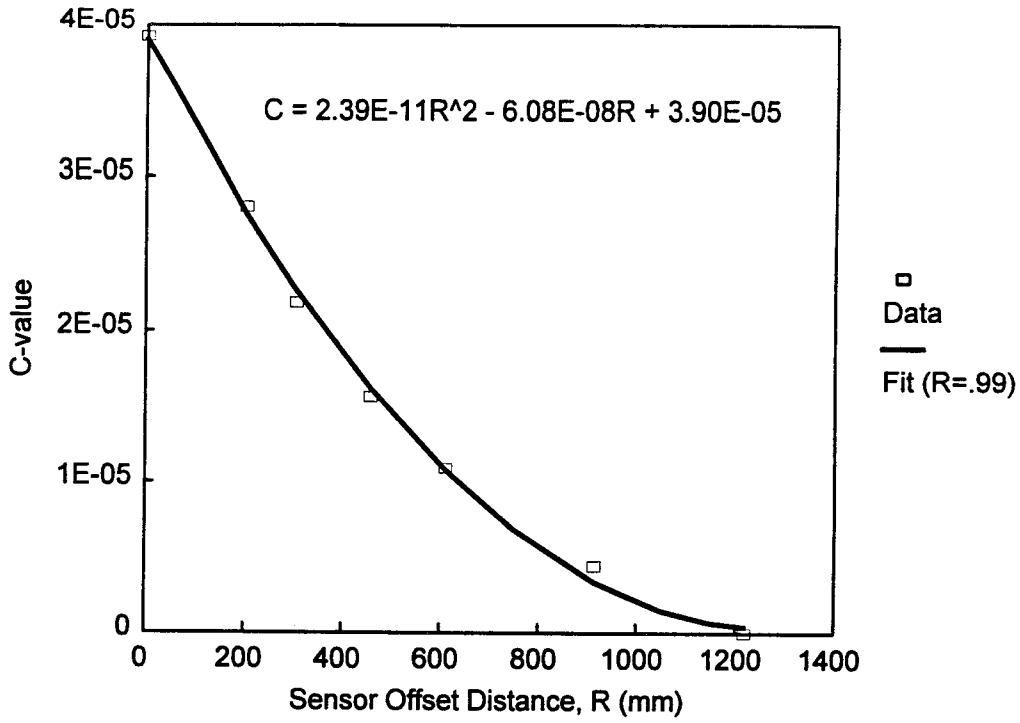

Figure C.4. Variation of C-values with sensor offset distance and its quadratic least squares fit (from all seven sensor deflections at all six sites).

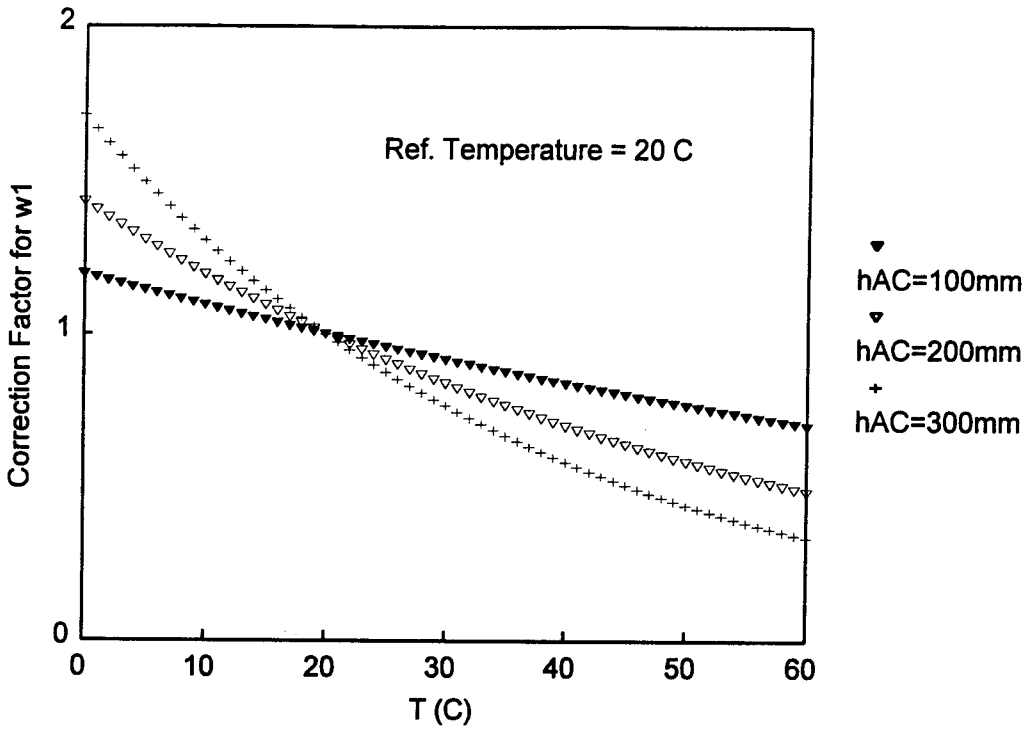

Figure C.5. Typical computed deflection correction factors for different asphalt layer thicknesses. (a) For center (R = 0 mm) deflections.

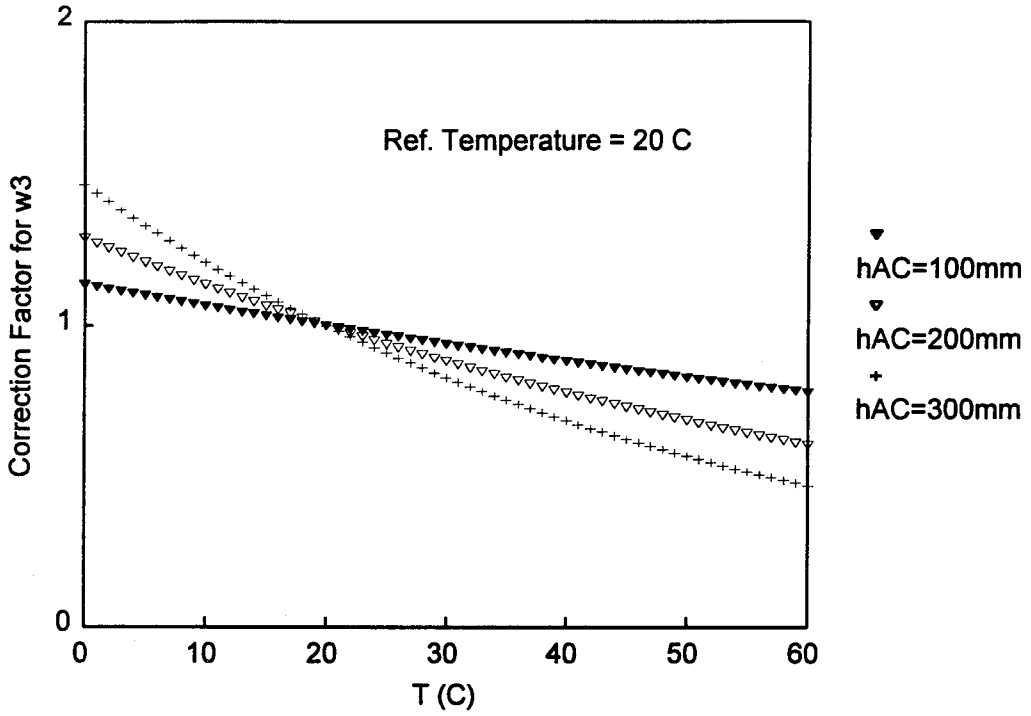

Figure C.5. (Continued). (b) For third sensor (R = 305 mm or 12") deflections.

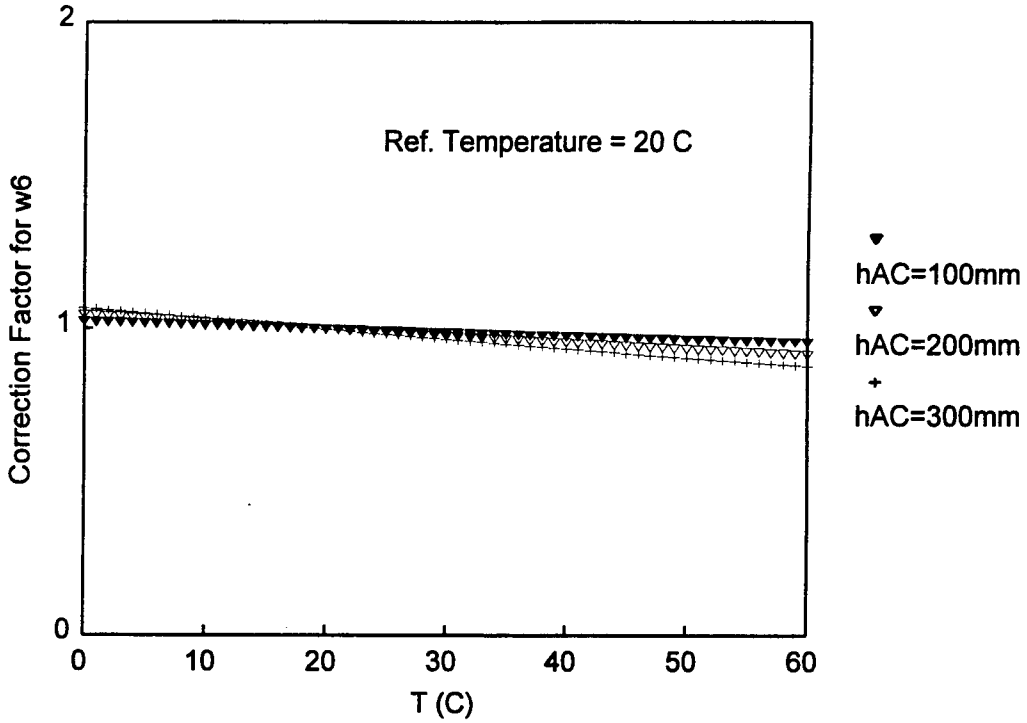

Figure C.5. (Continued). (c) For sixth sensor (R = 914 mm or 36") deflections.

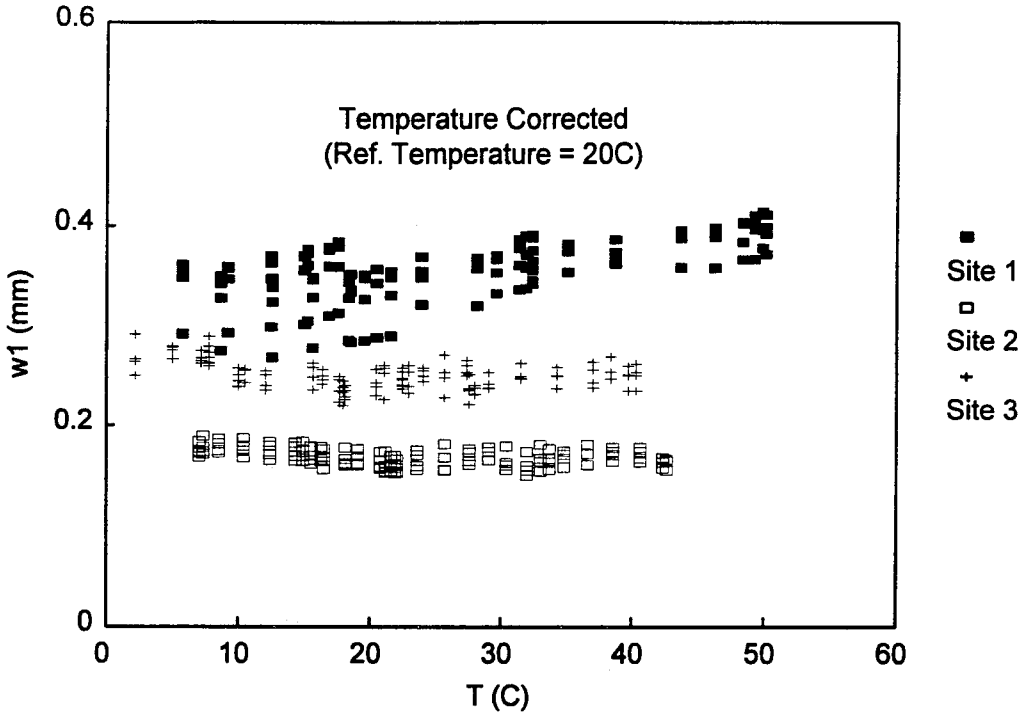

Figure C.6. Deflections corrected to a reference temperature of 20°C. (Deflection data were used in modeling). (a) Center (R = 0 mm) deflections.

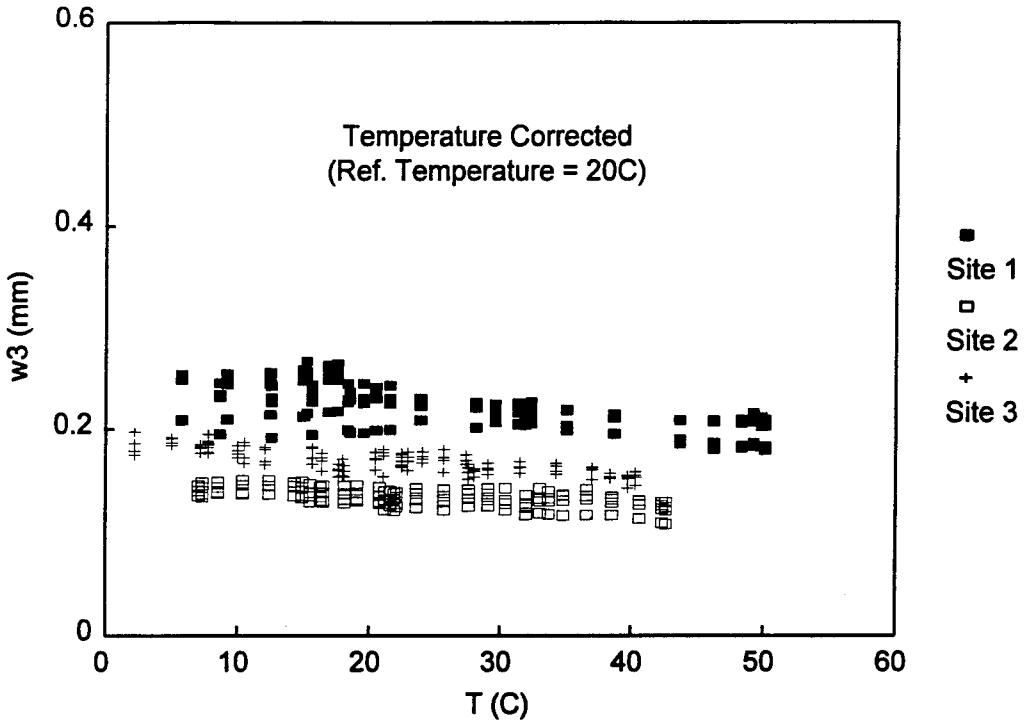

Figure C.6. (Continued). (b) Third sensor (R = 305 mm or 12") deflections.

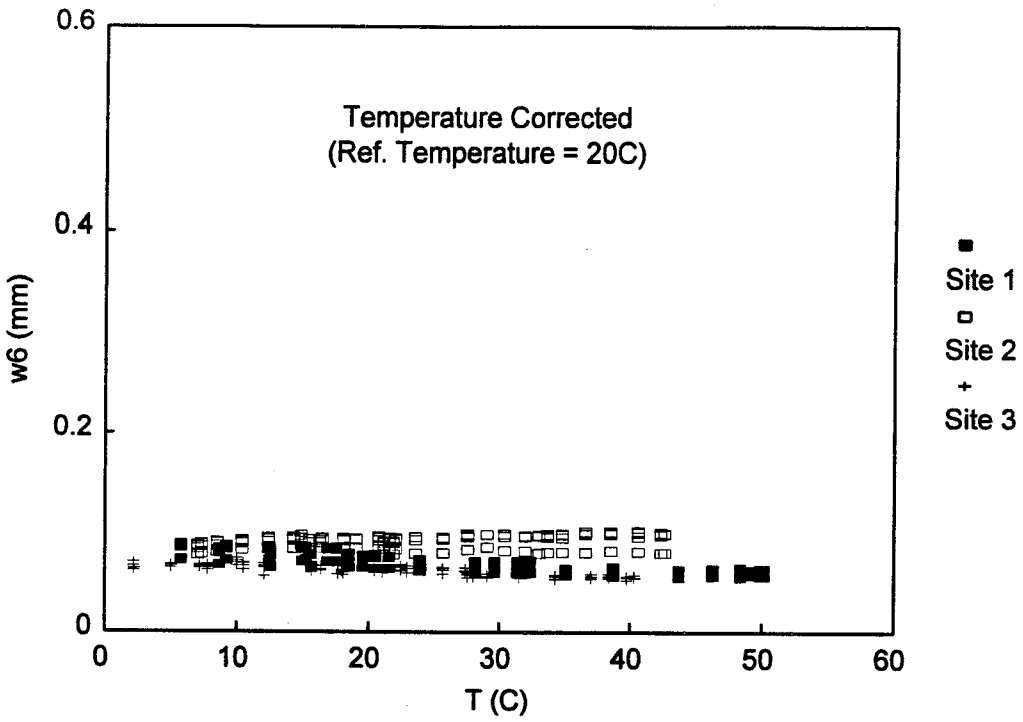

Figure C.6. (Continued). (c) Sixth sensor (R = 914 mm or 36") deflections.

obtained are plotted in Figures C.6(a)-(c) for w_1, w_3, and w_6, respectively. Overall, the corrections are good, which is manifested by near-horizontal alignment of the corrected data (signifying independence of the corrected deflections of temperature). A slight under-correction of the center deflections from Site 1 and w_6's from Site 2, and a minor over-correction of the center deflections from Site 2, are observed. These minor deviations can be attributed to the *averaged* nature of Equation C.8; it should be remembered that the equation has been derived based on a series of least squares curve fits of the temperature dependence of the measured deflection data. Though not presented in this paper due to space limitations, similar findings were observed with corrected deflections from the other three sites not shown in Figures C.6(a)-(c).

Even though the corrections demonstrated in Figures C.6(a)-(c) are good, one may see that these cannot serve as a proper *validation* of the model, because the data has been used in developing the model. However, these results still serve as meaningful proof of the soundness of the model with respect to its mathematical structure and generality. It is to be noted that there are only three constants involved in the correction model, Equation C.8, but we are dealing with a great number of combinations of three active variables (T, h_{AC}, and R). If the model were not developed on a proper phenomenological basis (and thus did not take a proper mathematical form), the results might not necessarily be positive, and any good results could be claimed to be fortuitous.

For an additional check of the model, we now would like to apply the model to a set of data not used in developing the model above. The data, shown in Figure C.7(a), were obtained from four different sites within the central region of North Carolina. These test sections were either full-depth asphalt pavement (Sites A and C) or pavement with an aggregate base course (Sites B and D). The thickness of asphalt layers for Sites A, B, C, and D, were, respectively, 190, 89, 229, and 140 mm. Mid-depth temperatures of asphalt layers were directly measured from the pre-installed thermocouples. Records of only the center deflections only are used here.

Figure C.7(a) indicates that the deflections from the sections with thicker asphalt layers (Sites A and C) are much more temperature dependent than those from thinner sections, and thus require greater corrections. Figure C.7(b) shows that the overall corrections appear to be satisfactory, except that the data from Sites A and C (with thicker asphalt sections) are somewhat under-corrected. Based on this particular observation, the model appears to under-correct the deflections from sections with thick asphalt layers. However, it is still difficult to judge whether the deviation is due to the deficiency of the model or due rather to the exceptional behavior of the tested sections.

In order to enhance the reliability of the model, a re-calibration of the model using a larger data base of FWD deflections and corresponding pavement temperatures (either measured or predicted) and other pertinent parameters (including asphalt thickness and sensor offset distance) can be made. Also, when a geographic factor is essential, the model calibrated using the field data retrieved within that particular geographical region should be used.

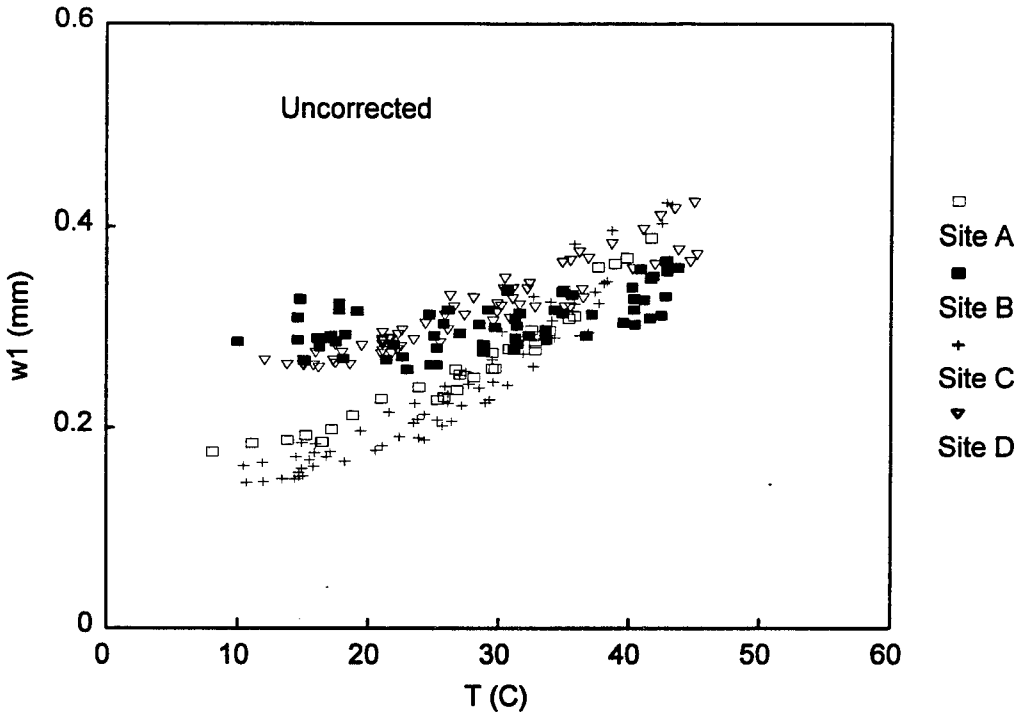

Figure C.7. FWD deflections from other sites (not used in model development). (a) Uncorrected deflections (at R = 0 mm under P = 40 kN or 9 kips).

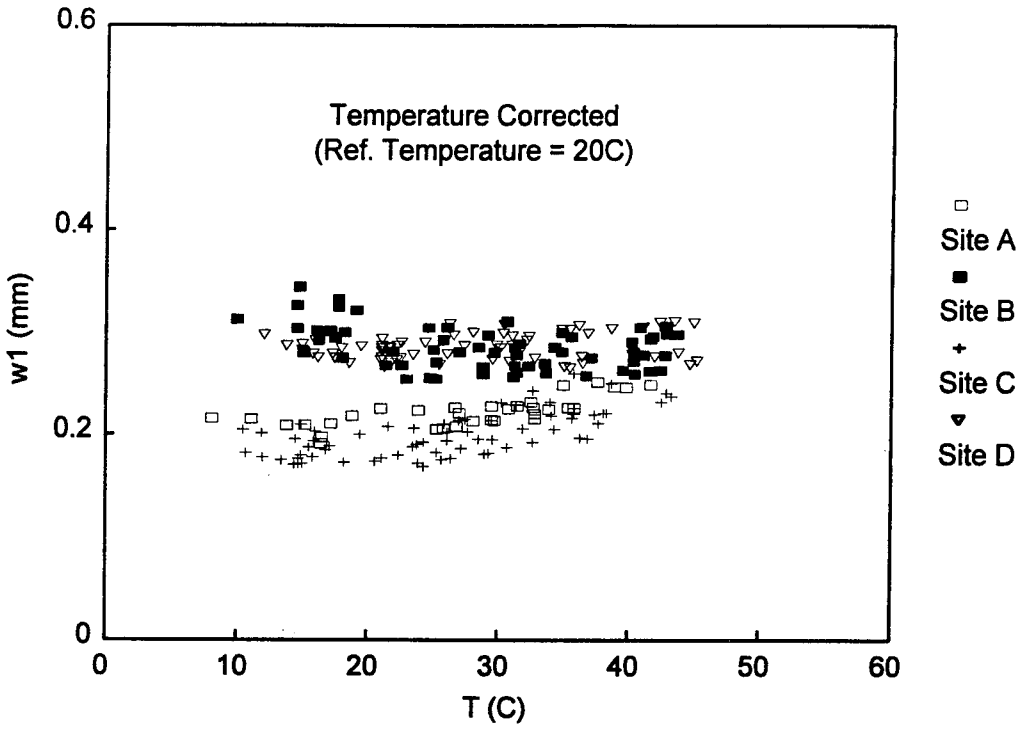

Figure C.7. (Continued). (b) Corrected deflections (to reference temperature of 20°C).

C.5. Discussion

In comparison with Equation C.8, the model proposed by Kim et al. (48) for correction of center deflections, takes the following form:

$$\lambda_w = 10^{-A(h_{AC})^B (T-20)} \quad \text{(C.9)}$$

where h_{AC} is the AC layer thickness in *mm*, T is the temperature in ℃, and the constants A and B are given, respectively, to be 5.807E-6 and 1.4635 for sections along the wheel path, and 6.560E-6 and 1.4241 for sections along the lane center. It can be readily seen that, with $R = 0$ in Equation C.8 and $A = 3.90E\text{-}5$, $B = 1$ and $T_0 = 20$ in Equation C.9, Equation C.8 reduces to Equation C.9. In Equation C.9, the effects of asphalt thickness are modeled by a power law in h_{AC}; while in Equation C.8, the effects are modeled by a simple, linear function of h_{AC} with a zero y-intercept. This simplification appears to be reasonable in view of the corrections demonstrated in Figures C.6(a)-(c) and Figure C.7(b).

Let us briefly consider the temperature correction of backcalculated asphalt-mixture moduli in contrast to the deflection correction. It was pointed out by Park and Kim (50) that the temperature dependence of modulus is much simpler than that of deflection. An asphalt modulus is a thermoviscoelastic *material* property and thus is a function of temperature and (loading) time; whereas the deflection is a *system* property dictated by a set of material *and* geometrical parameters of the system including asphalt thickness (h_{AC}) and radial offset distance (R). Kim et al. (48) proposed the following form of a modulus correction model based on a statistical analysis of backcalculated moduli and pavement temperatures from the central region of North Carolina:

$$E_{T_0} = \lambda_E E_T \quad \text{(C.10)}$$

where E_{T0} is the modulus corrected to the reference temperature T_0, E_T is the backcalculated modulus of the asphalt mixture at temperature T, and λ_E is the temperature-modulus correction factor defined by:

$$\lambda_E = 10^{m(T-T_0)} \quad \text{(C.11)}$$

in which m is a positive constant. Equation C.11 was obtained from the observed trend that the logarithm of the modulus is a linearly decreasing function of temperature.

Equations C.5 and C.11 are of the same form, except that $-n$ in Equation C.5 corresponds to m in Equation C.11. Since both m and n are positive values, this correspondence means that λ_E and λ_w behave inversely to each other; for instance, for $T > T_0$, the modulus correction factor is greater than unity (thus scaling up the backcalculated modulus), while the deflection correction factor is less than unity (thus scaling down the measured deflection). Another major difference between m and n is that while m is a constant, n is a function of asphalt thickness (h_{AC}) and radial offset distance of the sensor (R) as indicated by Equations C.6 and C.7. Kim et al. (48) reported $m = 0.0275$, but a recent study based on a more extensive database generated within North Carolina

indicated that $m = 0.0262$ is a better choice. Figure C.8 shows the temperature-modulus correction factor defined by Equation C.11 with $m = 0.0262$ and $T_0 = 20°C$.

Finally, even though the model has been developed based on deflection data obtained from seven sensors with a particular set of spacings, the model is believed to be applicable to deflections obtained by FWDs with sensor spacings different from those used in this work; Figure C.4 shows a rather strong correlation between C-values and offset distance, suggesting any arrangement of sensors (in terms of their radial spacings) may be well accepted.

C.6. Summary

A phenomenological temperature correction model for FWD deflection basins (consisting of deflections at different offset distances) was successfully developed based on a statistical analysis of measured deflections and temperatures. Detailed steps for developing such a model are presented and illustrated through the use of the data obtained from pavements within North Carolina.

The relationship between deflection and pavement temperature was found to be characterized roughly by their linear relationship on a semi-logarithmic scale. The temperature dependence of the deflection was found to be influenced by the thickness of the asphalt layer and the offset distance of the deflection sensor. The resulting correction model uses a very simple and straightforward algebraic equation without requiring iterative or closed-loop computations.

The model was demonstrated to yield required corrections satisfactorily. Both the original data set which was used in developing the model and other independent data sets not used in model development were used in testing the model. Even though the mathematical structure of the model is fixed, the constants involved in it can be revised (or customized) using a particular database available in a given region. The necessary procedure for doing this is presented.

A temperature-modulus correction model previously given by Kim et al. (48) has been re-calibrated using a larger data base generated within North Carolina, and its correction capability has been enhanced.

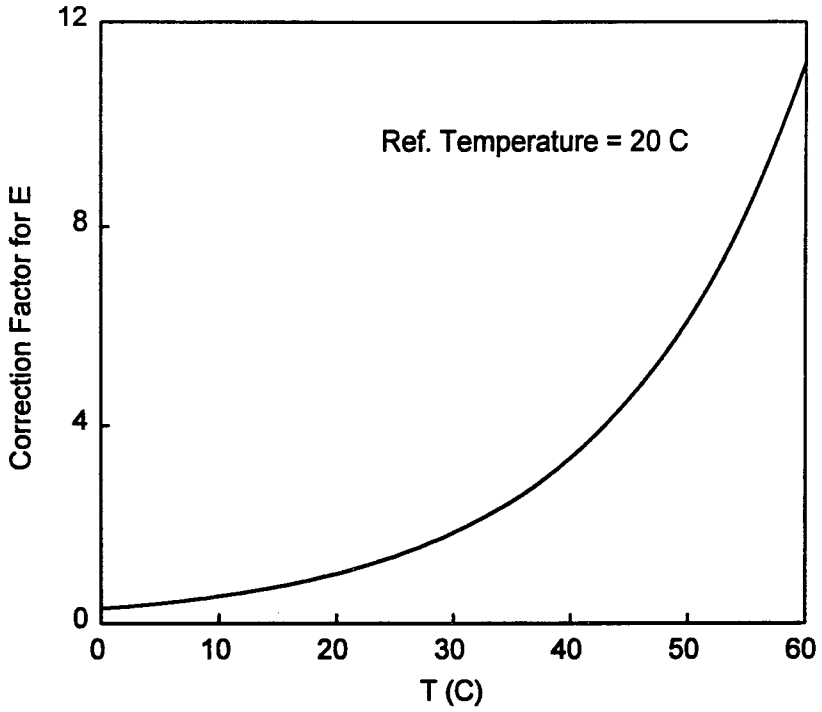

Figure C.8. The modulus correction factor computed according to Equation C.11 (with $m = .0262$ and $T_0 = 20°C$).